EUROPEAN ORGANIZATION FOR NUCLEAR RESEARCH

SUMMARY OF PRESENTATIONS MADE AT THE SPECIAL OPEN SESSION

OF THE INTERSECTING STORAGE RINGS COMMITTEE, 9th JANUARY 1979

The Future Use of the SFM Detector

Antiproton-proton Collisions at the ISR

edited by K.M. Potter

Geneva, April 1979

INTRODUCTION

Consideration of the long term physics programme at the CERN ISR started in 1976 when it became clear that in order to carry out any new large project at CERN it would be necessary to close the ISR for reasons of manpower and budget. This very fact of a machine with a limited lifetime underlined the need for a complete understanding of the physics capabilities of the ISR. Workshops were held in both 1976 and 1977 to discuss possible future programmes. One of the possibilities discussed at these workshops was the use of antiprotons colliding against protons to allow the study of the $\bar{p}$-p interaction up to $\sqrt{S}$ = 62 GeV.

By the end of 1978 the SPS collider project was under way, based on an antiproton accumulator ring using stochastic cooling. At its November 1978 meeting the ISRC heard of technical studies which had been made of methods of bringing antiprotons from this accumulator to the ISR, and recommended for approval a scheme which would make 26 GeV antiprotons from the CERN PS available for injection into ring 2. This recommendation was approved by the Research Board on 16th November 1978.

In order to prepare the physics programme with this new facility which is expected to be available during 1981, a special Open Session of the ISRC was held on 9th January 1979. A number of physicists who had in most cases already expressed interest in the possibilities offered by $\bar{p}$-p collisions at the ISR, were invited to give brief presentations of their ideas. These talks were not necessarily based on formal letters of intent and were intended simply to provoke discussion and hopefully generate new ideas in order to ensure that the ISR antiproton programme yields the maximum possible physics output in what is likely to be a relatively short time. An early approval of the LEP project could limit the use of antiprotons in the ISR to a period of little more than 18 months.

The recently upgraded Split Field Magnet (SFM) Detection system is expected to play a leading role in the antiproton programme while, on the other hand, it had become a matter of some concern that interest in its use for protons was waning, at least when judged by the number of physicists using it. For these reasons the first part of the meeting focussed attention on this detector in particular, with presentations of the advantages gained by the upgrading programme and reports from the current experiments.

This document is a collection of summaries of the talks given at this Open Session of the ISRC as listed below.

* * * * *

I. THE UPGRADED SPLIT FIELD MAGNET DETECTOR

P.G. Innocenti - CERN-EF

FOREWORD

A few years of ISR operation made it clear that an improvement to the SFM detector was desirable in order to allow the continuation of the physics programme. By 1975 possible areas of improvement could be singled out:

a) Increase redundancy of track information to ease pattern recognition in general and cover some areas previously neglected.

b) Introduce particle identification as far as compatible with magnet structure and efficient MWPC layout.

c) Reduce background by a thin vacuum chamber.

d) Switch to a more recent computer with CERN standard software.

The upgrading of the SFM detector took place in 1976 and 1977. Comparative performance is shown in what follows with reference to:

1. vacuum chamber and shim
2. multiwire proportional chambers
3. particle identification
4. trigger, data acquisition, online
5. reconstruction programs.

1. Vacuum chamber and shim

The vacuum chamber material is a serious source of event associated background mainly though γ conversion and δ rays.

The old vacuum chamber was elliptical both in the central region and in the downstream arms in order to accommodate field on and field off operation.

The new vacuum chamber (I4 yoyo) is made of corrugated thin cylinders and some spherical surfaces; it must be moved from field on to field off operation to accept full beam intensity (see fig.1). The quality of the vacuum chamber can be quantified by the thickness traversed by a particle emerging from the interaction point (see fig.2). Alternatively, by the weight of material of the chamber:

weight of central section

old	16.9 kg
new	8.0 kg

weight of downstream arms

old	2.6 kg/m
new	0.8 kg/m.

The magnetic channel (shim) around the upstream arms was shortened to allow an improvement of the MWPC layout at the end of the central section of the vacuum chamber. Field measurements on the SFM model were adequate for calculating a new field table.

No appreciable loss of beam time was introduced by operation with compulsory field on; the influence of the shorter shim could be properly corrected for.

2. MWPC layout

The increase in redundancy of information for pattern recognition was achieved by doubling the number of wire planes. However, cost of the improvement could be contained within acceptable limits by going from a wire spacing of 2 to 4 mm (with the exception of the compensator chambers), hence confining the modifications to the chamber mechanical

construction and keeping the number of electronics channels unchanged. Approximately 1/3 of the chambers were left untouched, 1/3 had minor modifications (remove one wire out of 2) and 1/3 was heavily modified or completely rebuilt (see fig.3). The success of the operation in terms of acceptance is shown by the rapidity vs. azimuthal angle plots of fig. 4, 5 and 6.

After the modifications the detector has operated 15 months without breaking a single wire. Failure of readout electronics, including bad contacts, is of 0.3% per year, with no detectable ageing so far.

3. Particle identification

The performance of the various particle identification devices will be described in the reports by R415 and R416.

With reference to fig.7, a list of the particles identifiers is given here:

1) Cherenkov counters inside magnet gap
2) outer Cherenkov counters
3) Pb-glass array
4) Pb-scintillator sandwiches
5) TOF system
6) dE/dx chambers
7) liquid Argon calorimeter.

4. Trigger, data acquisition, online

The trigger principle based almost exclusively on the MWPC was retained, with addition of particle identification in the trigger when needed.

Three levels of trigger are operational:

FAST	(ns)	{ MWPC FOR's { particle identifiers
SLOW	(μs)	{ MWPC MOR's { (groups of 16 or 32 wires) { particle identifiers
FILTER	(ms)	{ small computer reading a { selected fraction of event { and doing simple calculations

Data acquisition is now based on a PDP 11/45 replacing the EMR 6130. The standard CERN PDP 11 Data Acquisition System is used. The connection to the Network has replaced the backup by the CII 10070 (see fig.8).

5. Offline reconstruction programs

The new detector layout required a change in software on account of the geometry of the MWPC and of the addition of particle identifiers. Moreover, the added redundancy made possible the utilization of new methods in pattern recognition and geometry.

The reconstruction programs were rewritten to cope with the new situation, with special attention to:

- accepting events with large number of digitizations coming from the new detector layout and in view of efficient reconstruction of very high multiplicity events;

- reducing computer time per track;

- by being modular
  a) make early use of track fit and vertex reconstruction in pattern recognition,
  b) allow trigger dependent selections to be used at any time for special space regions,
  c) be transportable to other detectors.

The average size of the event from MWPC is roughly unchanged:
- more planes ↗↗
- more angular coverage ↗

- smaller wire clusters ↘
- thinner vacuum chamber ↘↘
- more distributed absorbers (chambers) for slow particles ↘

However, the information from the particle identifiers represent an appreciable addition.

The performance of the reconstruction programs can be summarized as follows:

- 85 to 90% single track efficiency
- <5% events rejected
- 2 s of CDC 7600 CP time per event with $<n>_{ch}$ = 16.

FIGURES

Fig.1   Plan view of a) the old vacuum chamber, and b) the new vacuum
         chamber around the beam crossing point.

Fig.2   Thickness of Fe traversed by a particle emerging from the
         intersection point in a vertical plane for both old and new
         vacuum chambers.

Fig.3   MWPC Layout (for R416). Chambers with single cross hash /////
         have been transformed from 2 to 4 mm wire spacing; chamber
         with double cross hash XXXX have been heavily modified or re-
         built.

Fig.4a   Experimental y vs ϕ acceptance plot for old detector.
    4b   Calculated y vs ϕ acceptance plot for upgraded detector, no
         $\delta p/p$ cut.

Fig.5   Calculated y vs ϕ acceptance plot for upgraded detector, $\delta p/p \leqslant .3$.

Fig.6   Experimental y vs ϕ acceptance plot for upgraded detector,
         $\delta p/p \leqslant .3$ (from R415).

Fig.7   Layout of experiment R415 with indication of the particle iden-
         tification equipment (see section 3).

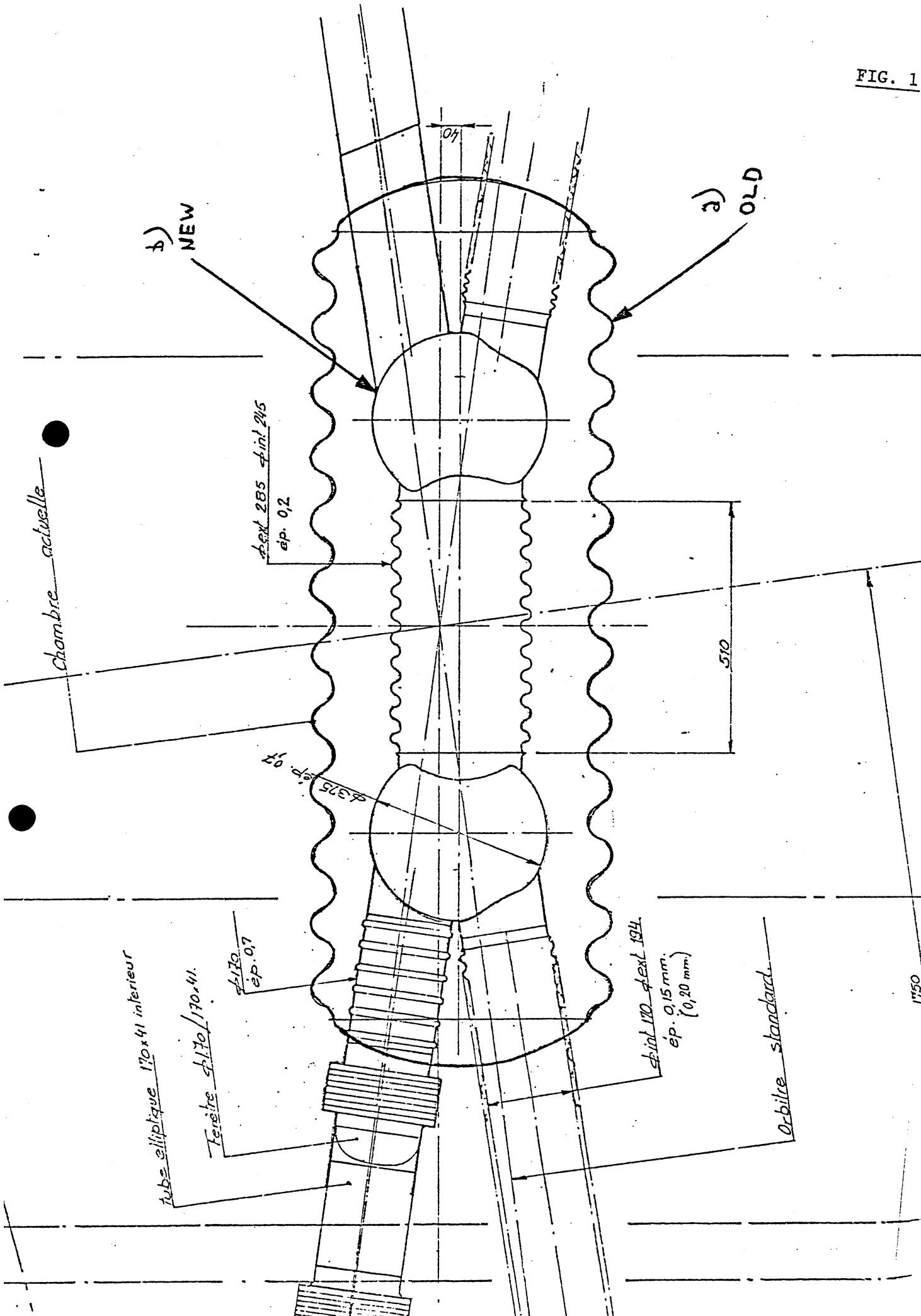Fig.8   Data acquisition and computer block diagram.
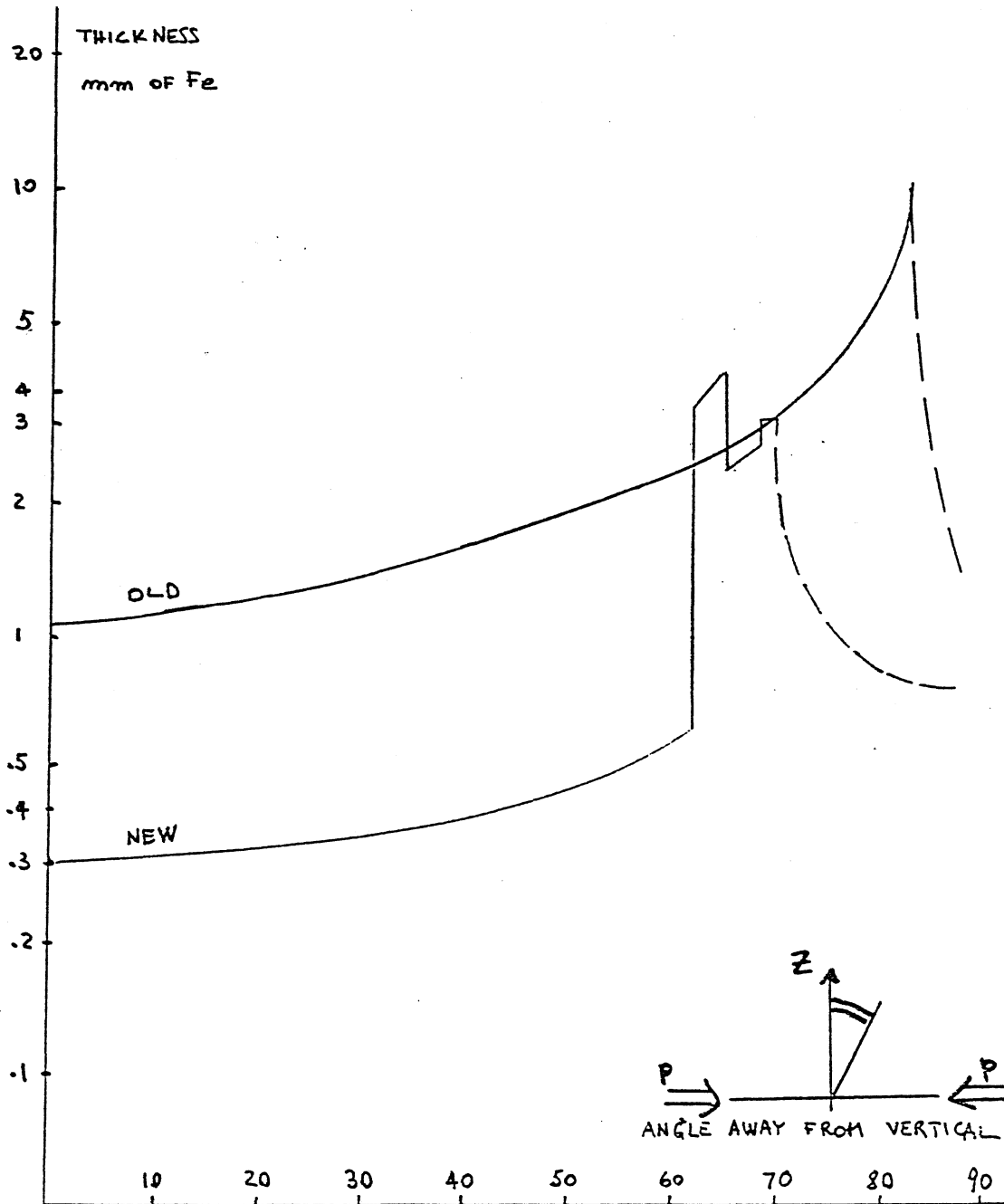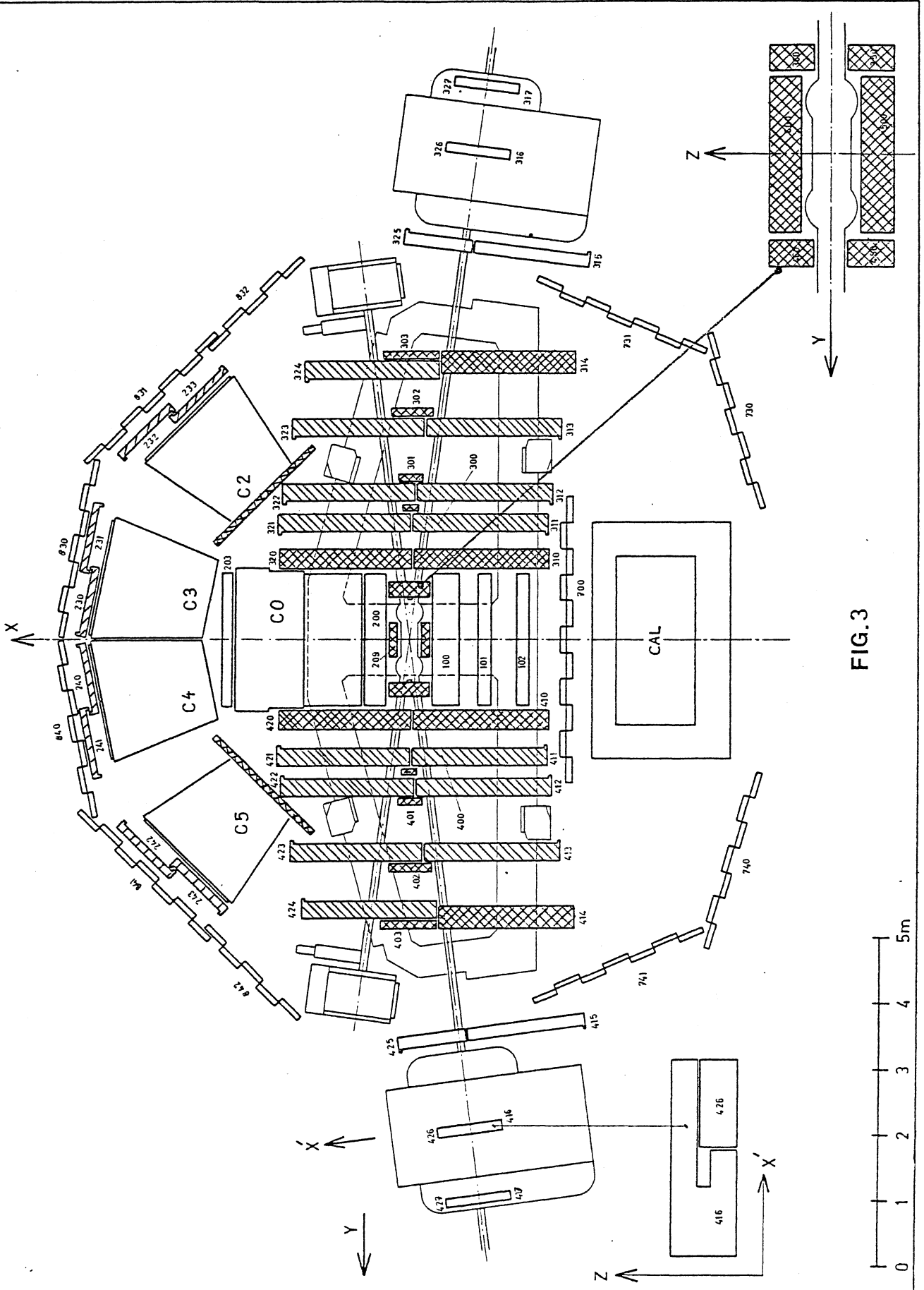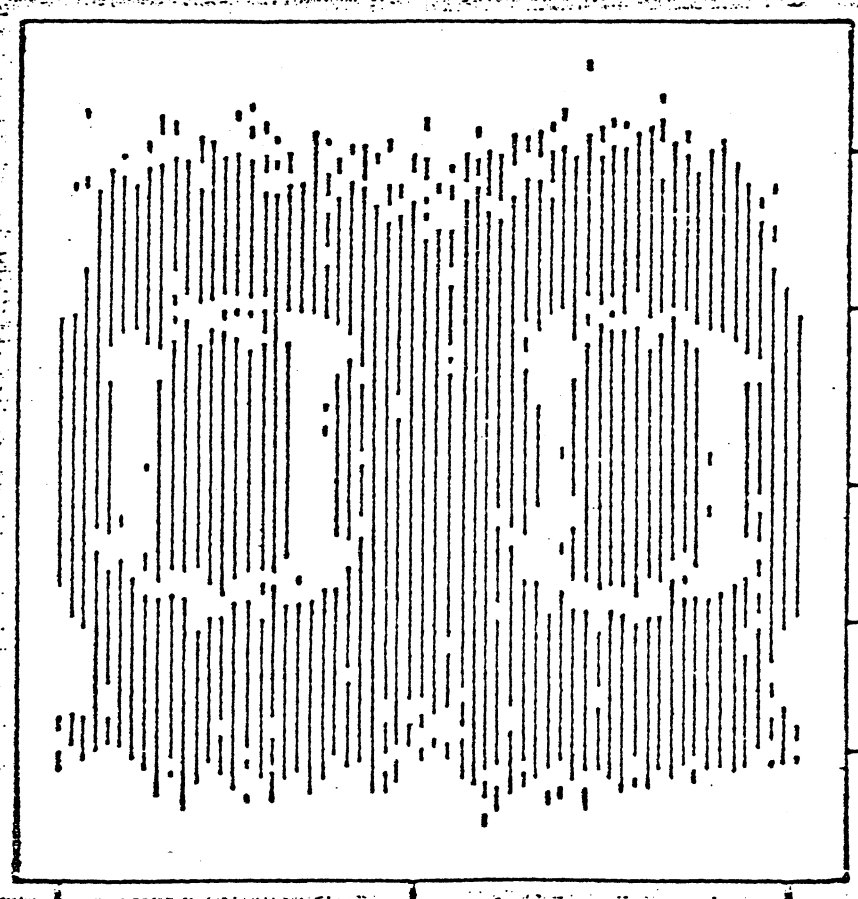
FIG. 1

FIG. 2

FIG.3

FIG. 4b

FIG. 4a

Old detector   Improved detector

Acceptance as function of rapidity "y" and azimutal production angle "φ"

FIG. 5

FIG. 6

Fig 6c

FIG.7

SFM ONLINE COMPUTER SYSTEM, JAN. 79
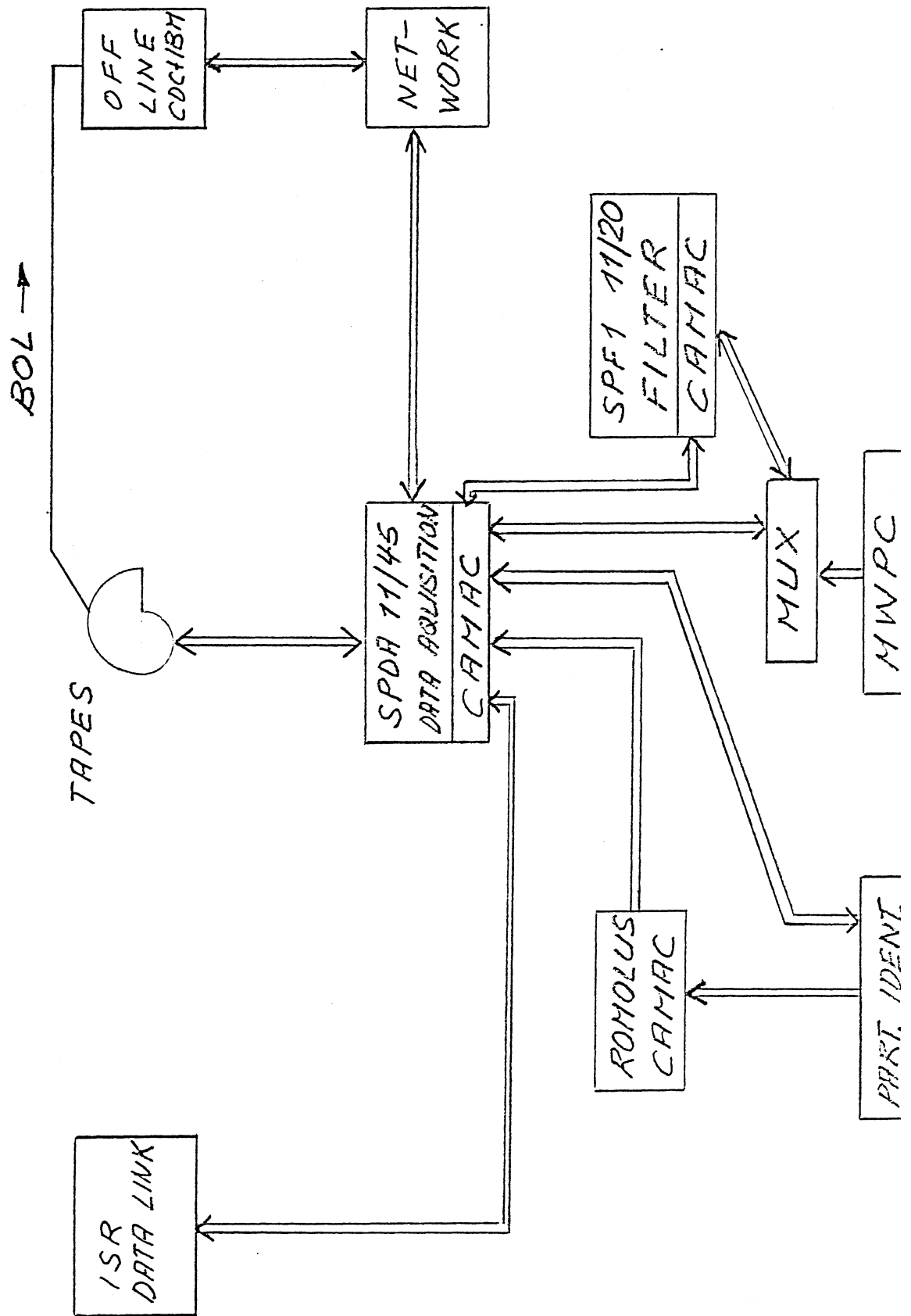
Fig. 8

II. REPORT FROM EXPERIMENT R 415
Study of Events with Large-Angle Electrons in the SFM

Bologna-CERN Collaboration

M. Basile, G. Cara Romeo, L. Cifarelli, A. Contin, G. D'Ali, R. Del Re, B. Esposito,
P. Giusti, T. Massam, F. Palmonari, G. Sartorelli, G. Valenti, G. Visco, A. Zichichi.

(Presented by T. Massam - CERN-EP)

Since this report is intended as a contribution to the discussions on the future use of the SFM it will emphasise our experience in carrying out an experiment at that facility rather than present a traditional sort of progress report.

Some of the points relevant to future experiments are :

a) the time scale involved in getting an experiment through the selection system, building installing and comissioning it;

b) the possible evolution of the experiment as it goes through this process

c) the cost,

d) how well can particle identification be made and over what solid angle.

e) The acceptance of the resultant system for physical processes (as opposed to single particle acceptance).

f) How do the various parts of the resultant apparatus perform.

Proposals to use the SFM for electron detection were made by us at the end of 1974 and the beginning of 1975. Another experiment, known as R416, with certain similar features was subsequently proposed and in early 1976 the ISR approved the part of the physics (and most of the apparatus) which was common to both experiments. In June 1978 the first serious quantity of data was taken but data with the system including the electromagnetic detector of the Argon calorimeter could be taken only in the last two periods of 1978 . So, there may be a three year time scale between proposing the experiment and being able to analyse data.

The Apparatus

Fig.1 shows the setup. Since there is one paper devoted to the SFM and its wire chamber system and there is report on R416 this description will mainly serve to point out differences between R415 and R416. The two main differences are 1) the arrays of lead-scintillator

sandwiches and 2) lead glass Čerenkov counters which are used to give an improved energy resolution near 90° and give an extra rejection against hadrons in the electron selection. These were components which R416 did not wish to use and after discussion the ISRC allowed us to include them. As well as these we also proposed to have a downstream time of flight counter and downstream gas Čerenkov counters for e and K detection. They are shaded in Fig.1. R416 did not want these because they considered that they would destroy the track finding ability of the detector system for too large a part of the single particle acceptance. These features were not accepted by the committee.

Aims and Triggers

The physics aims of R415 can be summarized as the investigation of a) The physics associated with electron production, that is principally charm production and e^+e^- pairs where possible.

b) The physics associated with neutral particles which carry a high transverse momentum, for example jets.

To collect data covering this physics, the following triggers have been set up :

T1. A single electron.

T2. An electron pair.

T3. A wide angle γ -pair (mainly for calibrations using π^o decay).

T4. A high electromagnetic energy release. (Effectively the total π^o energy flow into a detector array).

T5. Unbiassed events (for calibration of efficiencies).

T6. Penetrating charged particles. (Tagged particles which penetrate the electromagnetic shower detectors. Used for setting up and calibration).

Costs

Concerning cost, we believe that a detailed analysis of the costs of running an experiment at the SFM would be very interesting and useful, but this seems to have not been done. We give as an aperitive a few rough figures in the table below. Costs are expressed as FrSw/sec of data taking time. Thus though the analysis time will be spread over a much longer period than the data taking, it is at data taking time that

the analysis cost is committed.

Table I.   Some costs.

Electrical Power (of the SFM) _ _ _ _ _ _ 0.06 FrSw/sec

Physicist Power _ _ _ _ _ _ _ _ _ _ _ _ _ 0.14

Unfiltered electron event reconstruction 40.0

(at 10 triggers/sec)

Filtered electron event reconstruction 0.4

Magnetic tapes _ _ _ _ _ _ _ _ _ _ _ _ _ 0.01

An important point about analysis costs is that they should not in general be based on simulations made with 'unbiassed' or 'average' events. As an example of this we find that when we trigger on electrons, the multiplicity of the events which have to be reconstructed increases by a factor of 1.5 with a corresponding increase in analysis cost.

What does the physics signal look like?

A simulation of the electron spectrum to be expected near 90° can be conveniently made by taking the decay of a 2 Gev particle to the $Ke\nu$ state using a Bourquin-Gaillard type of production angular distribution. Fig.2 shows the results for electrons produced parallel and antiparallel to the ISR centre of mass motion. Because the spectrum, especially on the antiparallel side where the main electron detection is made, is at low energy, the trigger settings are a compromise. One would like to select as low an electron energy as possible but as the threshold is decreased the background trigger rate increases very rapidly. consequently a trigger threshold of 0.7 to 0.8 Gev has to be used.

Now, when the electron is detected, where does the K meson go? Fig.3 shows the population of a projection of the K phase space. It is a scatter diagram of the polar angle of the K relative to the leading beam direction against its momentum. The conclusions are that the K almost forgets the electrons direction and the K energy spectrum is mostly below 2 Gev.

If the K meson from the decay of an associated particle in the

same event is to be observed, there will be even less angular correlation.
Fig.4 shows the K spectra observed when there are no coincidence requirements
and it shows that it is sufficient to have particle identification up to
1.5 Gev momentum. As the mass of the decaying particle increases, these
spectra will scale so the best possible velocity and momentum resolutions
should be achieved to avoid lowering the efficiency for higher masses.

Examples of the acceptance.

 In the plan view of Fig.1, the acceptance with particle identifica
tion looks large but detailed calculations give a less optimistic picture
as the numbers tabulated below will show.

Table II.   Some acceptances.

 . Single electron detected in $\overset{\vee}{C}$ counters,
   wire chambers and shower detectors. _ _ _ _ 4.0%
   e^+e^- pairs.   Mass = 3 Gev _ _ _ _ _ _ _ _ _ 0.15%
                         Mass = 5 Gev _ _ _ _ _ _ _ _ _ 0.4%
   Ke pairs from X—>Ke .   Mass = 2 Gev _ _ _ _ 0.17%
                         Mass = 5 Gev _ _ _ _ 0.4%

How does the apparatus behave?

 To avoid duplication we will discuss just the parts of the
apparatus which are particular to R415 or about which we may have a dif-
ferent approach. About the SFM detector system itself it suffices to say
that the chambers, gas system and electronics are kept in good working
order by the SFMD team and the detector works well so that one can con-
centrate on commissioning new equipment and taking data without having to
worry about chasing detector faults.

 Firstly we will consider the time of flight system because this
illustrates some of the difficulties at the SFM. Difficulties arise
because the interaction diamond is extended and there is no unique flight
path over which one can define a base-line with 'start' and 'stop' counters
to measure the time interval. All the counters are 4 to 5 metres from the
intersection point. In each event several particles, of unknown velocities,
cross the counters. Some coincidence condition determines the start of

the time encoder circuits and all the time information available is the relative delays of the particles arriving at the counters.

Before any time analysis can be made, many events have to be reconstructed so as to determine the relative intrinsic delays of the photomultipliers and the effective velocity of light in the sintillators. When these calibrations are available, then the particle identification techniques can be tried and tested. To make the particle identification, each event has to be reconstructed so as to give the momentum of each particle and its trajectory length from the vertex to the counter. Then, in general, all possible mass values have to be assigned to all possible tracks so as to obtain estimates of the times of the tracks at the vertex. The solution with the lowest X^2 for the spread of these vertex times is taken as the best solution. In some cases the sandwich detectors can be used to verify the time of flight system. In particular for events where an electron has been positively identified, the sandwich time information provides an independent interaction time determination.

Since the sandwich counters are close to and directly behind some of the time of flight counters, distributions of the time difference between corresponding counters can be made as shown in Fig.5. The resolution in time difference is seen to be 0.44 nsec which verifies that in the ISR environment the TOF counters have a resolution $\sigma = 0.3$ nsec.

Fig.6 shows some of the hundred determinations of the effective velocity of light in the TOF counters. Track reconstruction gives the position relative to the counter centre and this together with the time information from the photomultipliers gives the light propagation velocity inside the counter on an event to event basis. Once the velocity has been determined, the resultant resolution can be checked by histogramming the difference between the position determined from reconstruction and that determined from time differences. See Fig.7. A cut on this distribution helps to clean events by rejecting badly reconstructed tracks, ghost tracks and randoms of various kinds.

As mentioned above the most direct way to determine the
interaction time is to use a relativistic $(\beta = 1)$ particle, i.e. the
identified electron.

Fig.8 shows the first results which we have obtained displayed on a momentum
velocity diagram, and Fig.9 shows the mass distribution obtained with the
same data. These results indicate that the average background of pions
in the K sample up to 1.5 Gev/c is about 50%. No selection in timing ac-
curacy, path length accuracy and momentum reconstruction accuracy (it can
be as low as 30%) has been made in this analysis. A more precise determina-
tion of the interaction time is obtained when considering the time information
from all particles which hit the TOF counters.

Measurement quality is taken into account by a likelihood
method which will not be described in detail here. Suffice to say that
the best X^2 value of the vertex times is used to give a time determination
and then a normalized probability W is defined so that for each track in
the event W_{π} , W_K , W_p give the probabilities that the particle is a
π , K or proton respectively. To understand the results, shown in Fig.10,
11 and 12, consider W_K in Fig.11. When W_K is near to 1 the track is identified
as a K. Tracks which fall in the peak at $W_K = 0$ have been identified as
a good π or p in the W_{π} or W_p distributions. When all the tracks are
relativistic, the solution is indeterminate and $W_{\pi} \approx W_K \approx W_D = 0.33$.
The actual value of W at which one should cut to accept a track as
identified will be determined by simulation studies. For the present we
accept events with $W > 0.95$. Table III below shows the uncorrected fractions
of identified tracks in various momentum groups.

Table III. Track identification.

P GeV/c	Fraction Identified			
	π	K	P	All.
< 0.5	0.74	0.035	0.017	0.79
0.5 - 1.0	0.46	0.083	0.022	0.56
1.0 - 1.5	0.14	0.059	0.100	0.30
1.5 - 2.0	0.011	0.001	0.070	0.082
> 2.0	0	0	0.026	0.026

Performance of the Electromagnetic Detector.

Fig.13 shows the $\gamma \gamma$ invariant mass spectrum in the π^o region. This serves as an energy calibration check and shows the background level in the π^o identification. The η region has a lot less statistics and we are still working on it. Fig.14 shows the present situation.

Performance of the Reconstruction.

Even though the SFM detector and software are now available almost as a "package deal", the user needs to test it. One way is to generate events with pairs of tracks of known momenta, to simulate the resultant chamber read-out and then put them through the reconstruction program. The first track finding program was called SINFIT and more recently a more accurate and faster SPLINE program has become available. Fig.15 shows the SINFIT results with a small systematic bias which shows up more clearly at higher momenta. Fig.16 shows the improvement of the spline parametrization. Notice that in both cases there are long tails of incorrectly reconstructed tracks and account must be taken of these as a source of background.

Performance of the Cerenkov counters.

It is difficult to check the Čerenkov counters in real time because the electron signal is only 10^{-3} of the flux of particles which are potential background sources. However when the electrons are recognized in the shower detectors and the tracks are reconstructed then the pulse height spectrum of the Cerenkov cell which the particle enters can be measured without background and compared with the shape expected from calibrations made in tagged particle beams. See Fig.17.

Some Electron Data.

Fig.18 shows the electron momentum spectrum observed near 90°. It is not yet corrected for resolution, but shows that the single electron to background ratio is not worse than 1/3. In some of our calculations for the proposal for this experiment we showed that with a rejection of 10^{-4} against pion pairs it should be possible to see the $J \rightarrow e^+e^-$ signal.

Now this should be true also if all the rejection is made on one of the particles and none on the second particle. This is an important point to demonstrate because such a technique can lead to a substantial gain in acceptance — a factor of ten in our case. Fig.19 shows the present state of this type of analysis.

The Argon Calorimeter.

The electromagnetic shower detecting part of the Argon Calorimeter has been made operational for the runs which we took just before Christmas, and work is just starting on the off-line auto calibration. Sets of four aligned dE/dx-measuring cells are chosen and then the spectrum in one of these cells is plotted for various pulse height cuts on the remaining three cells. The peak which emerges from the noise spectrum is the peak of non-interacting pions crossing the cells. See Fig.20.

To conclude I will summarize in Table IV below the numbers of events and the integrated luminosity collected with the various triggers.

Table IV. Data taken.

Trigger	Integrated Luminosity $x(10^{36} cm^{-2})$	Number of Events $x(10^6)$
Single Electron	17	14
Electron Pairs	12	1.1
Wide angle γ pairs	1.6	1.2
High energy neutral	5.6	0.5
Penetrating pions		1.0

FIGURE CAPTIONS

Fig.1 The layout of the experiment.

Notation. LG3, LG4 : Lead glass Čerenkov counter arrays.

SW2 to SW4 : Lead/scintillator sandwiches.

700 to 841 : Time of flight counter arrays.

C0 to C5 : Gas Čerenkov counters.

209 : Wire proportional chamber for dE/dx measurements.

LAC : Argon Calorimeter.

T, CF : Time of flight counters and forward Cerenkov

counters excluded from the experiment.

Others numbers : Multi-wire chambers of the SFM.

Fig.2 Electron spectra from the decay of a particle (mass = 2 Gev) to

$Ke\nu$. β^+ is in the direction of the centre of mass motion, β^-

is opposed to it. Global acceptance would be the spectrum if the

particle identification were extended to forward angles.

Fig.3 Direction/momentum correlation for K mesons in $D \rightarrow Ke\nu$ decay

when the electron is accepted near 90°. Angles are relative to

the leading beam direction.

Fig.4 K spectra in various angular regions without electron coincidences.

Top and bottom refer to the regions above and below the intersection

region where identification cannot at present be made. The

remaining notation is as in Fig.2.

Fig.5 Time of flight spectra between a Time of Flight counter and the

nearest sandwich counter. Spectra from two different counter

pairs are shown.

Fig.6 Examples of determinations of the velocity of light in the
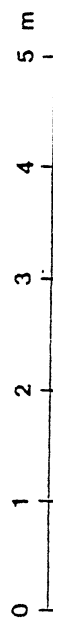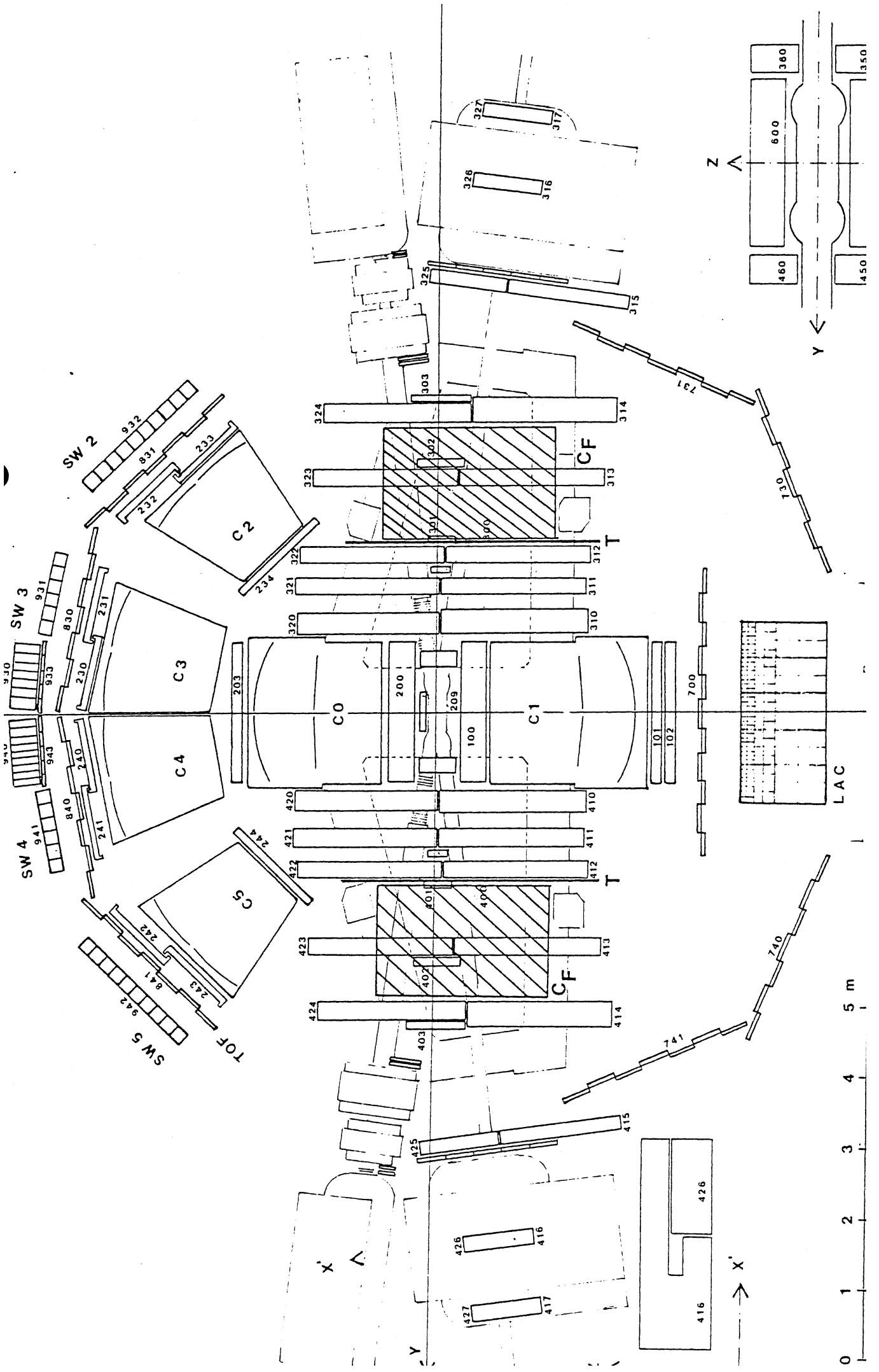
scintillators.

Fig.7   Comparisons of the two methods of position determination. Z_t is the position along the counter determined using the time difference method. Z_G is that obtained by extrapolating the particle trajectory found in the event reconstruction.

Fig.8   Showing the π, K and p bands in the velocity/momentum scatter diagram. All events with momentum uncertainty less than ± 30% are included.

Fig.9   The mass spectrum derived from Fig.8 using events with momentum less than 1.5 Gev/c.

Fig.10   Showing for various momentum ranges the distributions of W_π , the probability that a given track is a π.

Fig.11   Showing, for various momentum ranges, the distribution of W_K, the probability that a given track is a K.

Fig.12   Showing, for various momentum ranges, the distributions of W_p, the probability that a given track is a p.

Fig.13   Showing the $\gamma\gamma$ invariant mass spectrum and background in the region of the π^0.

Fig.14   The $\gamma\gamma$ invariant mass spectrum in the region of the η.

Fig.15   Showing the reconstruction accuracy of the SFM detector and the SINFIT reconstruction program. Tracks of known momentum are generated by Monte-Carlo.

Fig.16   Showing the reconstruction accuracy of the SFM detector and the SPLINE reconstruction program. Tracks of known momentum are generated by Monte-Carlo.

Fig.17   Showing the pulse height distribution from electrons in a $\check{\text{C}}$erenkov counter.

Fig.18   The single-electron spectrum near 90° and a comparison with pion spectra.

Fig.19   The invariant mass spectrum between an $e^{\pm}$ and any other charged track of the opposite sign.

Fig.20   Showing the pulse height spectra in a single cell of the Argon calorimeter.   The cuts refer to pulse height selection in three other cells which are aligned with the cell being calibrated.

$\frac{dN}{dPe}$

e Spectra without K coincidence

e spectrum in β^+

e spectrum
in β^- telescope

A.

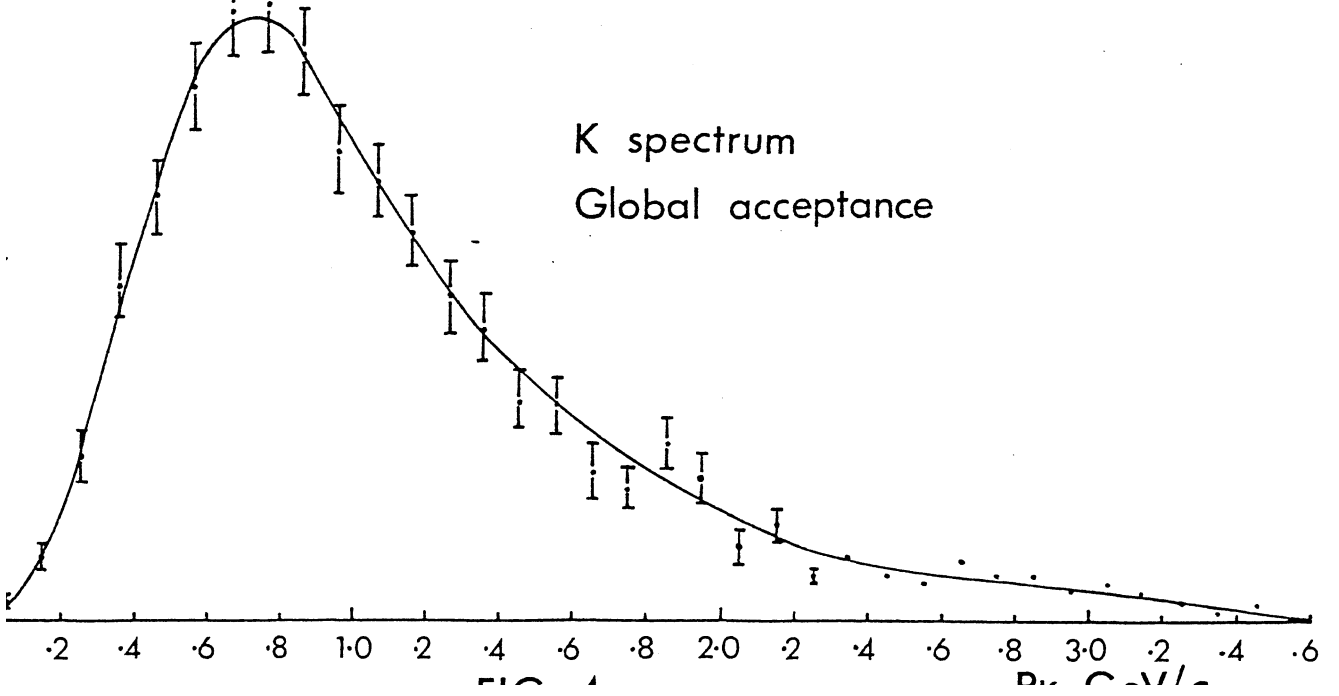Electron spectrum
Global acceptance
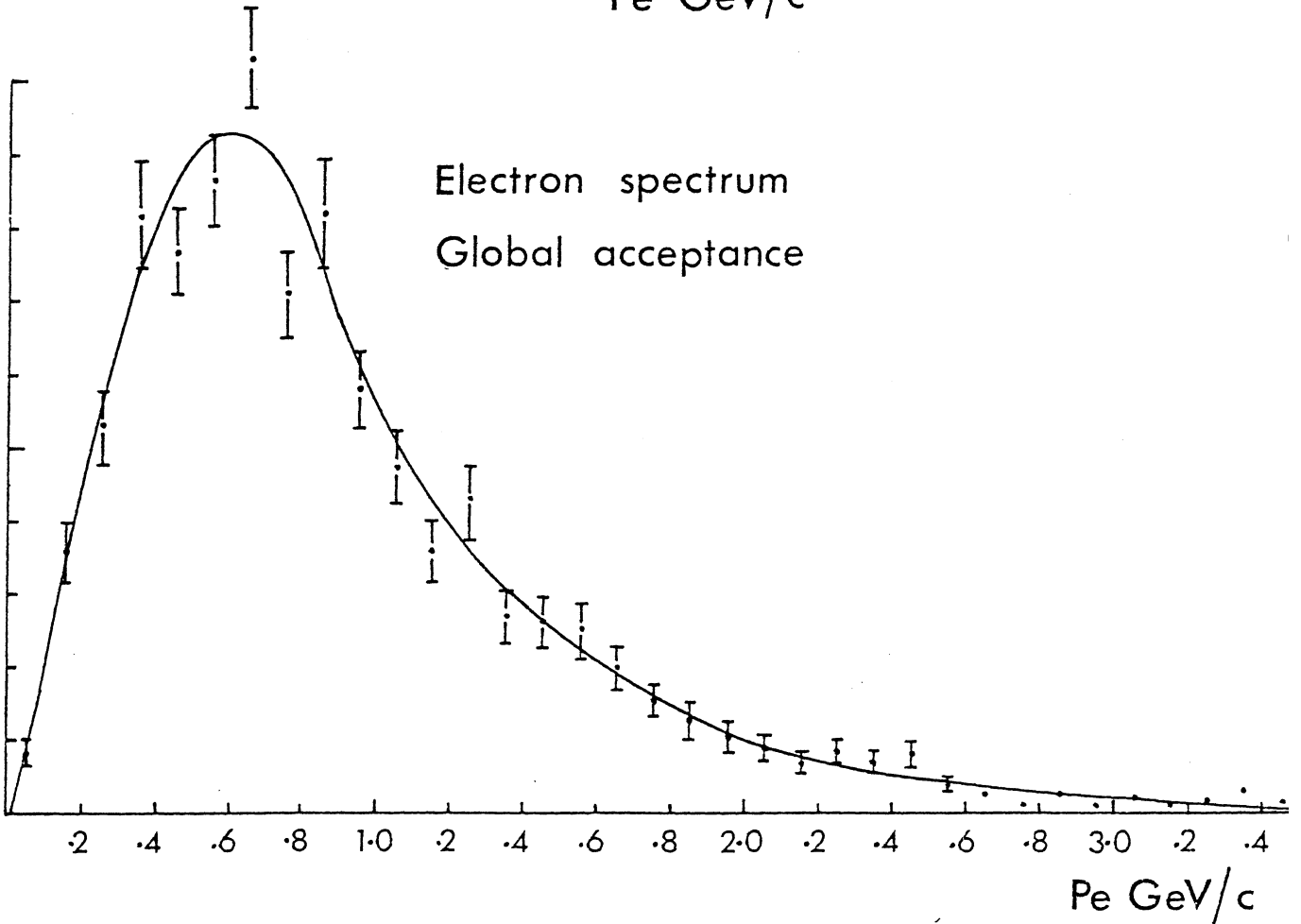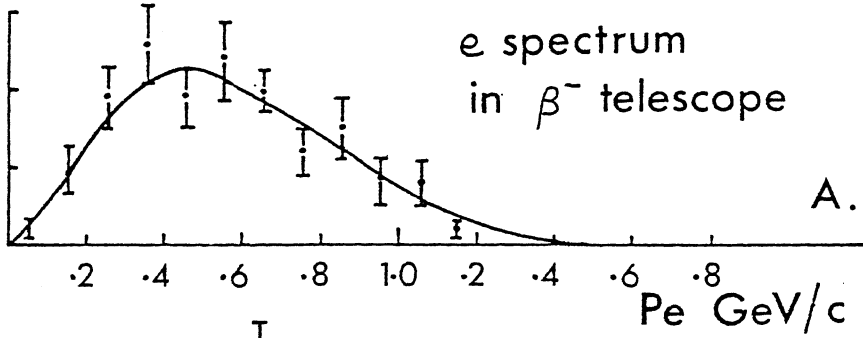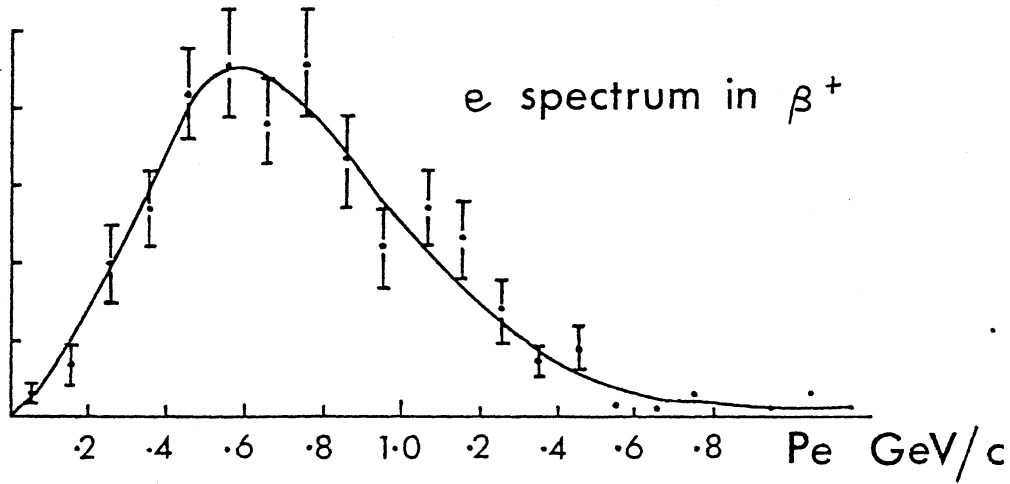
FIG. 2

e in β^-. Where does K go ?
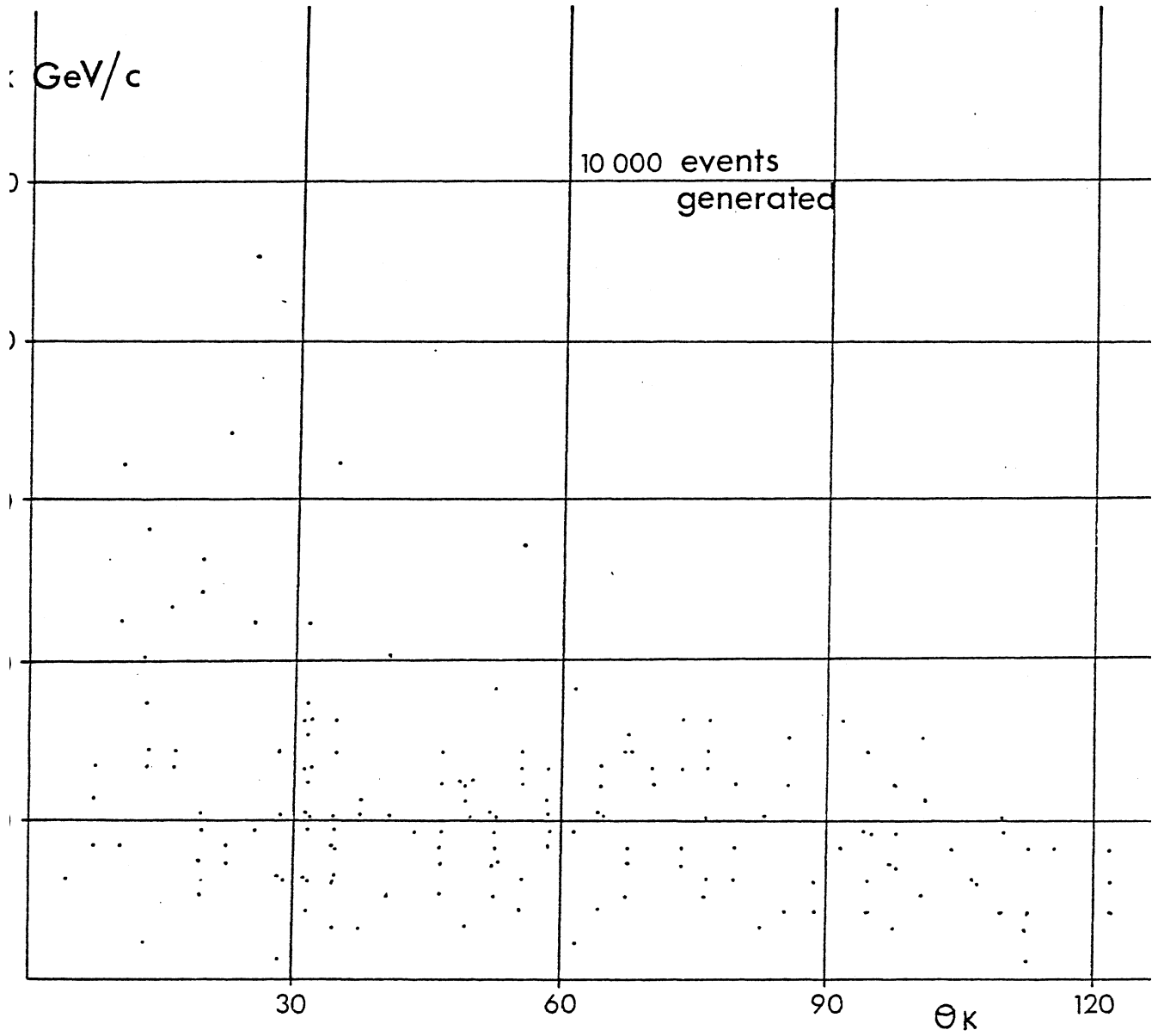
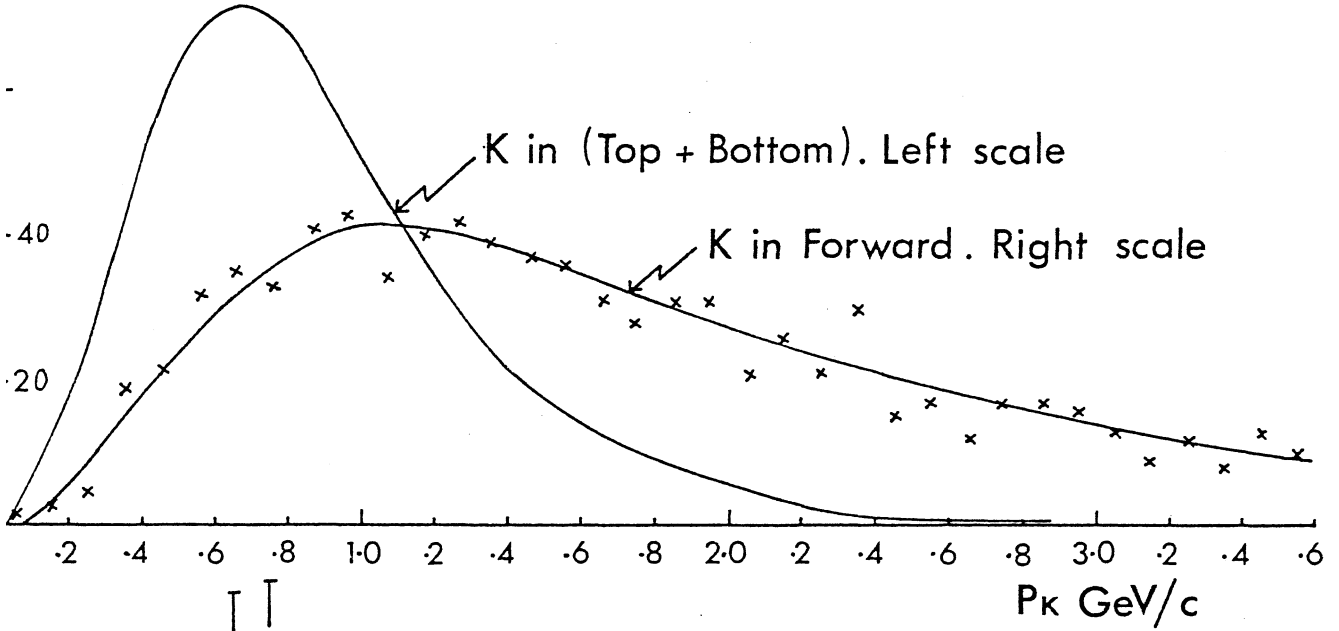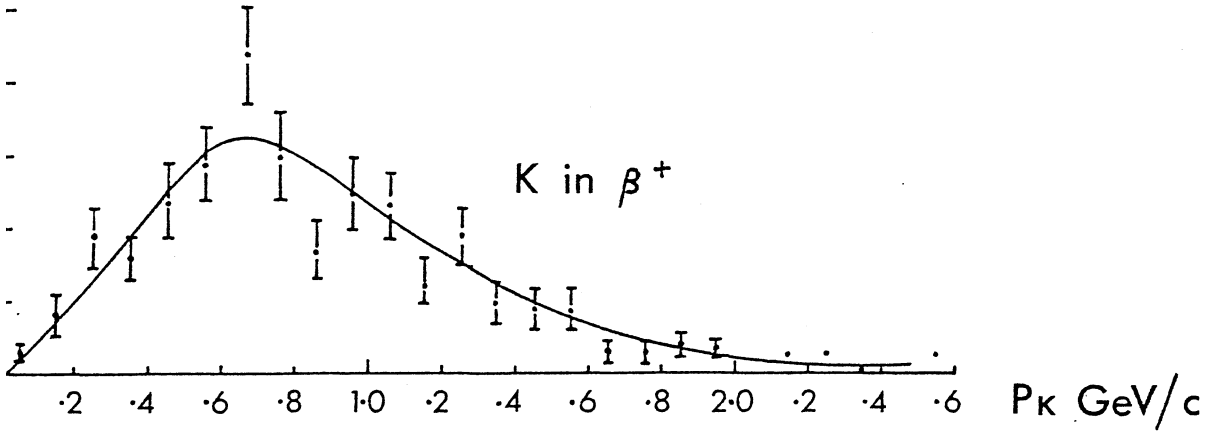FIG. 3

K Spectra without e coincidence

K in β^-

P_K GeV/c

K in β^+

P_K GeV/c

K in (Top + Bottom). Left scale

K in Forward. Right scale

P_K GeV/c

K spectrum

Global acceptance

P_K GeV/c

FIG. 5

FIG. 6

FWHM = 9 cm

(GE on)
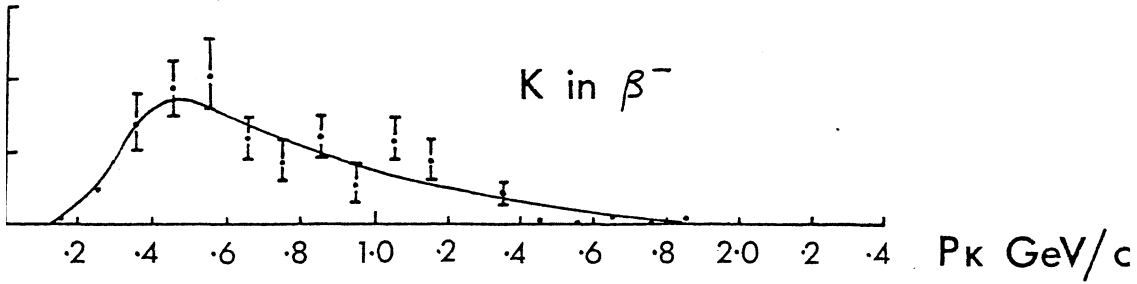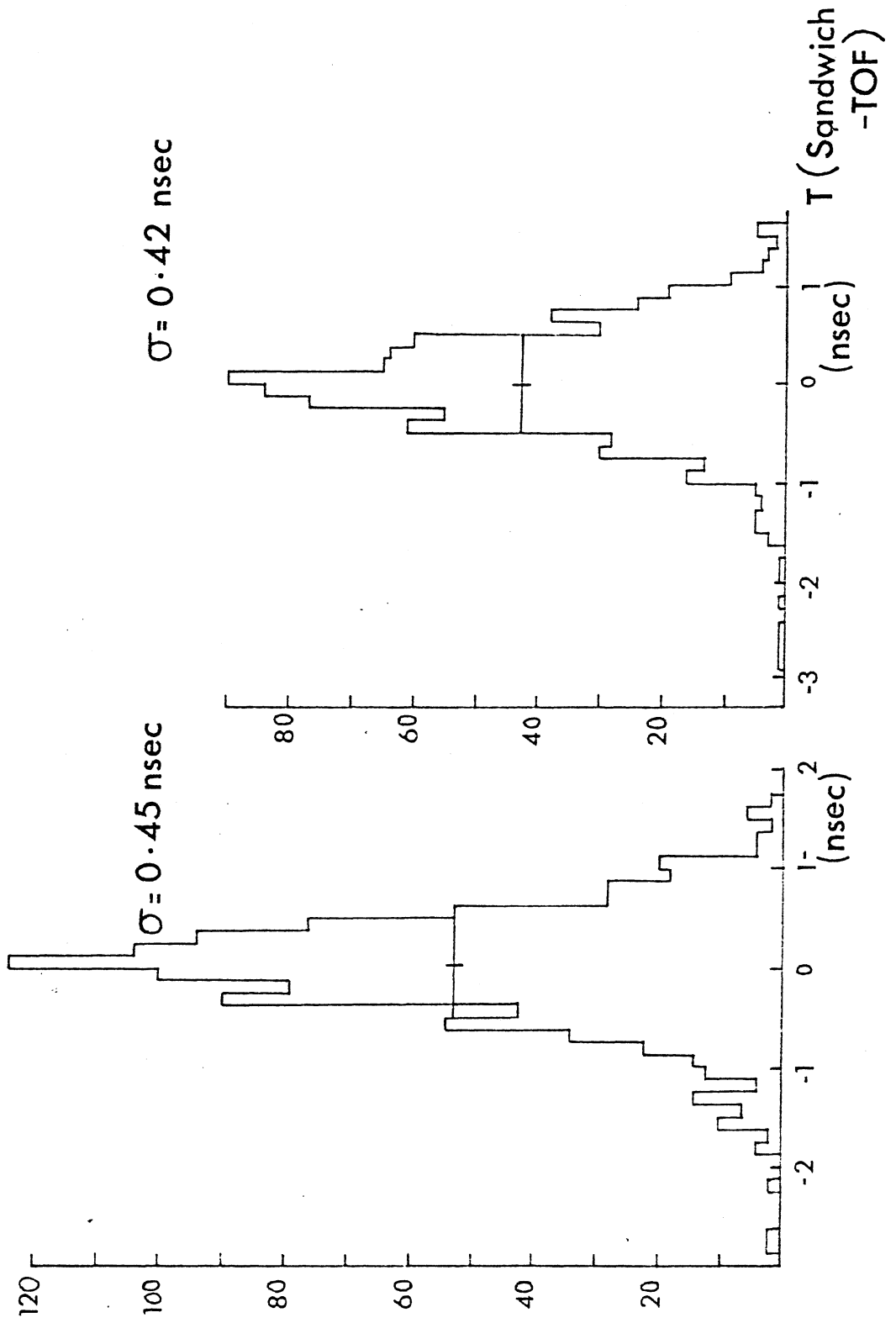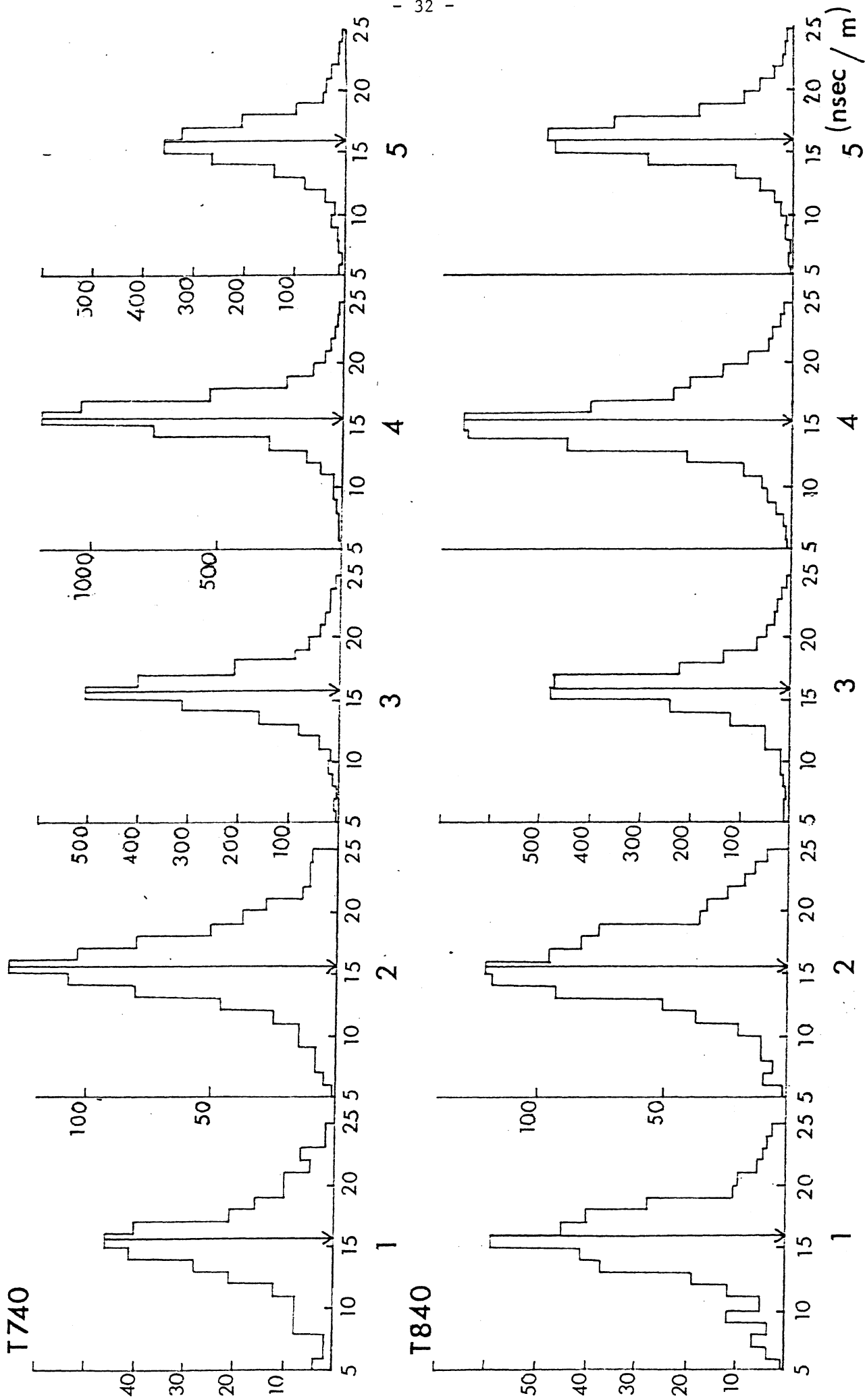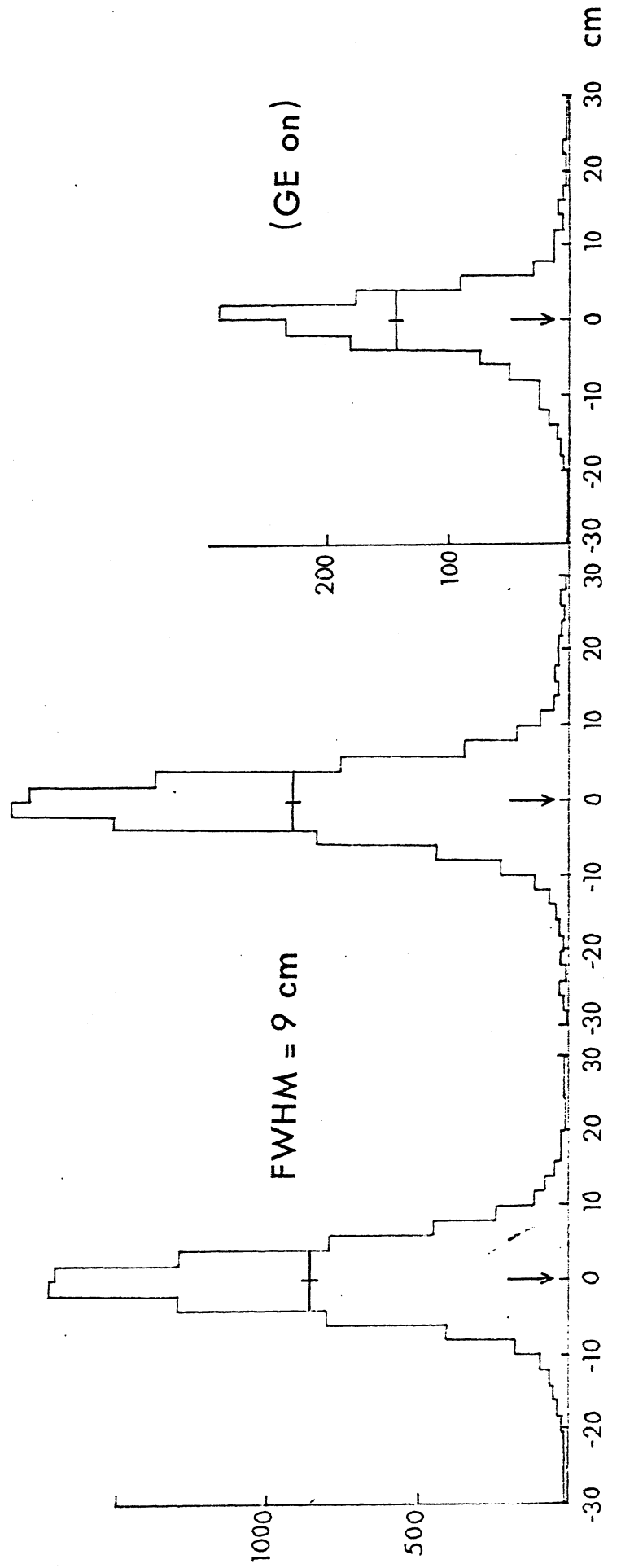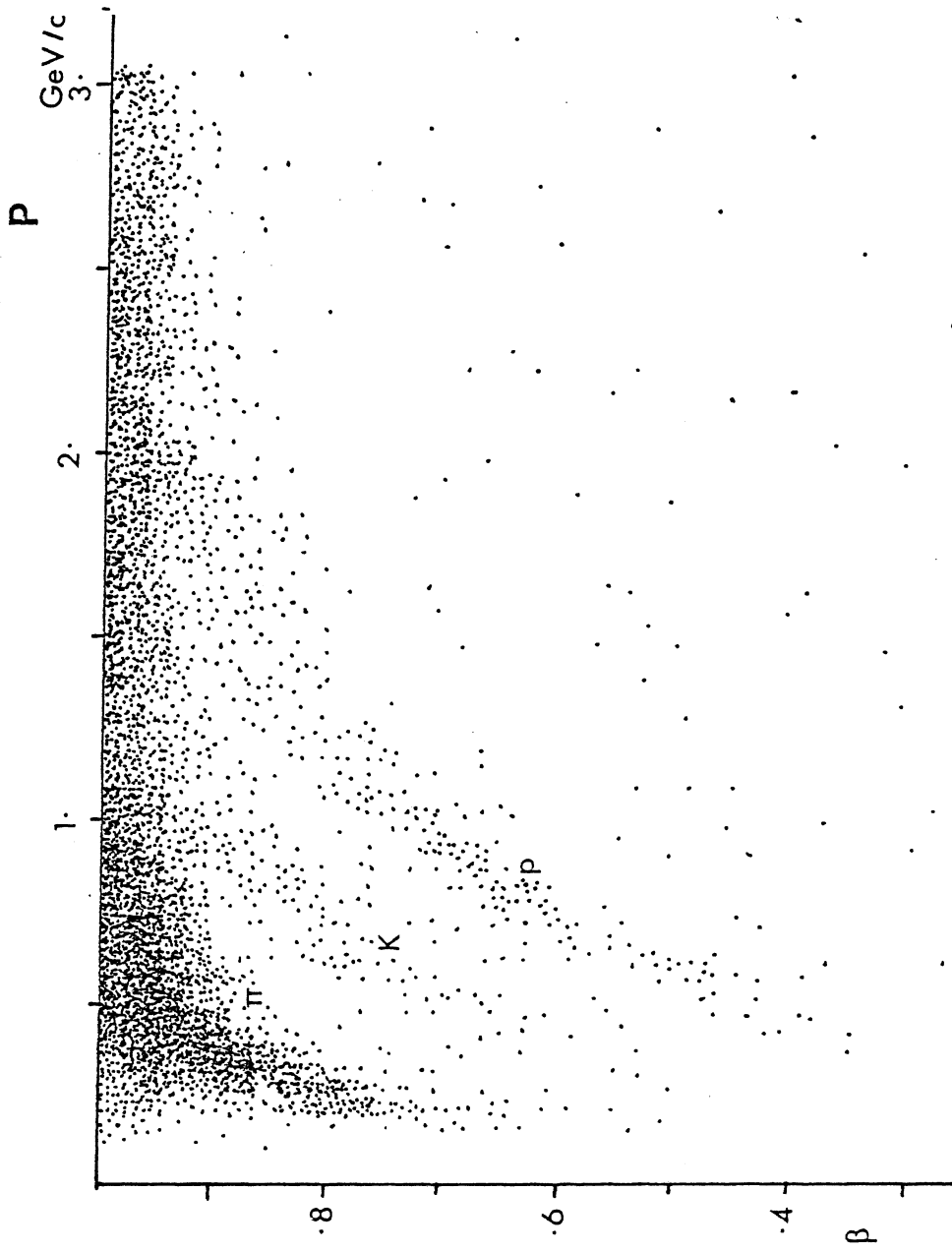
FIG. 8

Start given by the identified
eletron ($\beta = 1$) 3796 events

P < 1·5 GeV/C   2990 particles

FIG. 8

Particle probability for pions

Events

125

1140
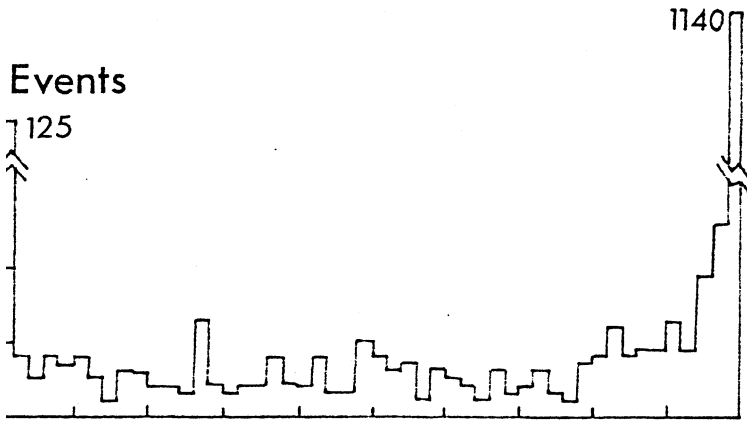
P < 0·5 GeV/C
1583 tracks

544

1241

0·5 ⩽ P < 1 GeV/C
2886 tracks

355

185
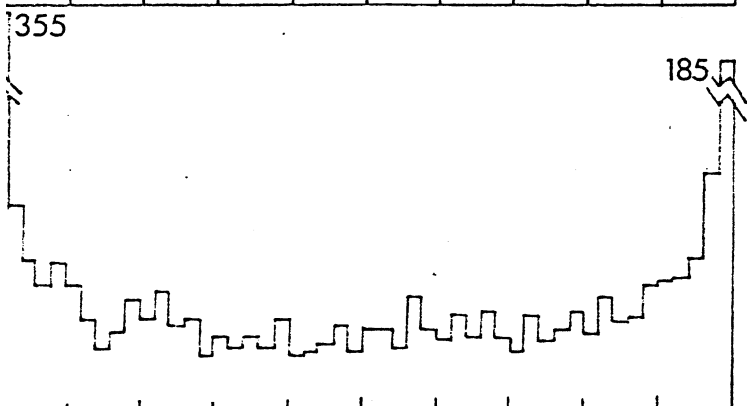
1 ⩽ P < 1·5 GeV/C
1743 tracks

207
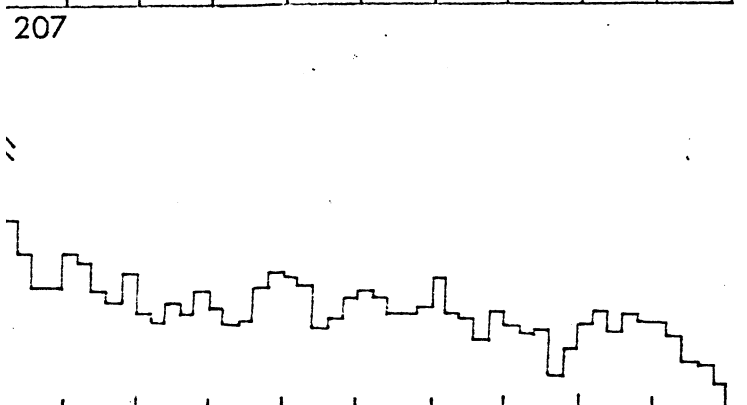
1·5 ⩽ P < 2 GeV/C
1490 tracks

P ⩾ 2 GeV/C
3085 tracks

0.1   0.2   0.3   0.4   0.5   0.6   0.7   0.8   0.9   1 W_π
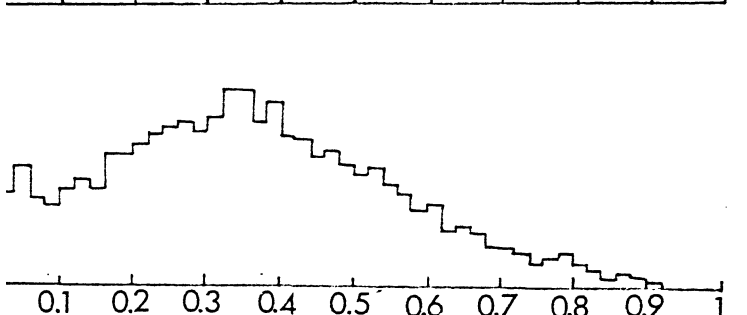
FIG. 10

Particle probability for kaons

P < 0·5 GeV / C
1583 particles

0·5 ≤ P < 1 GeV/
2886 particles

1 ≤ P < 1·5 GeV/
1743 particles

1·5 ≤ P < 2 GeV/
1490 particles
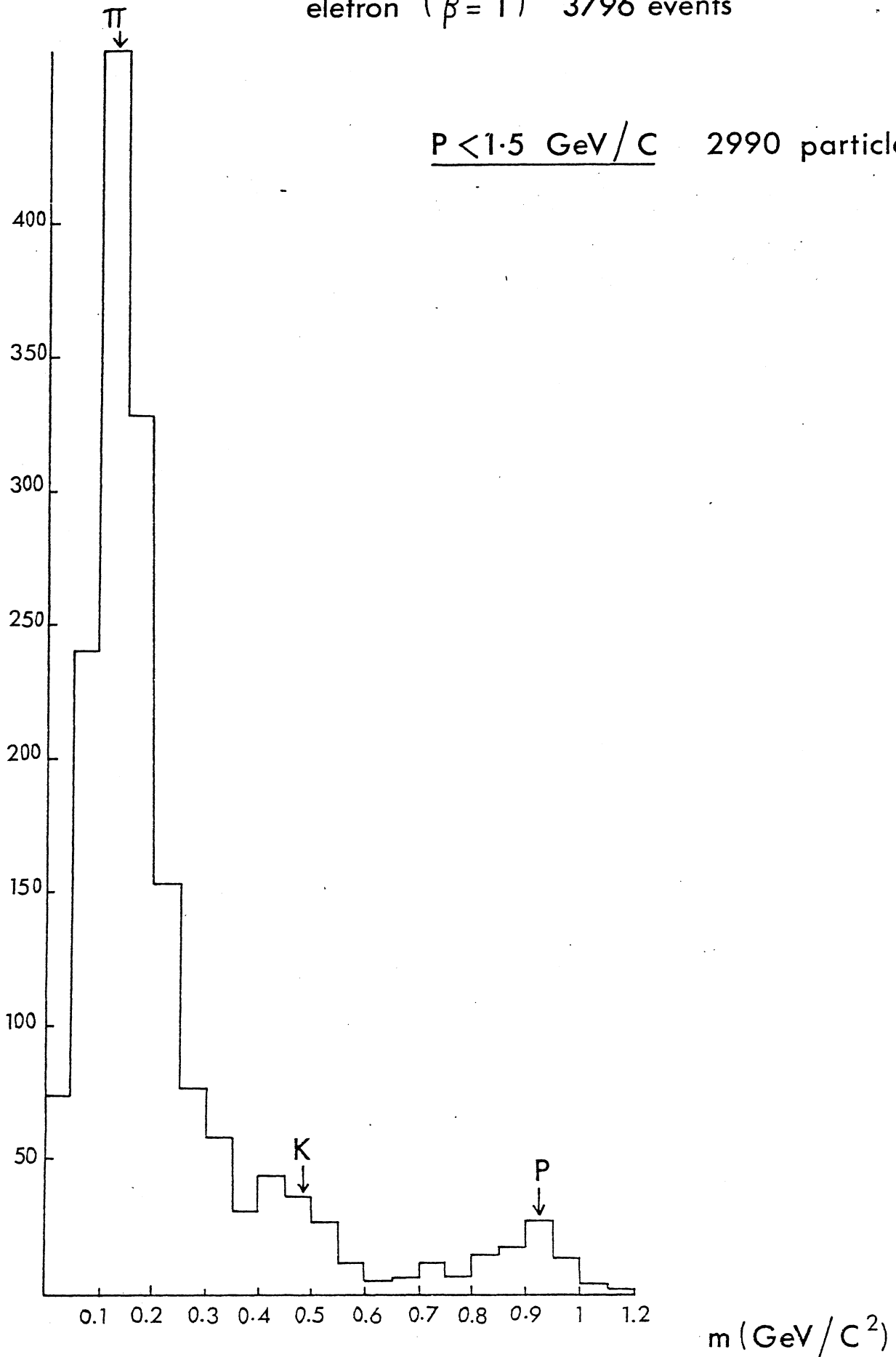
W_K

P ≥ 2 GeV / C
3085 particles
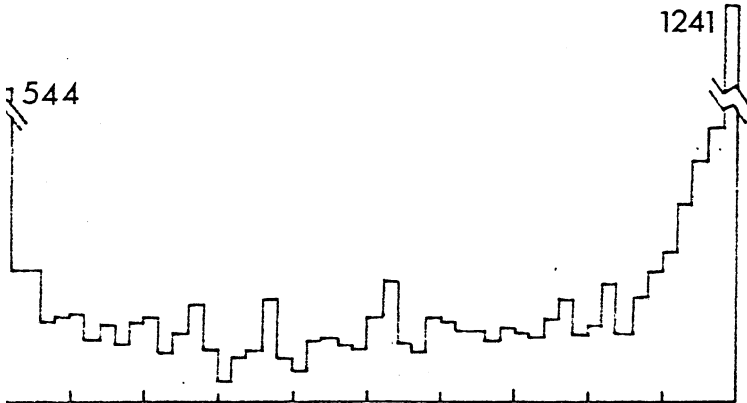4327 events
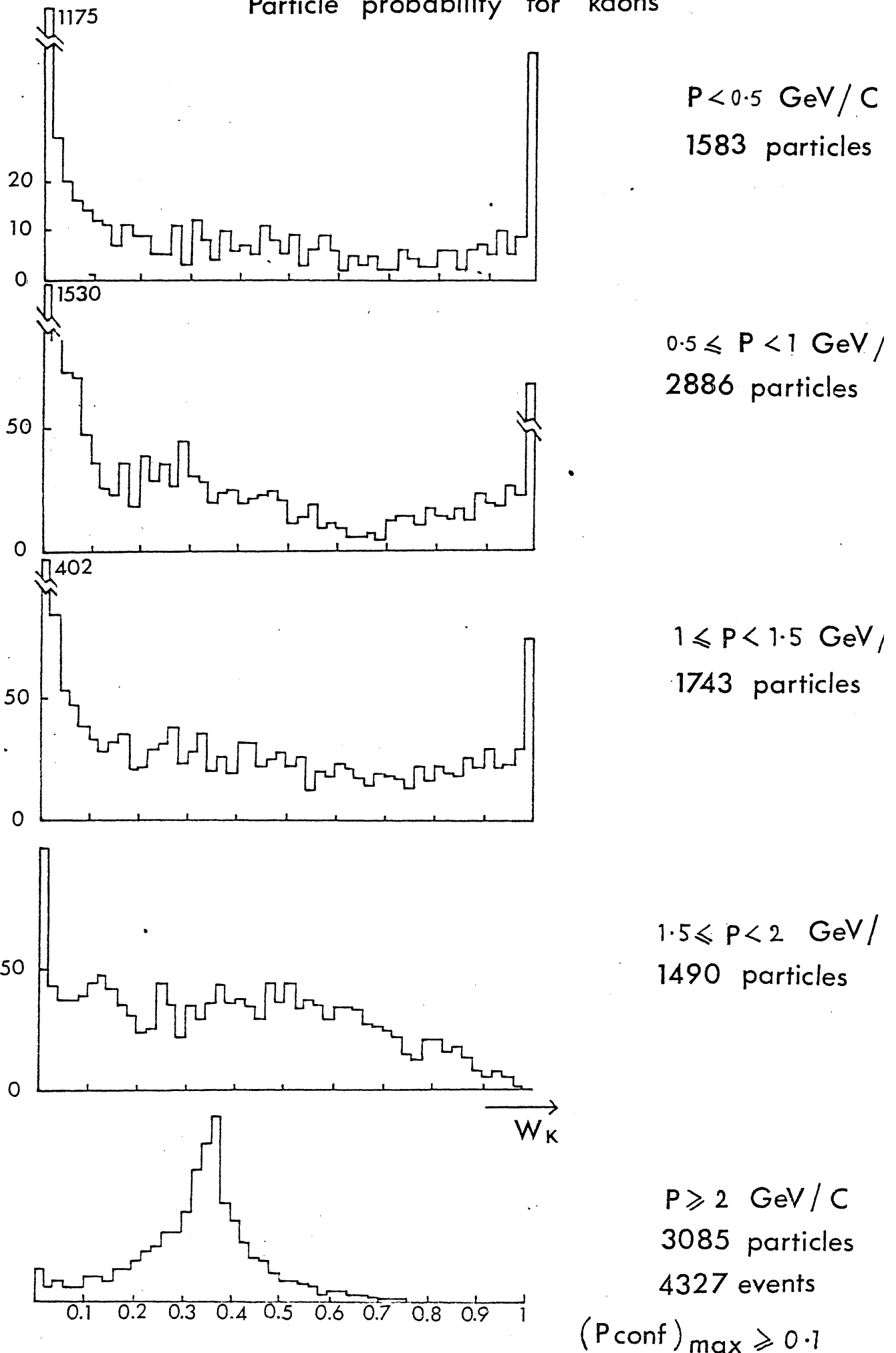
$(P conf)_{max} \geqslant 0·1$

FIG . 11

Particle probability for protons
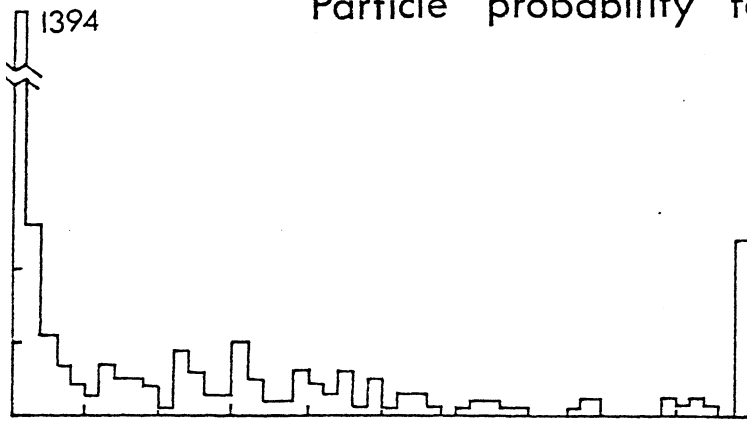
P < 0·5 GeV/C
1583 particles
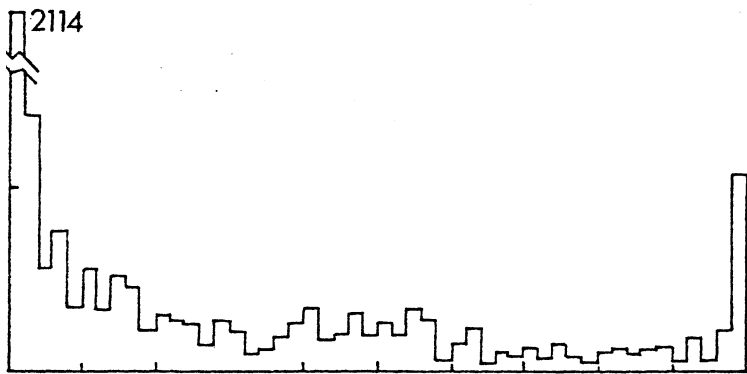
0·5 ≤ P < 1 GeV/C
2886 particles
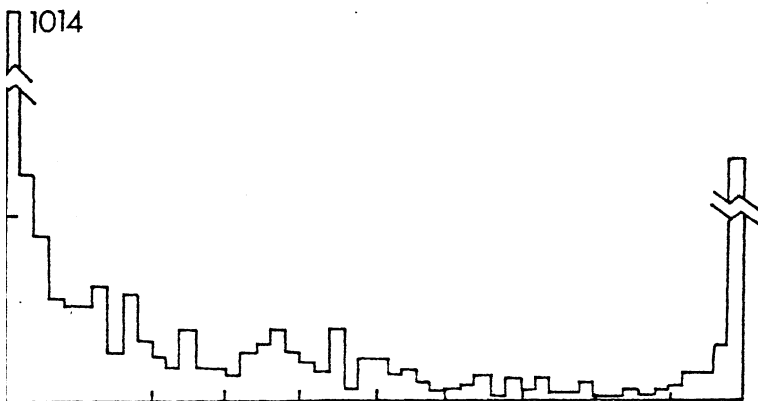
1 ≤ P < 1·5 GeV/C
1743 particles
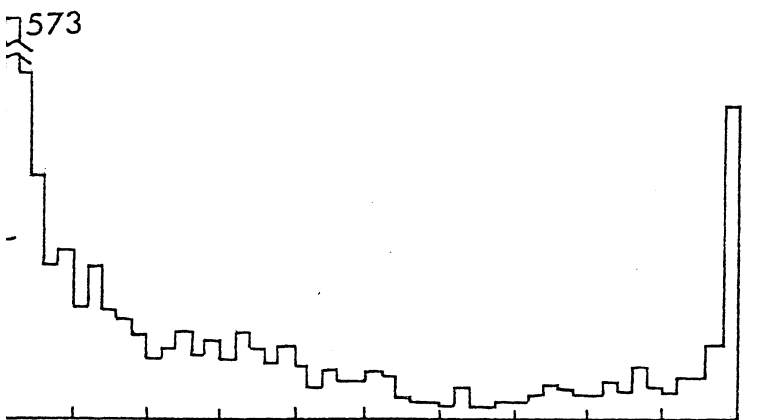
1·5 ≤ P < 2 GeV/C
1490 particles

W_P

P ≥ 2 GeV/C

3085 particles

4327 events

$(P_{conf})_{max} ≥ 0·1$

FIG. 12
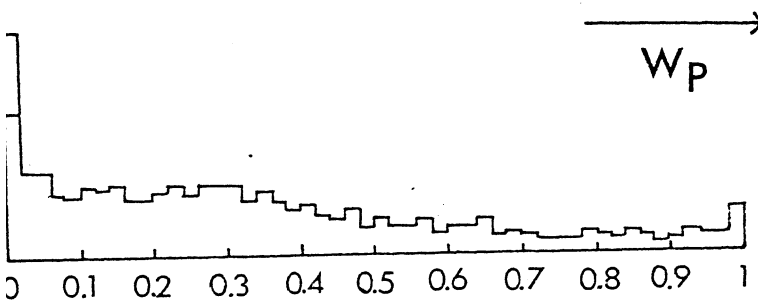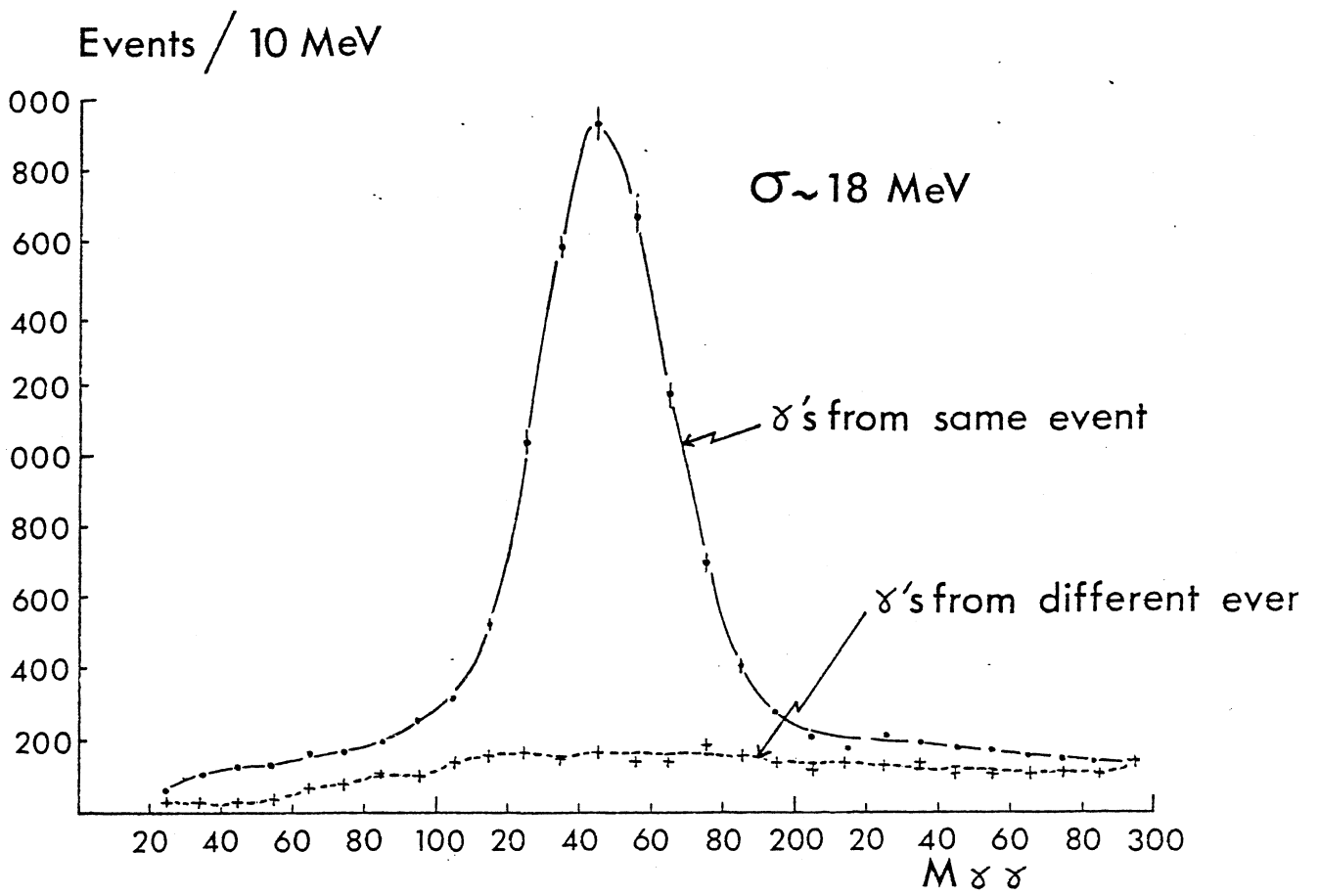
FIG . 13
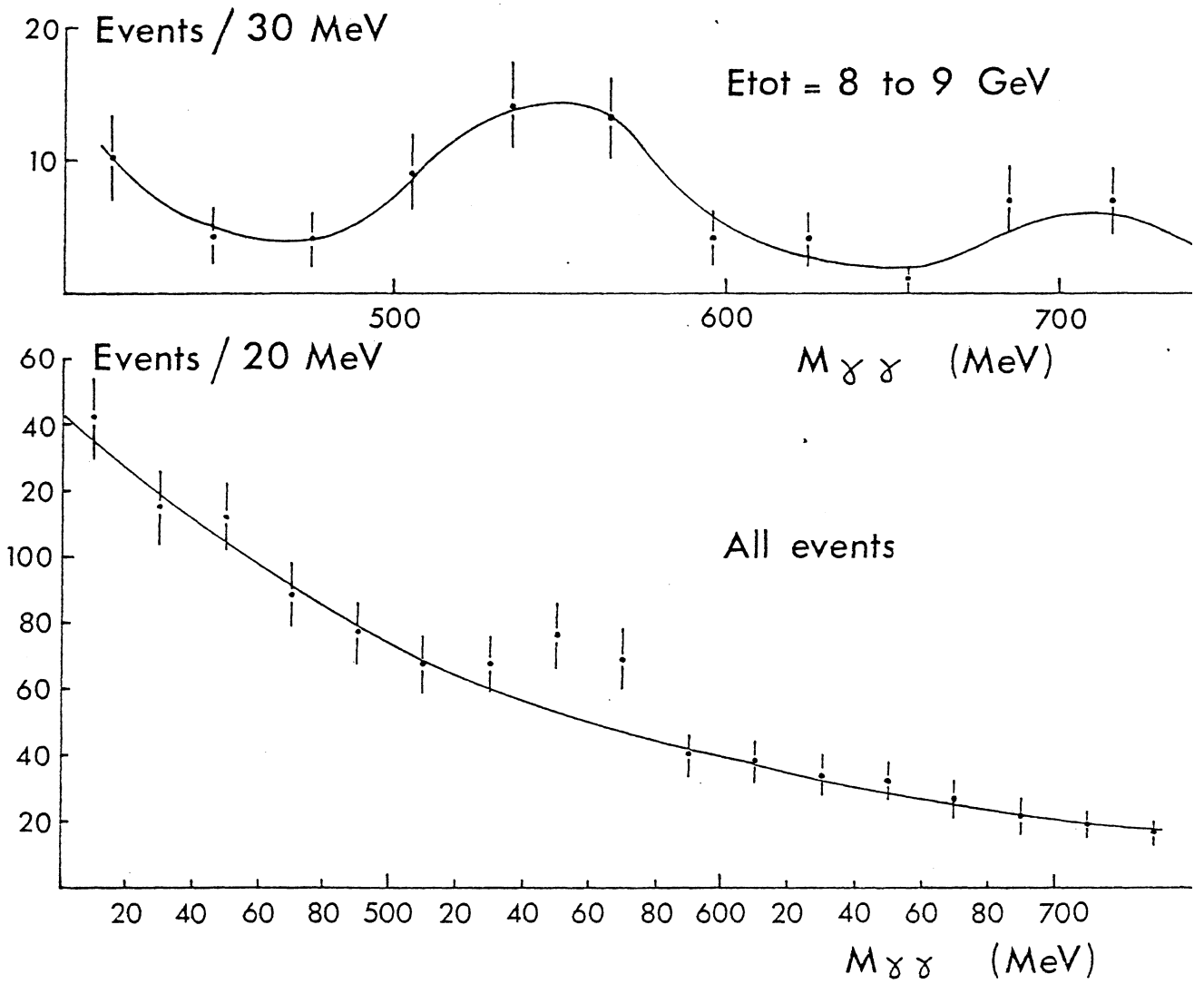
FIG.14
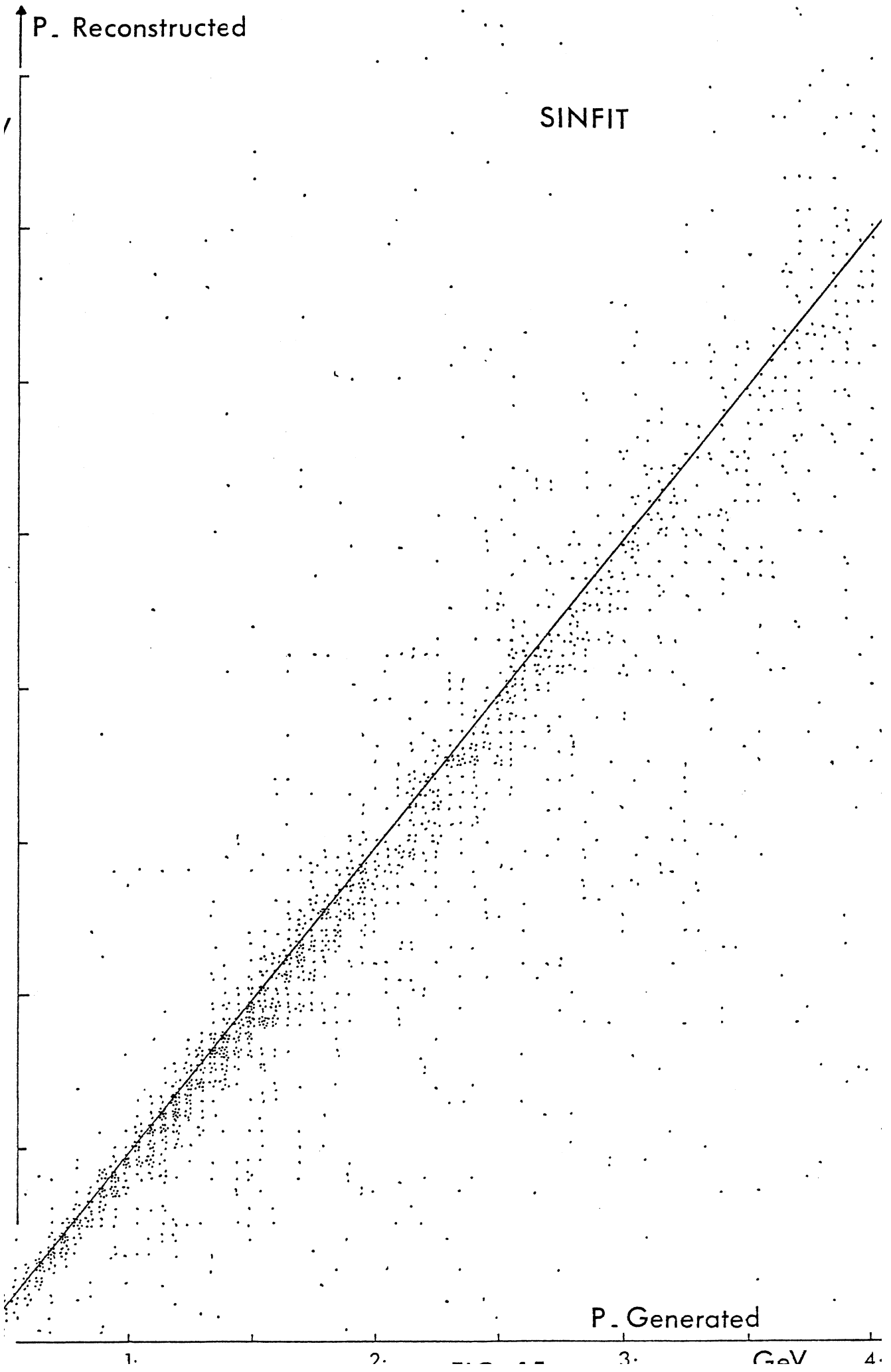
Reconstructed

SPLINE

P. Generated

GeV

- 43 -
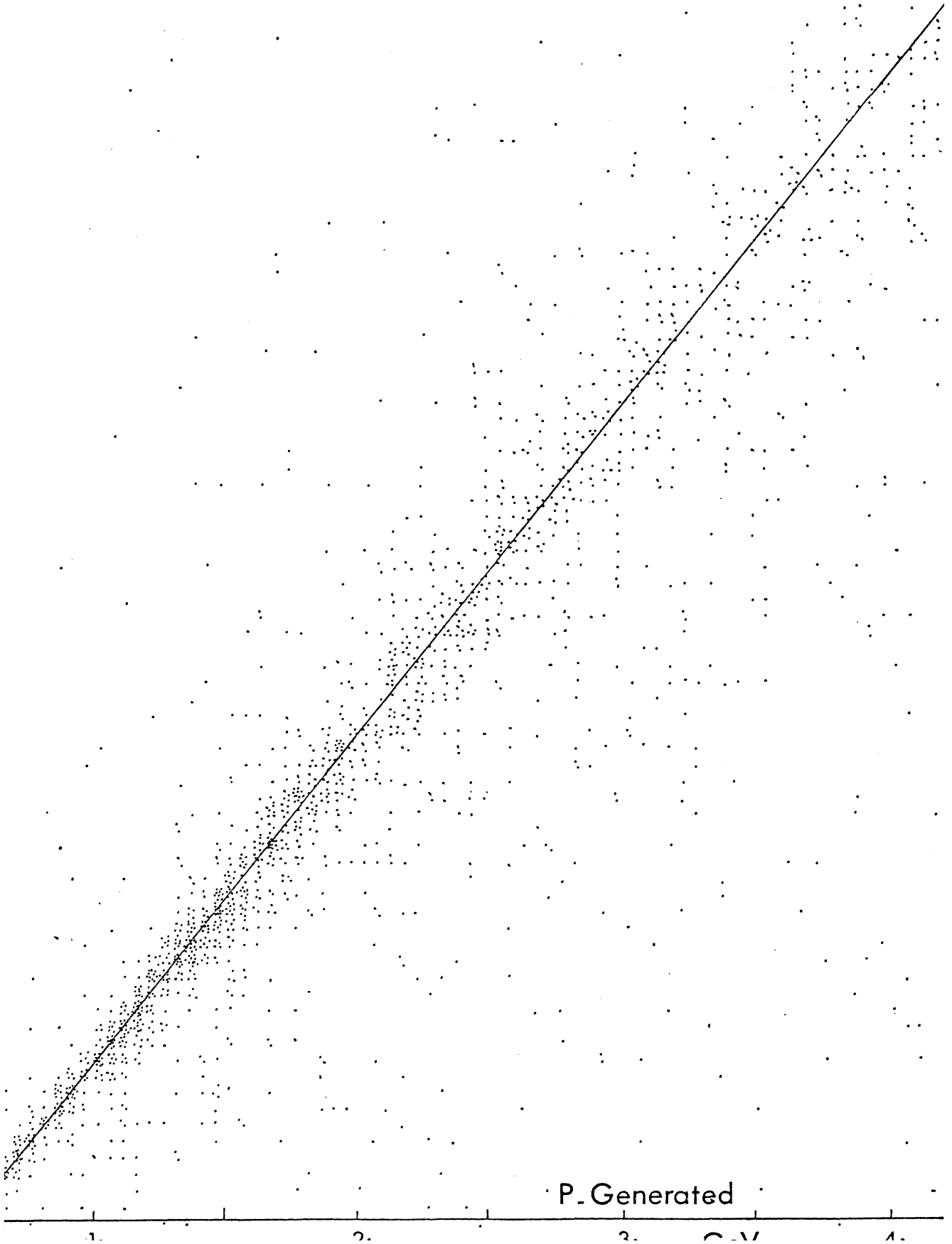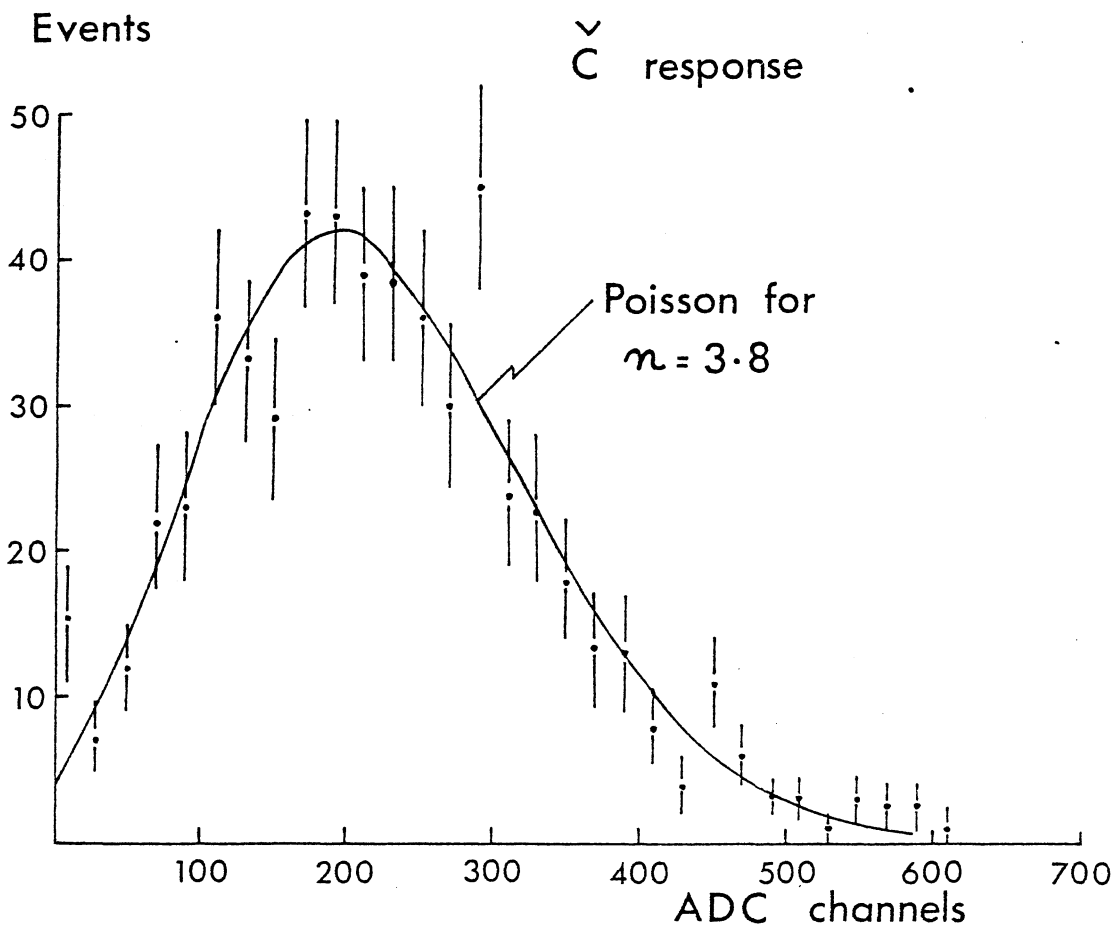
FIG.17
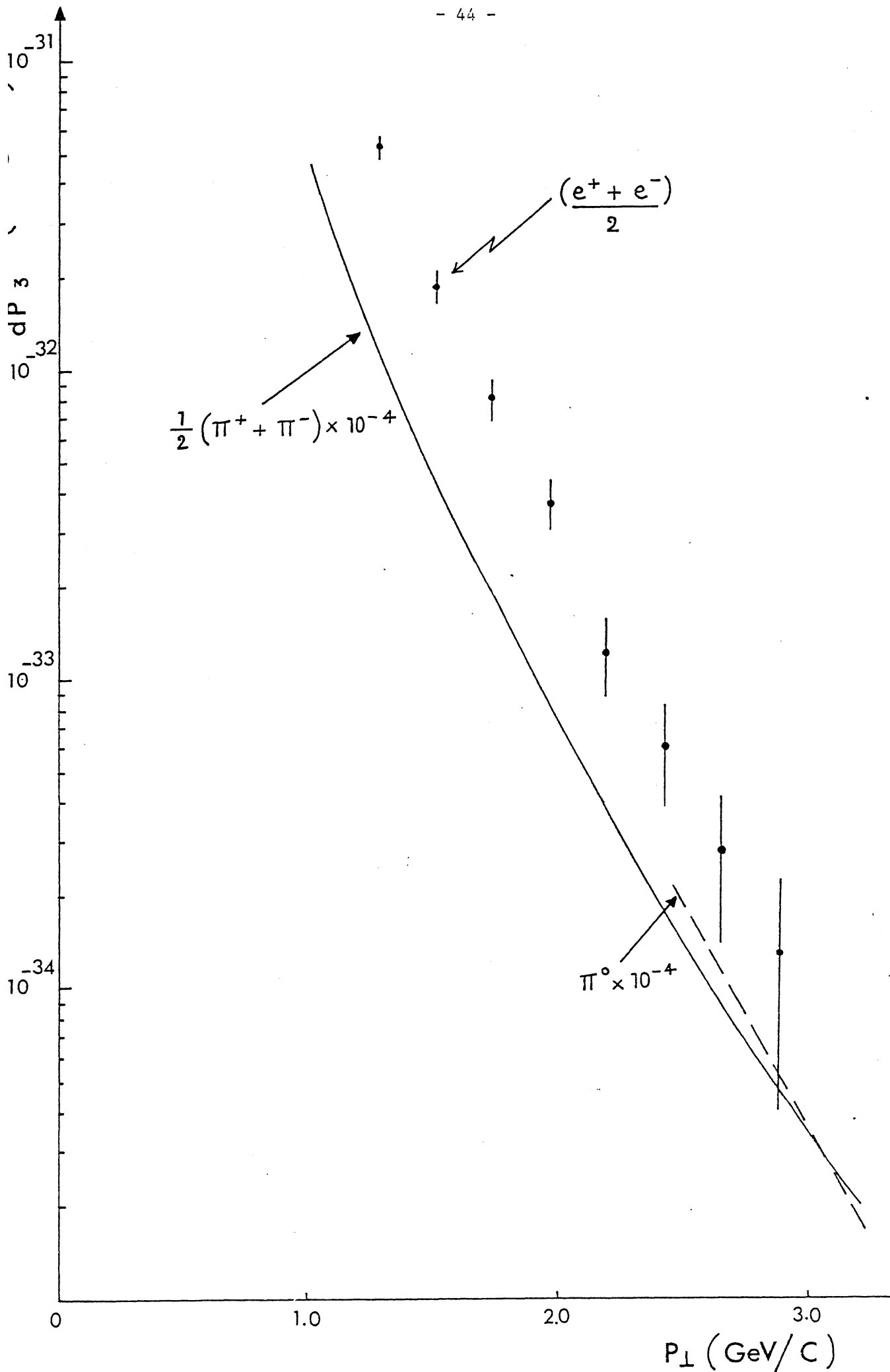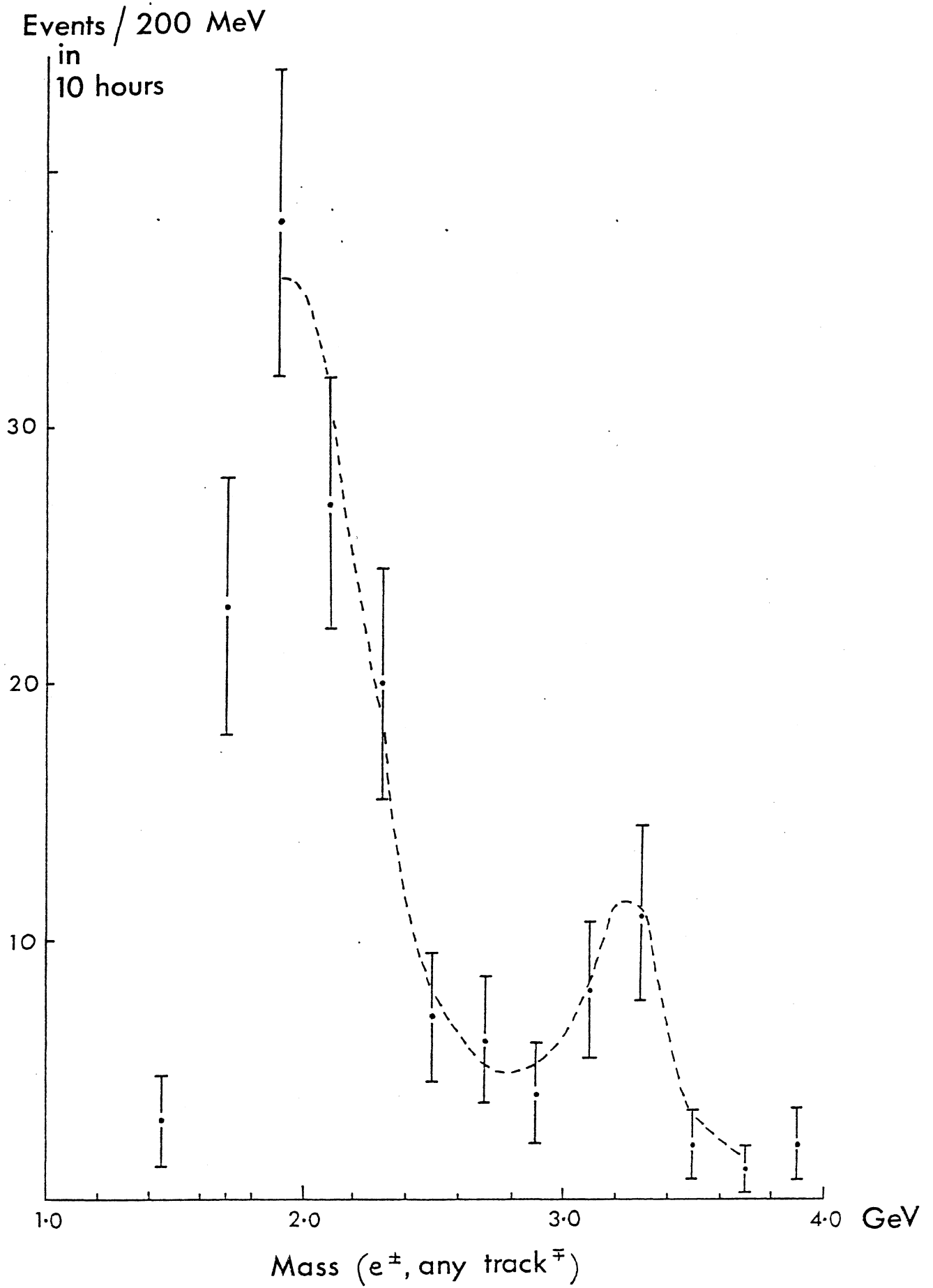
FIG .19
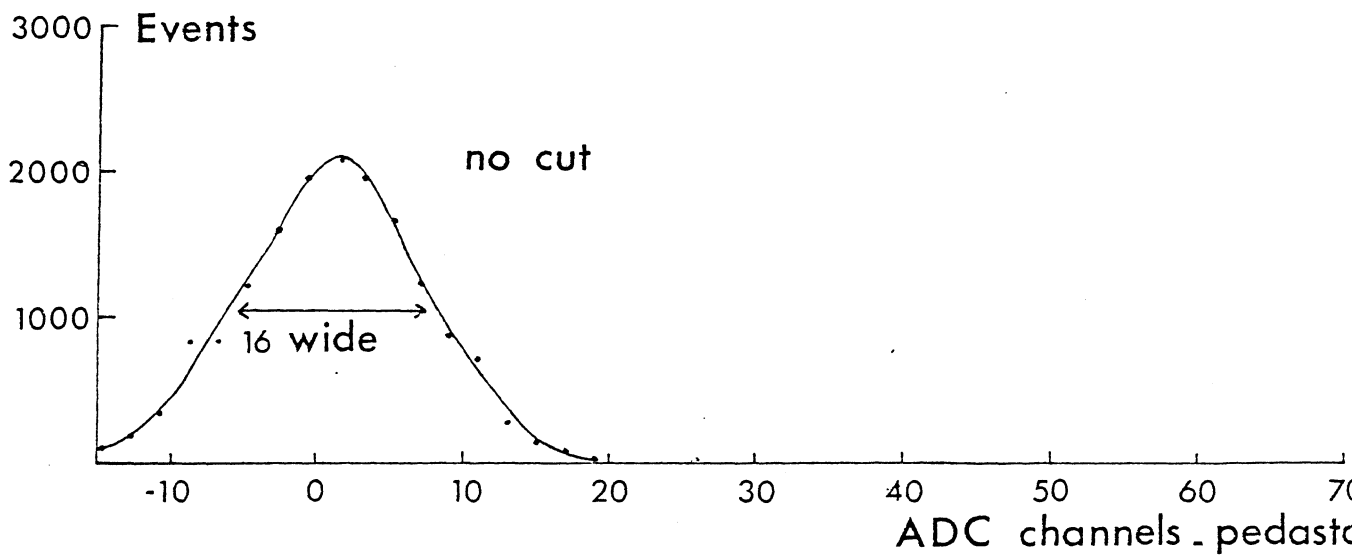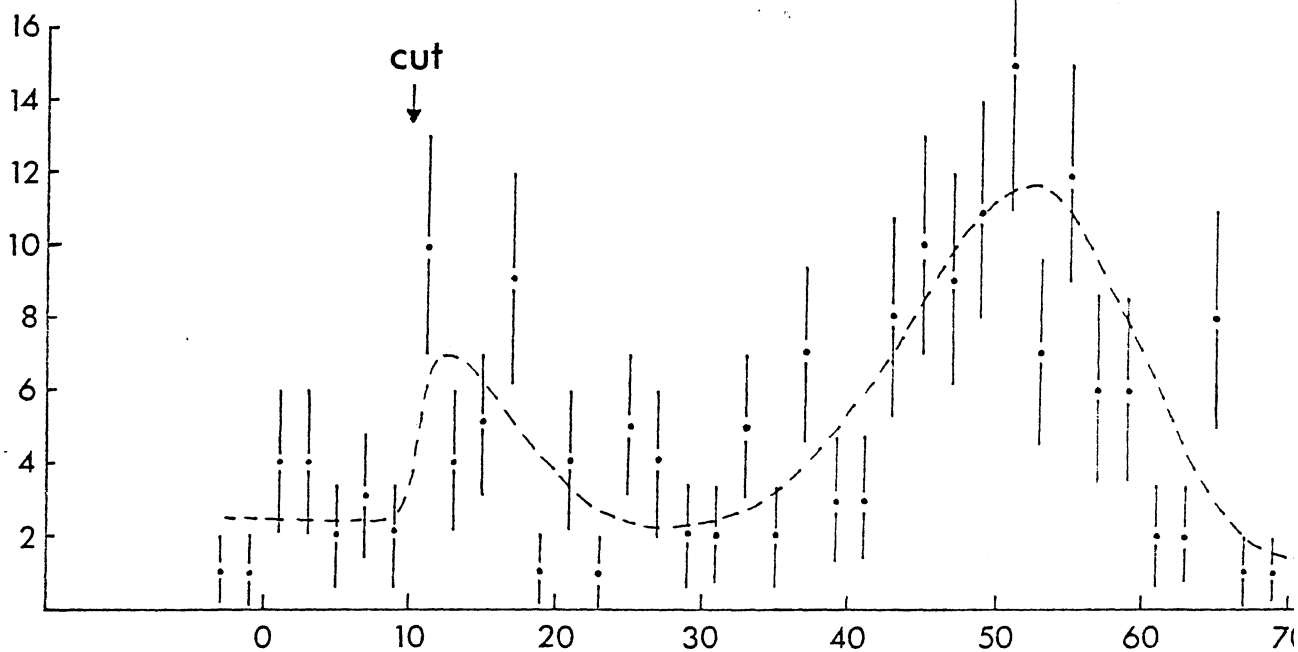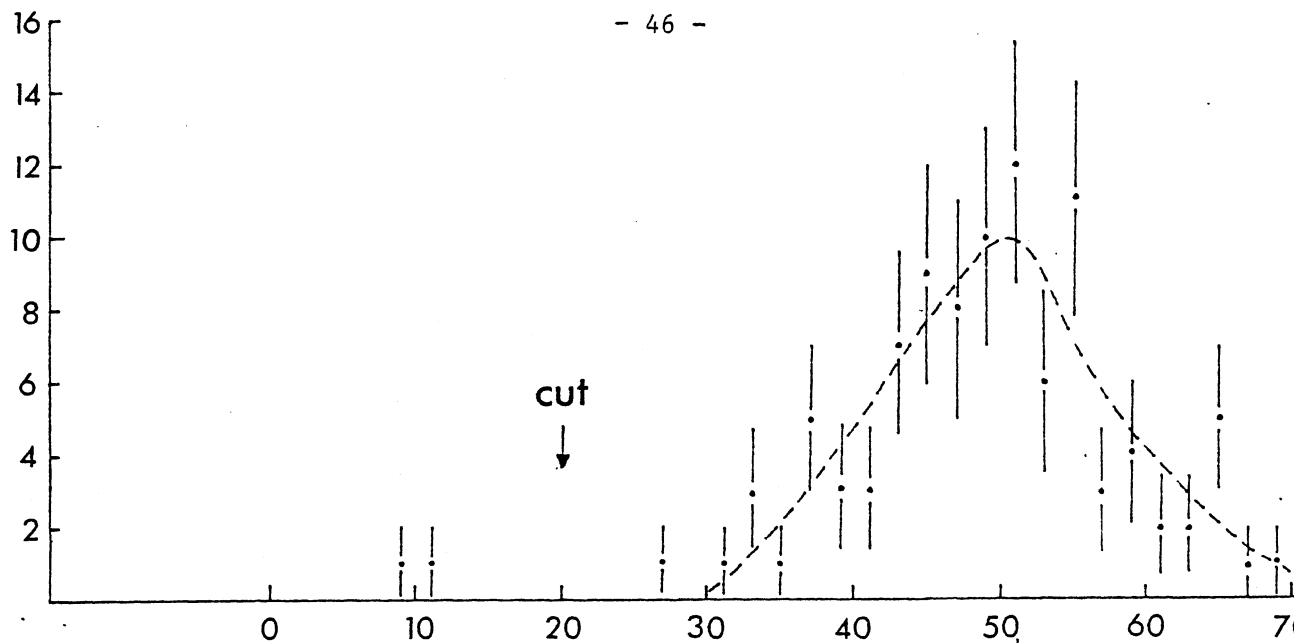
FIG . 20

III. <u>REPORT FROM EXPERIMENT R 416</u>

<u>STUDY OF RARE EVENTS AT THE SFM</u>

CERN-Collège de France-Dortmund-Heidelberg-Lapp(Annecy)-Warsaw-Collaboration

(Presented by H.D. Wahl - CERN-EP)

.

<u>Introduction</u>

The following is a brief description of the present status of experiment R 416 (January 1979). The following headings will be used :

      1. Aim of experiment

      2. History, timescale

      3. Apparatus and trigger

      4. Data processing

      5. Data taken and analysed

      6. Results (some mass distributions)

      7. Conclusion, future plans

For details of the apparatus, see the presentation of P.G. Innocenti in these proceedings and the written status report to the Intersecting Storage Rings Committee (ISRC 78-11).

1. <u>Aim of experiment</u>

The aim of experiment R 416 is the study of full events associated with :

(a) trigger on hadron with high p_T (> 5 GeV/c) around $\theta = 45^{\circ}$

     - study event structure (jet studies etc.)

(b) trigger on low momentum electron
     ($p_T \gtrsim 500$ MeV/c) around $\theta \simeq 90^{\circ}$

- charm production via :

$$pp \rightarrow D_1 + D_2 + X$$

with

$$D_1 \rightarrow K + \Pi\text{'s}$$

$$D_2 \rightarrow eK\nu + \Pi\text{'s}$$

The single electron in the D_2 decay is used as a trigger, the expected improvement in the charm/non charm ratio being approximately a factor of 10^3.

The aim is then to identify the D_1-meson via its K and Π decay products.

2. Curriculum vitae of experiment

date	event
Jan. 75	letter of intent submitted
Feb. 75	1st proposal submitted
May 75	1st proposal refused
Oct. 75	2nd proposal submitted
April 76	2nd proposal approved
Dec. 76	scheduled SFM physics program finished (R 417)
	- start dismantling of detector and rebuilding chambers
June 77	start installation
Nov. 77	first test data with high p_t and e
Feb. 78	full detector and external equipment installed
March 78	run-in of detector
April 78	debugging and data taking
Aug/Sept. 78	data taking
Dec. 78	charm signal seen

3. Apparatus and Trigger

(i) Trigger

The general layout of the SFM detectors and particle identifiers is shown in Figure 1. The electron trigger EL is defined as :

$$EL = PIF \times C \times DC \times F1$$

where PIF = fast trigger, coincidence of FOR's of chamber in trigger region

$$C = CO \times (C3 + C4)$$

DC = slow trigger : 'roads', coincidence pattern of MOR's (16 wire groups)

FI = filter : track finding and momentum cut-off

The trigger solid angle $\Delta\Omega$ is approximately 0.17 sr with an overall efficiency of 0.4 and deadtime losses of 15%.

There is no on-line electron pair rejection. The trigger rates for $L = 10^{31}$ cm^{-2} sec^{-1} are typically :

	EL	P1
fast	340	35 K
× DC	35	3.5 K
× FI	12	1.3 K
DAQ	10	40

(ii) Cerenkovs :

Details of the 5 atmospheric C-counters are given below

Counter	Gas	Threshold e(MeV)	Π(GeV)	purpose	$<n_e>$
CO, 3, 4	N_2	21	5.7	e-trigger	$\simeq$ 4
C2, 5	Freon 12	11	3.0	Π-identif. in high p_T	$\simeq$10

(iii) dE/dx chamber

A small dE/dx chamber next to the vacuum chamber of the interaction region consists of 4 gaps (3V, 1H), wire spacing 4 mm with a sensitive area 57 × 27 cm^2 and solid angles $\Delta\Omega \simeq 2$ sr. It has an energy resolution of about 50% FWHM and its uses in the experiment are :

- e-trigger (slow)
- trackfinding in trigger region
- rejection of close (unresolved) pairs by pulse height (Figure 2)
- rejection of open (resolved) pairs
- particle identification

Π/p/K up to $\simeq$ 400 MeV

p/non p up to $\simeq$ 700 MeV.

(iv) Time of flight counters

The time of flight system consists of 67 scintillation counters 225 × 40 × 2 cm^3 or a total area of 60.3 m^2. 56 are at a distance of 5 m and 11 at a distance of 3.6 m. The total solid angle $\Delta\Omega$ is 1.6 sr. An intrinsic time resolution of 0.6 ns FWHM has been achieved.

The system provides particle separation :

Π/K/p up to approximately 1 GeV

and   p/non p up to approximately 1.8 GeV.

A typical TOF mass distribution is shown in Figure 3.

4. Data Processing

The average number of observed tracks $<n_{obs}>$ is high ($\simeq$ 17) so that full reconstruction is extremely time consuming ($\simeq$ 11 sec IBM). A selection is made to restrict full reconstruction to that subsample of events which is of interest for the physics goal.

(a) Selection program

- identify the trigger track and hence reject fake triggers
- match the trigger track with the C signal and check consistency in the dE/dx chamber
  (all planes hit, clustersize O.K.)

- cut on dE/dx pulse height (< 40)
- geometrical cuts (exclude low field region)
- p_T-cut (> 0.5 GeV/c).

This gives reduction factors of :

      $\simeq$ 65 for data taken without on-line filter (spring)

      $\simeq$ 13 for data taken with filter (autumn)

The computing time used is approximately 140 ms (IBM) per input event.

(b) 'In/out' trackfinding
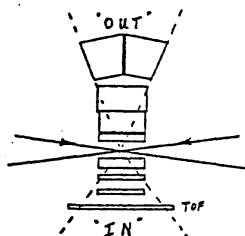
Concentrate on those events where a track is found opposite to the trigger.

This gives a reduction factor of 2 to 3.5, depending on the trigger p_T cut-off.

(c) 'Crash program' for charm search

    Fast search for K/p candidates in 'IN' region (without track reconstruction). A further reduction factor of 7.6 is obtained $(m_{TOF}) > 0.3)$.

5. Data taken and analysed

(a) 'Spring' data (period 2)

$$Ldt \simeq 1.2 \times 10^{36} \ cm^{-2}$$

total number of triggers $\simeq 3 \times 10^6$
of these, 46 K were fully processed,
30 K with an 'IN' track.

(b) 'Autumn' data (periods 5, 6)

$$Ldt \simeq 7.6 \times 10^{36} \text{ cm}^{-2}$$

total number of triggers $\simeq 10^7$

processed through the 'crash programme' and

yielded $\simeq$ 50 K events with a K/p candidate

in the 'IN' region.

The present status is that $\simeq$ 35 K events have been written on a Data Summary Tape. In terms of computing time, the job is 90% complete. Total computing time used so far is :

$\simeq$ 430 hours IBM at CERN

$\simeq$ 200 hours at Collège de France.

Production at Heidelberg is now starting.

5. Results

Very preliminary results have been obtained so far. The data, which was processed through the 'crash programme' shows a D signal of 3.8 standard deviations in $K^- \pi^+ \pi^+$ and $K^+ \pi^- \pi^-$, when the $K^{\pm} \pi^{\pm}$ has the K^* mass, additional cuts in p_T and X were also used. This is shown in Figure 4.

A similar signal has recently been found in data taken in experiment R 407/408 (Figure 5). This is an event sample taken with a K^- trigger ($\theta \simeq 8^\circ$, $<p_T> \simeq 1.1$ GeV/c) and the D signal of about 5 standard deviations is seen in $K^- \pi^+ \pi^+$ when the $K^- \pi^+$ correspond to the K^* mass. The rather high cross-section suggests that forward production of D is important.

More details of this last result are given in CERN/EP/Phys/78-45 (22nd December 1978) which has been submitted to Physics Letters B.

6. Conclusions

The detector + external equipment are working satisfactorily as is the software (though the latter is not yet complete).

The physics goal of the experiment is achievable since a charm signal has already been seen in both the central and forward regions.

Lots of work remains to be done; in particular, to complete the software and to continue data processing of the events so far neglected.

In order to understand the physics of charm production cross-sections must be obtained. The aim will also be to extract information which might be used to do an even better experiment.

The immediate future plans of the collaboration are to concentrate on analysis, in particular using the K/p selection provided by the dE/dx chamber and to look for V^0's.

Finally, thanks are due to the ISR Operations and Experimental Support Groups, the SFM Detector Group, and EF Instrumentation and DD On-line Support Groups.

Figure captions

Fig. 1   :   Layout of the SFM detectors as used in experiment R 416.

Fig. 2   :   Pulse-height distribution in the dE/dx chamber obtained with
                    the electron trigger. The energy loss measurements are
                    corrected for angle and saturation effects. The first peak
                    corresponds to one electron, the second to unresolved electron
                    pairs.

Fig. 3   :   Typical time of flight mass spectrum p < 0.7 GeV/c.

Fig. 4   :   A preliminary invariant mass distribution in $K^-\Pi^+\Pi^+$ and
                    $K^+\Pi^-\Pi^-$ where the $K^+\Pi^+$ has the K^* mass (890 ± 40 MeV). A peak
                    of 3.8 standard deviations above background is seen at the
                    mass of the D meson.

Fig. 5   : $K^-\Pi\Pi$ mass distributions from experiment R 407/408. At least
                    one of the two $K^-\Pi$ combinations has a mass in the K^* region

                         (a) $K^-\Pi^+\Pi^+$

                         (b)   sum of $K^-\Pi^+\Pi^-$ and $K^-\Pi^-\Pi^-$

Fig. 3

Fig. 4

K⁻ππ mass spectra with (K⁻π) in K*

a) K⁻π⁺π⁺

b) (K⁻π⁺π⁻) + (K⁻π⁻π⁻)

M (K π π) , GeV

Number of combinations / 80 MeV
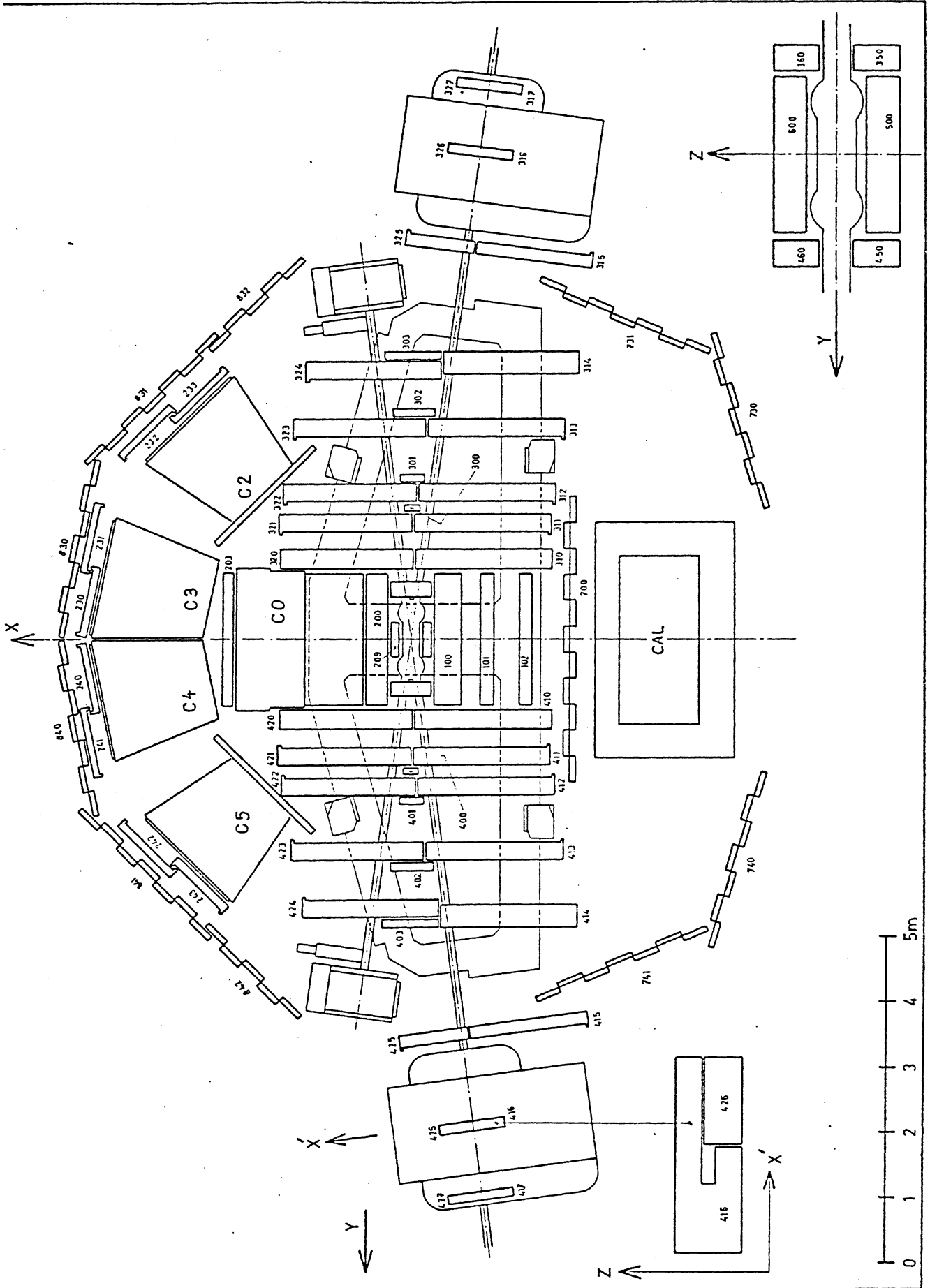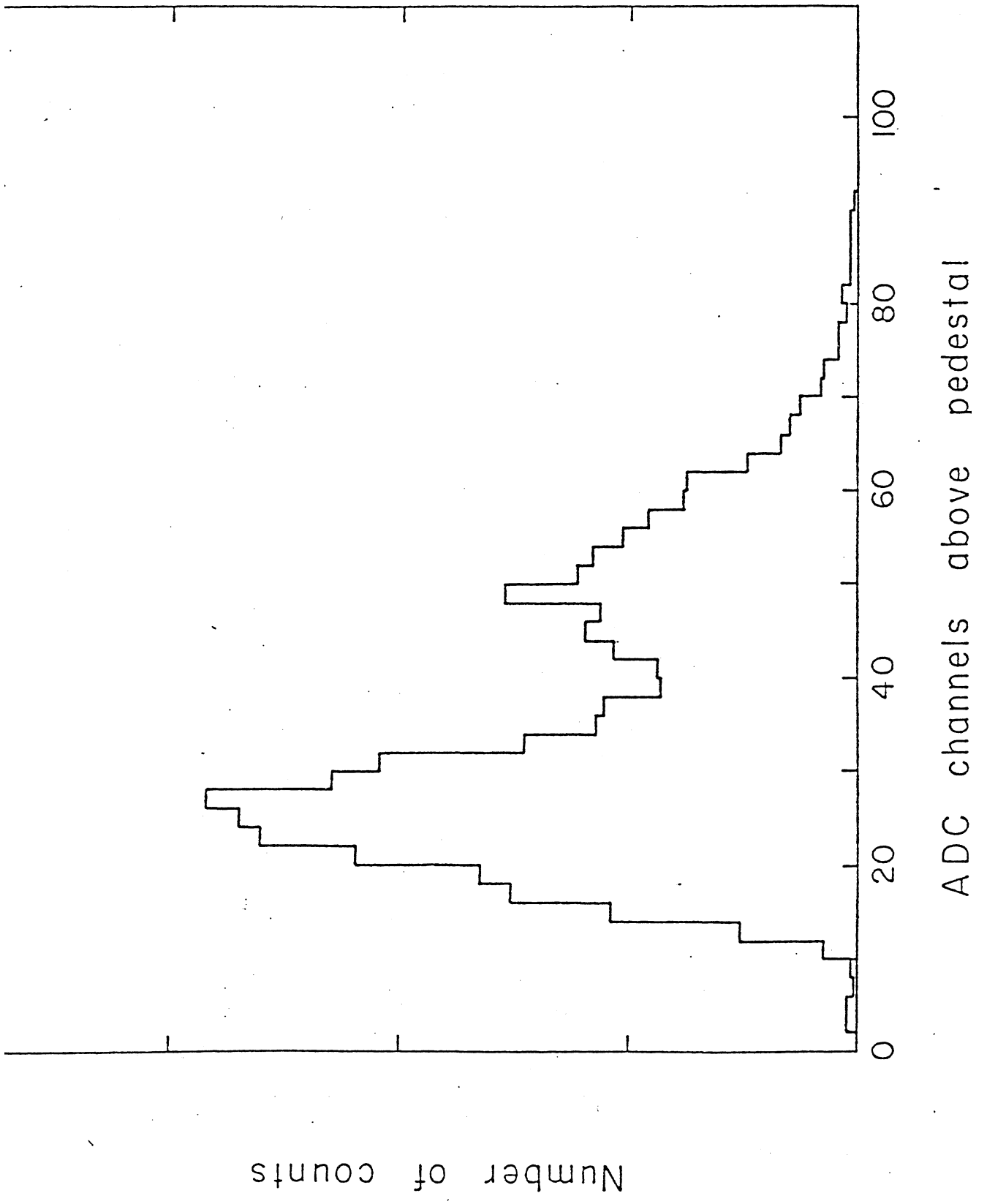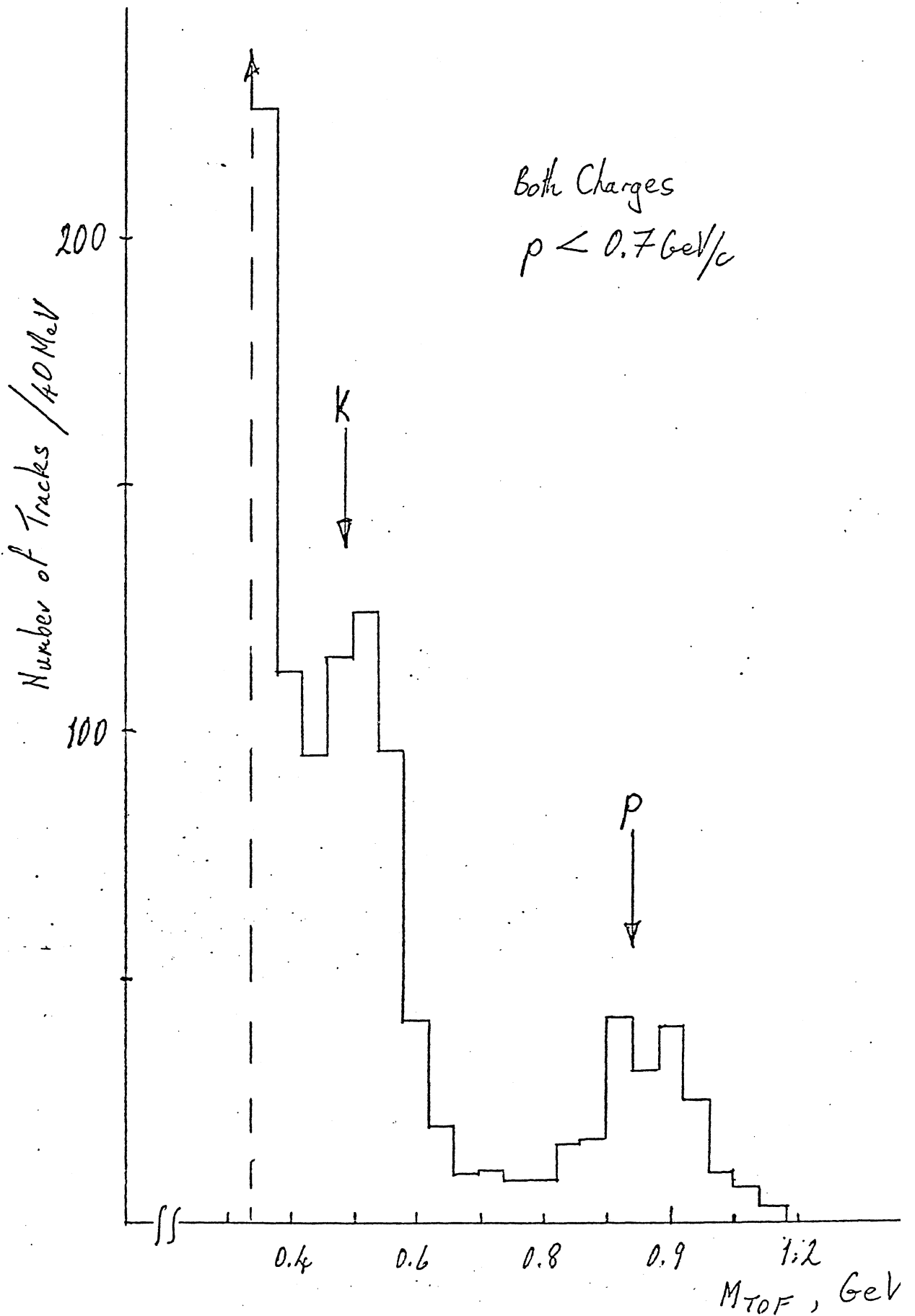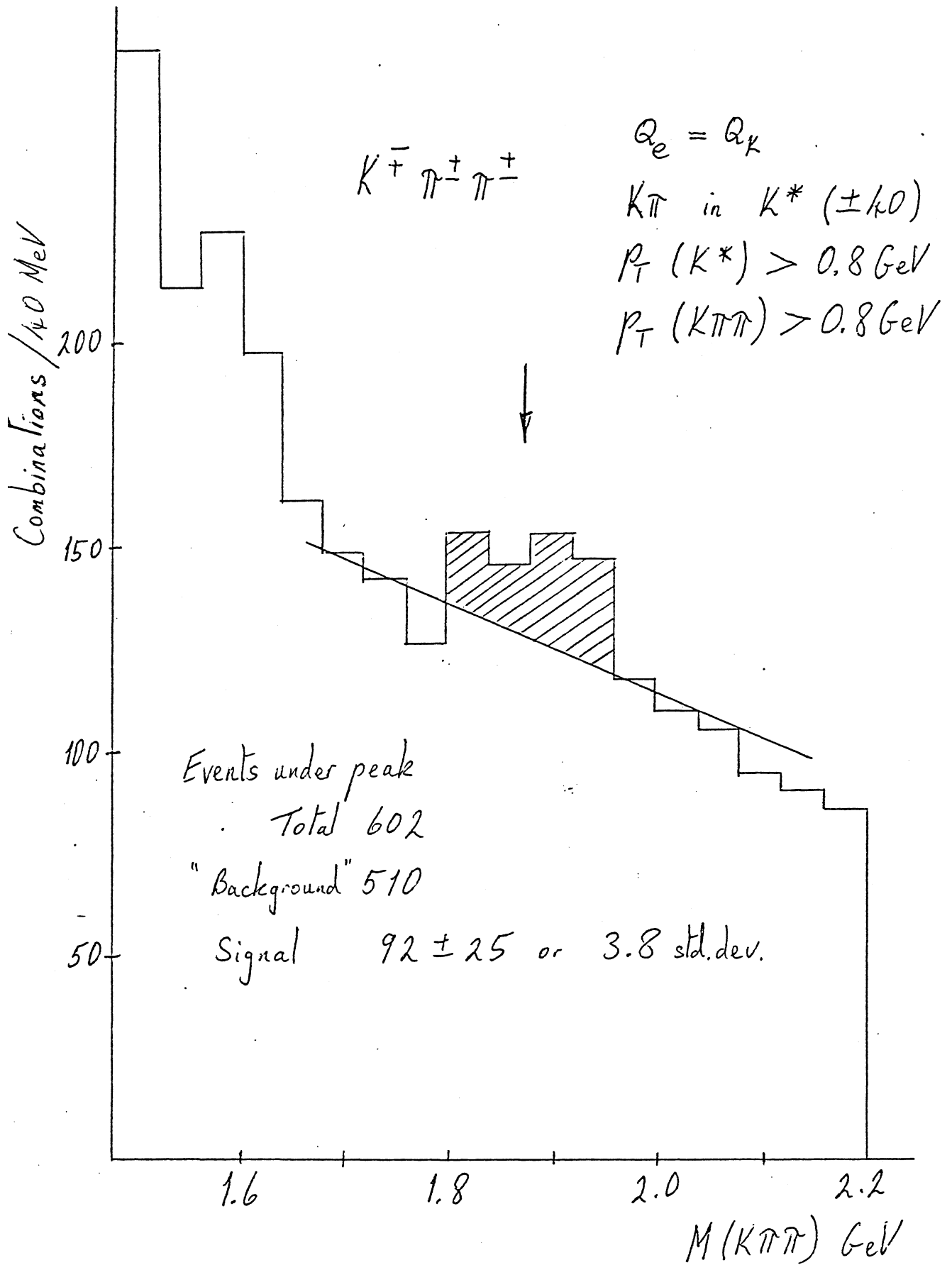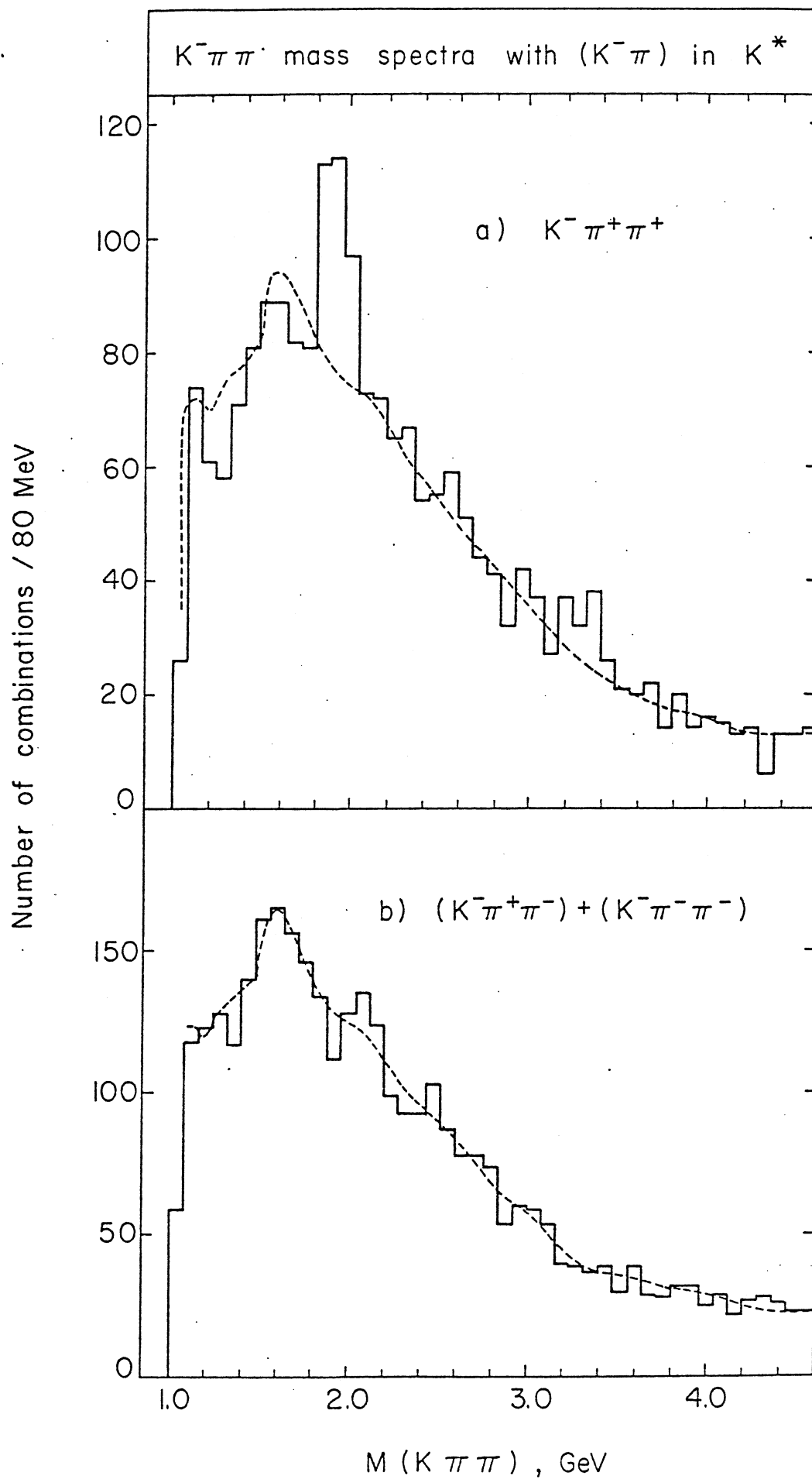
IV. STUDY OF α-p-COLLISIONS WITH THE SFM

M.A. Faessler - CERN-EP

Acceleration of α-particles in the PS and storage in the ISR is technically possible, although the amount of effort necessary for this kind of program has still to be estimated. In the following we discuss a few physics aspects which make the study of α-p-collisions an interesting subject in our opinion. We think of doing a "soft ware experiment" - according to a classification used at the workshop - with the SFM as it stands. The advantage of using α-particles will be explained below in some more detail, but we want to anticipate the result : The use of α-particles lies essentially in the fact that, as targets, nuclei are $A^{2/3}$ times bigger hadrons in transverse (to the beam) dimension and $A^{1/3}$ times denser hadrons in longitudinal direction than the proton, for the fast components (partons, quarks, gluons) of the projectile.

The experimental approach to study α-p-collisions which we envisage is to study global correlations in phase space of particle and flavour densities. This is a lesson from high p_T physics : A break through in understanding the dynamics which underlies high p_T events was achieved when global correlations in phase space were studied transverse to the beam axis [1] - in an experiment using the SFM. The fact that opposite side jets are found (and expected to be found for q-q-scattering) at different relative rapidities, makes it clear why other approaches (inclusive $d\sigma/dp_T$ at fixed x_F or y, or integrated over x_F or y, 2-particle correlation function etc) could not give a clear picture of the 4-jet structure of high p_T events. Mainly correlations transverse to the beam axis have been studied, for the correlations between high p_T jets and the beam fragmentation regions more measurements would be useful.

To my knowledge, little attention has been paid, in normal, low p_T interactions, to correlations along the beam axis until recently. There were measurement many years ago, of 2 particle correlations in rapidity but it seems that people soon got attracted by the presence of strong short range y correlations which were nicely explained by cluster production. The long range in y correlations which were seen, were attributed to energy and momentum conservation and to diffractive dissociation and by these statements they were dismissed. At least I could not find any detailed discussion of the measured long range y correlations in literature. Almost by analogy to high p_t physics, one would guess that

back to back correlations along the beam axis would teach something on low p_t dynamics.

This can be seen most intuitively if one considers different constituent models. Recently it has become popular to apply constituent models to low p_t normal hadronic interactions after all the successes of explaining deep inelastic processes by the parton model and more modernly by QCD. There is not enough time to explain in detail what the different soft constituent models would predict about correlations along the beam axis. It would require a lot more homework too.

The following is a summary of a quick and superficial study of the subject : Consider the fragmentation regions which are according to most opinions dominated by the valence quarks. Whether there are back to back correlations of the opposite fragmentation regions or not depends essentially on how actively the valence quarks participate in the primary interaction. In models with passive valence quarks (I), there are no such correlations, to first approximation, like in Feynman's original proposal [2] for soft hadron hadron collisions where only the wee partons interact or in Van Hove's and Pokorski's model [3] where the role of the wee partons is taken by the neutral gluons. In both cases, the valence partons or quarks pass the scene as spectators.
On the other side, if valence quarks participate actively (II), you will see correlations, as in the additive quark model [4] (In this model, the quarks are not point-like constituents).
There is a recent calculation by Brodsky and Gunion [5] which gives an almost quantitative support to these statements since they calculated gluon exchange which I have put into the first category and quark interchange which clearly belongs to the second category.

So much for the general hadron hadron interaction including pp collisions. The usual question to answer now is why complicate it and use nuclear targets ? The answer : because nuclei and specifically the α in the ISR will amplify the correlations,if there are any!

Consider α-p-collisions in the models with passive valence quarks. The valence quarks of the projectile p would find the second and following nucleons which they encounter as transparent as they did the first nucleon. Only after leaving the α, they would dress up or recombine in a similar fashion as for the pp case. The projectile fragmentation region would look exactly the same , no matter if you observe at the α side that one or 2 or maybe even 3 or 4 nucleons have been hit. (apart from small corrections due to energy and momentum conservation).

Since there is no correlation for one interaction, there is no amplification by rescattering.

It is different if the valence quarks participate actively. In this case, rescattering means that the quark which interacted first will interact again or one of the quarks which was spectator in the first collision will interact. Thus one loses more and more of the passive spectator quarks which give the fast final hadrons.

I think here it is obvious that the correlation observed for 1 scattering will be amplified.

A small complication in the case of nuclei has been omitted. It arises from the fact that the distances between nucleons or rather the time between 2 successive collisions is finite. This is really a small complication. It is common wisdom that internucleon or intranuclear distances are negligibly small for the fast quarks or partons. You might see it this way : The first interaction destroys the coherence of the incoming hadron states such that after some time they will fall apart into the final observed hadrons.

Now the time or distance it takes for the fast components to fall apart is long. One can explain this fact using lorentz dilatation or lorentz contraction but even m simply if one states that the fast components all have almost light-velocity and small velocity differences. Therefore it takes a long way in the Lab. to separate th

The conclusion is that the space time configuration of the fast quarks (+ the accompanying gluons) remains practically unchanged between two collisions. In this sense for the fast partons the nucleus is like a big hadron or rather a big hadron in transverse dimension and a dense hadron in longitudinal dimension.

Now to summarize what I have said and what I haven't said. We would like to study α-p collisions in the ISR in order to look for the correlations which I mentioned and a lot of other things which I had no time to mention. The ISR can reach the maximum energy for α-p collisions among existing accelerators and has the advantage of studying the collision in the CM system (almost).

Therefore, the α-p option in the ISR is a unique chance, if it exists, which will not be offered by any other machine for many years to come. In addition, at the ISR there is a detector installed and working well, the SFM. This detector is as ideal as an existing detector can be for measurements of global correlations in phase space.

REFERENCES

1)   P. Darriulat et al., Nucl. Phys. $\underline{B107}$, 429 (1976)

      See also J.D. Bjorken in Proc. of Summer Inst. on Particle Physics
      SLAC (1975)

2)   R.P. Feynman, Photon-Hadron-Interactions (Benjamin, N.Y. 1972)

3)   L. Van Hove and S. Pokorski, Nucl. Phys. $\underline{B86}$, 243 (1975)
      S. Pokorski and L. Van Hove, preprint Ref. TH 2427-CERN (1977)
      L. Van Hove, preprint Ref. TH 2580-CERN (1978)

4)   E.M. Levin and L.L. Frankfurt, JETP Lett. $\underline{2}$, 65 (1965)

      N.N. Nikolaev et al., CERN- Preprint Ref. TH 2541-CERN (Sept. '78)

5)   S.J. Brodsky and J.F. Gunion, Phys. Rev. D $\underline{17}$, 848 (1978)

V. PHYSICS WITH ANTIPROTONS AT THE ISR

M. Jacob - CERN-TH

1. Introduction

Physics with antiprotons in the ISR has been considered for a long time. Nevertheless, it was not until an intense source of antiprotons could be realistically envisaged, thanks to the use of cooling techniques, that an actual research programme could be discussed. Indeed, storage of antiprotons obtained from the SPS and directly injected into the ISR could provide a luminosity at the level of 10^{25} to 10^{26} only, hardly enough for a mere elastic scattering experiment. With cooling techniques, as presently developed for use in the SPS in its Collider version, luminosities as high as 1.5×10^{29} (10^{30} with the superconducting low β insertion) can be expected. A wide and most interesting physics programme can then be contemplated.

Physics with antiprotons at the ISR was discussed at length during the first ISR Workshop in 1976. The relevant conclusions have been summarized in the report by B.G. Pope, CERN/ISR/76-32. The matter was considered further, and at greater length during the second ISR Workshop in 1977. This resulted in an extensive report, ISR/2-9, with contributions from M. Braccini, A. Donnachie, U. Gastaldi, K. Hansen, K. Hübner, G. Matthieae and F. Vannuci. The conclusions of the specialized working group were summarized by P. Strolin in his final report ISR/2-16. This paper surveys all the key points of the physics programme which can be envisaged today. At the time of the ISR Workshop, expected luminosities were at the level of 2×10^{28} and 1.4×10^{29}, for standard and low β intersections, respectively. Since then, pre-acceleration in the PS and stacking, as now planned, will allow a very sizeable increase in the achieved luminosity. This is discussed by Ph. Bryant in these proceedings. We shall therefore take as a working hypothesis luminosities of 1.5×10^{29} and 10^{30}, for a standard and the low β intersections respectively. Such figures look very reasonable at the moment. The programme which can thus be contemplated is even more ambitious than the one foreseen a year ago.

The present note borrows much from ISR/2-9 and ISR/2-6 which should be consulted for a more detailed discussion. It consists of two parts. The first part puts together some general comments about the physics programme. The second part includes a set of figures showing recent ISR and Fermilab data. They illustrate the type of cross sections which can be envisaged for $\bar{p}p$

interactions since no large differences are expected between pp and $\bar{p}p$ induced reactions. For instance, one predicts a few percent difference at the total cross section level and, as the largest possible effect, one order of magnitude difference when considering the highest mass lepton pair which could be detected in $\bar{p}p$ interactions. Limitations associated with a luminosity of 10^{29} to 10^{30} can then be readily assessed.

2. General Features of $\bar{p}p$ Physics at ISR Energies

Experimentation with antiprotons at ISR energies will open a fresh door into existing physics. This is highly worthwhile. It is, however, unlikely that it will lead to the observation of completely new phenomena as those expected to occur at the very high energies reached with the SPS used as a collider. A host of interesting results can be collected in any case and this in a relatively short amount of time. The conclusions reached at the Workshop can be summarized as follows :

(i) the intense source of antiprotons which is being developed for use with the SPS and which will also be readily available for use with the ISR, provides large enough luminosities for an interesting programme of research, rich in highly topical questions

(ii) the large and powerful array of detectors available by 1981, and in particular the upgraded SFM and the AFM, can be used just as well for the analysis of $\bar{p}p$ interactions. More generally speaking, the ingenious experimentation techniques developed over a decade of intense activity at the ISR can be readily applied to the study of $\bar{p}p$ reactions.

(iii) over the ISR energy range one does not expect dramatic differences between pp and $\bar{p}p$ induced reactions. Nevertheless, differences are sizeable enough to be measurable and measuring them would provide very valuable tests of present ideas about the proton structure and about hadron interactions.

(iv) As shown in Figure 1, the ISR is unique for this programme. Expected luminosities according to three scenarios which can be considered at CERN are displayed as functions of centre of mass energy. A huge energy range is accessible at an acceptable loss in luminosity.

The Workshop therefore came up with a very positive recommendation. Within two years (1981 and 1982) all the looked-for data should be available.

Experimentation with antiprotons can be tentatively classified according to two main categories. In the first one, we have experiments which can be referred to as 'software' experiments. They correspond typically to rather large cross sections (σ > 1 μb say). The off line analysis is in general much longer than the data taking time proper which can be very short (a few days only in some cases). In the second category we have experiments which require a long running time to the extent that they are limited by the available luminosity. These experiments (large p_T and lepton pair production in particular) are very topical since they provide rather direct tests of hadron structure. They will benefit from the powerful detectors which have been gradually developed for experimentation at the ISR. One can say with confidence that one should at least be able to reach for $\bar{p}p$ the limits quoted for pp by 1977. This is already very satis

3. Expected Limits for the $\bar{p}p$ Programme

We consider in turn the different topics which are customary to the presentation of ISR physics (see for instance ISR/2-1).

(i) Total Cross section

The $\bar{p}p$ total cross section can be measured using techniques developed by the CERN-Rome-Pisa-Stony Brook experiments. The precision achieved could be at the level of 0.3 - 0.5 mb. This is very meaningful to the extent that the difference between the $\bar{p}p$ and pp cross sections is expected to fall from 2 to 0.7 mb over the ISR energy range (Figure 2). The $\bar{p}p$ total cross section is expected to rise by 1.5 mb. This could be verified with enough precision. Such an experiment should not request much running time.

(ii) Elastic scattering

A precise measurement of the elastic scattering differential cross section should also require only a small amount of running time. A good measurement of $\frac{d\sigma}{dt}$ in the diffractive peak region (0.05 < $|t|$ < 0.4 (GeV/c)) should only require a few hours (Figure 3a). This is particularly interesting for models of the Pomeron, since this t range covers the 'kink' region in high energy pp scattering and the 'cross-over' region for $\bar{p}p$ and pp scattering up to SPS energies. While a precise measurement of ρ looked marginal in 1977, the now expected increase in $\bar{p}$ current should make it possible with data taking time at the level

of a few days. The differential cross section at large $|t|$ could easily be studied up to $|t| \simeq 5$ $(GeV/c)^2$, this value corresponding to 10 days of running time at $L \simeq 10^{29}$. This is far beyond the dip region in pp scattering (Figure 3b).

(iii) <u>Diffractive studies</u>

By definition we do not expect any difference between pp and $\bar{p}p$ interactions. Nevertheless, a new round of experiments comparing pp and $\bar{p}p$ induced reactions studied with the same detector is highly worthwhile. This applies in particular to the Double Pomeron process for which better evidence still could be obtained. One should recall that correlation studies among the fragments of the hadronic state obtained in high mass diffractive exalation have not yet been made. This might be the occasion! The very high energy of the ISR is a precious asset.

(iv) <u>Exclusive exchange reactions</u>

Two beautiful experiments in the SFM have provided evidence for Regge behaviour, the leading trajectory taking over from Π exchange at high enough energy ($p_{lab} > 500$ GeV/c!). More examples should be welcome. One may, in particular, consider $\bar{p}p \rightarrow \bar{n}n$ and $\bar{p}p \rightarrow \bar{\Lambda}\Lambda$, with expected cross section at the level of 0.1 to 1 μb (Figure 4). The SFM is a very suitable detector for reactions listed under (iii) and (iv).

(v) <u>Low p_T dominant mechanisms</u>

Early research at the ISR (1972-1974) provided the key properties of production mechanisms. While some general understanding has emerged progress has been limited by the lack of suitable data. In particular, there is practically no information about correlations involving high mass particles (K, p, $\bar{p}$). Detectors are now such that a new round of minimum bias data collection and analysis has become highly worthwhile. This is a typical 'software' endeavour. Systamatic errors are to a large extent detector dependent. Available luminosities are more than enough. Consequently, doing such experiments with pp and $\bar{p}p$ initial states would add much interest to the programme and may provide very interesting clues. Studying the rise of the central plateau (a 30% effect over the ISR energy range) with an asymmetrical initial configuration should help going further to understanding it. More generally, the mechanisms responsible for quantum number excitation could be far better studied comparing $\bar{p}p$ and pp induced

reactions. Since 1974, the analysis of large multiplicity reactions, the analysis of reactions with slow protons and, in particular, the analysis of the fragmentation of the forward jets into very fast secondaries has made very sizeable progress. This now calls for more detailed experimentation. Again collecting $\bar{p}p$ and pp data would provide an extremely valuable supplement of information. Charm spectroscopy studies can now be envisaged with some confidence. Altogether, the programme which can now be carried out at the ISR looks even more interesting than the one which one can envisage for the EHS. Special triggers could allow for a specific study of annihilation mechanisms.

(vi)   Large mass lepton pairs

The success of the Drell Yan approach and the further insight offered by QCD, provide a direct link between the hadron quark structure and large mass (M > 3 GeV) lepton pair production. Analysis of the proton structure allows for precise predictions for $\bar{p}p$ induced reactions, which conversely would provide very valuable tests of present ideas. In principle, the larger the mass, the more interesting it is since Valence quarks have to play a more important role. As shown in Figure 5, a luminosity of 10^{29} should be enough to reach M = 5 while with 10^{30}, one could reach M = 10 GeV. Limits are estimated taking one event per day per GeV as the experimental limit. Ratios between $\bar{p}p$ and pp induced reactions are not yet overwhelming due to the relative small-ness of the relevant parameter M^2/s. Nevertheless, they are still sizeable : a factor 2 at 5 GeV and an order of magnitude at 10 GeV. Measuring such differences would be very interesting. The mass range 3 < M<9 GeV, over which such a comparison could be made with some precision, is already large and highly relevant. One expects larger differences at SPS energies (Figure 1). Nevertheless, the energy dependence of the predicted difference is also very much part of the required tests.

The production of narrow vector states is of course an important part of a lepton pair experiment. One expects that J/ψ production will be almost the same in pp and $\bar{p}p$ interactions at ISR energies. There is still a factor 6 difference at 40 GeV, which is interpreted as resulting from different competing mechanisms. Their relative roles should, however, change with increasing energy. One should in any case easily observe a very prominent J/ψ signal in $\bar{p}p$ reactions. This should allow

for tests of present ideas about J/ψ production. For the T one may
hope for a more pronounced signal in $\bar{p}p$ induced reactions than in
pp reactions. At $\sqrt{s} = 30$ GeV, the relevant $x(\ell cX)$ values actually
compare with those involved for J/ψ production at 40 GeV. An order
of magnitude difference in yields may then result in a detectable T
signal. It should be remarked that the very different $J/\psi/\psi'$ and
T/T' production ratios at SPS (Fermilab) energies are still puzzling.
The production of narrow states (this also includes the X states)
may thus reserve surprises.

(vii) <u>Large p_T production</u>

By 1977, inclusive production could be studied up to 9 GeV and it was
concluded that expected increases in solid angle coverage and detector
sophistication should compensate for the loss in luminosity when study-
ing $\bar{p}p$ reactions. Indeed, the new detectors have since allowed reaching
still larger values of p_T ($p_T \simeq 14$ GeV/c) and their use at $L = 10^{30}$
should allow triggering on large p_T particles up to $p_T \simeq 10$ GeV/c
(Figure 6). This is of great potential interest since one presently
expects that this includes the p_T range where quark-quark scattering
takes over from the gluon-gluon and gluon-quark contributions of
great importance at medium p_T. Furthermore, quark-anti-quark
annihilation in $\bar{p}p$ induced reactions is at the same level as quark-
quark scattering when studying wide angle production. This should result
in differences in yields and in specific quantum number effects, in
particular at the correlation level. The relative importance of
quark-anti-quark annihilation should also result in a sizeable increase
of the charmed particle yield at large p_T. Large p_T production turns
out to be rather complicated in the p_T range available for ISR
experimentation with antiprotons ($3 < p_T < 10$ GeV/c). Nevertheless,
this is the reason why comparison between $\bar{p}p$ and pp induced reactions
appears as so interesting. The AFM detector should be very well
suited for such studies. By 1981, jet triggering should also be
available. This should allow reaching still larger p_T values.

(viii) <u>What Else</u> ?

One should, of course, hope for surprises. One can, for instance,
mention that comparison between π^+ and π^- yields at 90° in $\bar{p}p$ induced
reactions allows for a test of CP invariance in large p_T production.
One should say, however, that from present knowledge what is at stake
is a better understanding of presently known hadronic processes rather

than something entirely new associated with the Valence anti-quarks of the antiprotons. This is, in any case, highly worthwhile. With the expected luminosity and the powerful detectors which are already available, or presently being completed, one can look forward to a very interesting programme.

— — — — —

PS. At the time of the ISR Workshop the $\bar{p}$ option was even summarized as follows (see ISR/2-0)

> Cherchant par ces cinq ans la pleine activité
> $\bar{p}p$ offre un champ de recherches nouvelles
> Le Cooling nous procure la luminosité
> Les Détecteurs sont là. Les projets s'ammoncellent.
>
> Néanmoins dans le cadre des théories des champs
> Rien ne singularise une antiparticule
> On ne peut escompter de désaccord flagrants
> Et de nombreux effets ne sont que minuscules.

This was however followed by a relevant quote from M. Tannenbaum in ISR/2-8, 'Never believe theorists'.
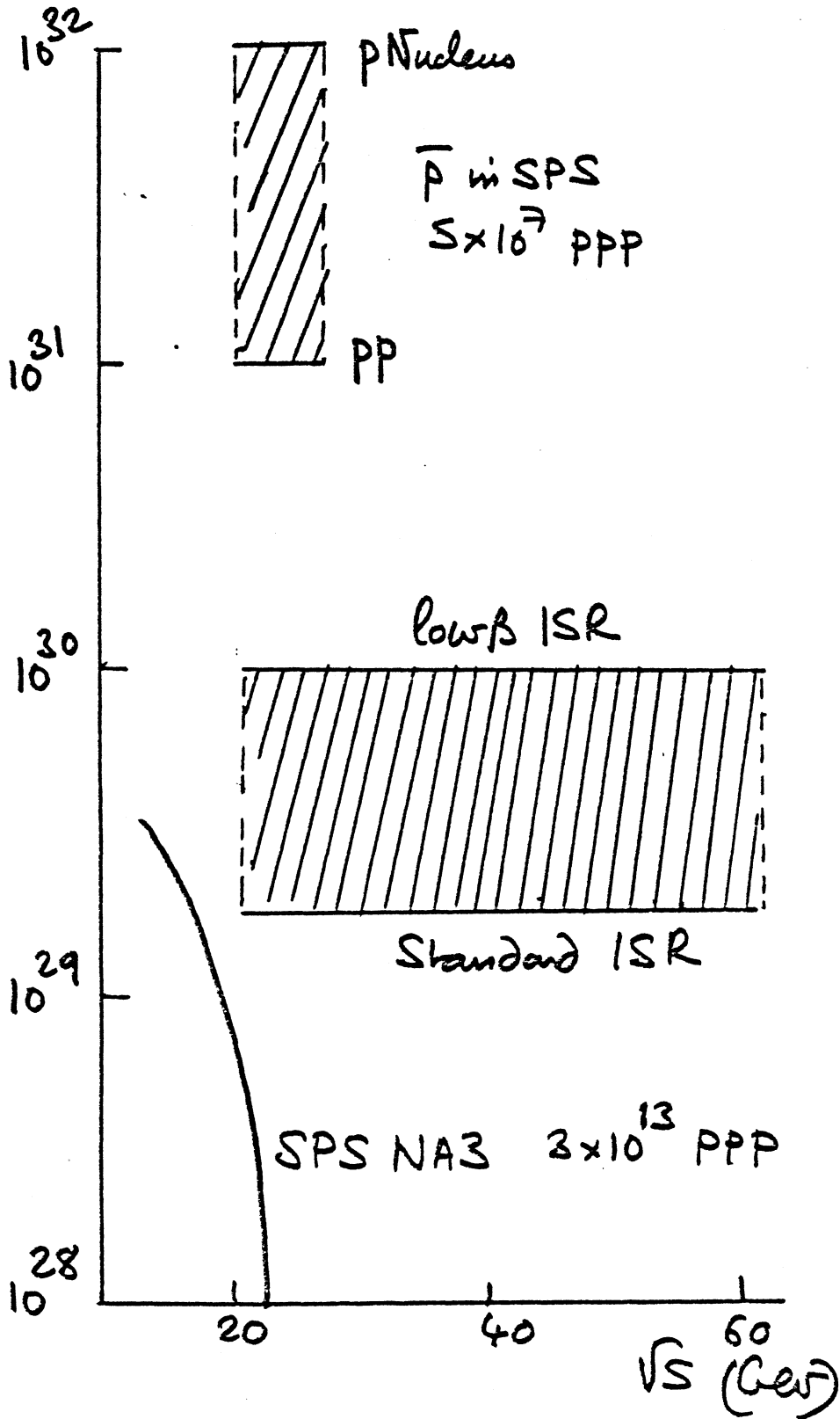
Figure 1 : 3 scenarios for p̄p research at CERN
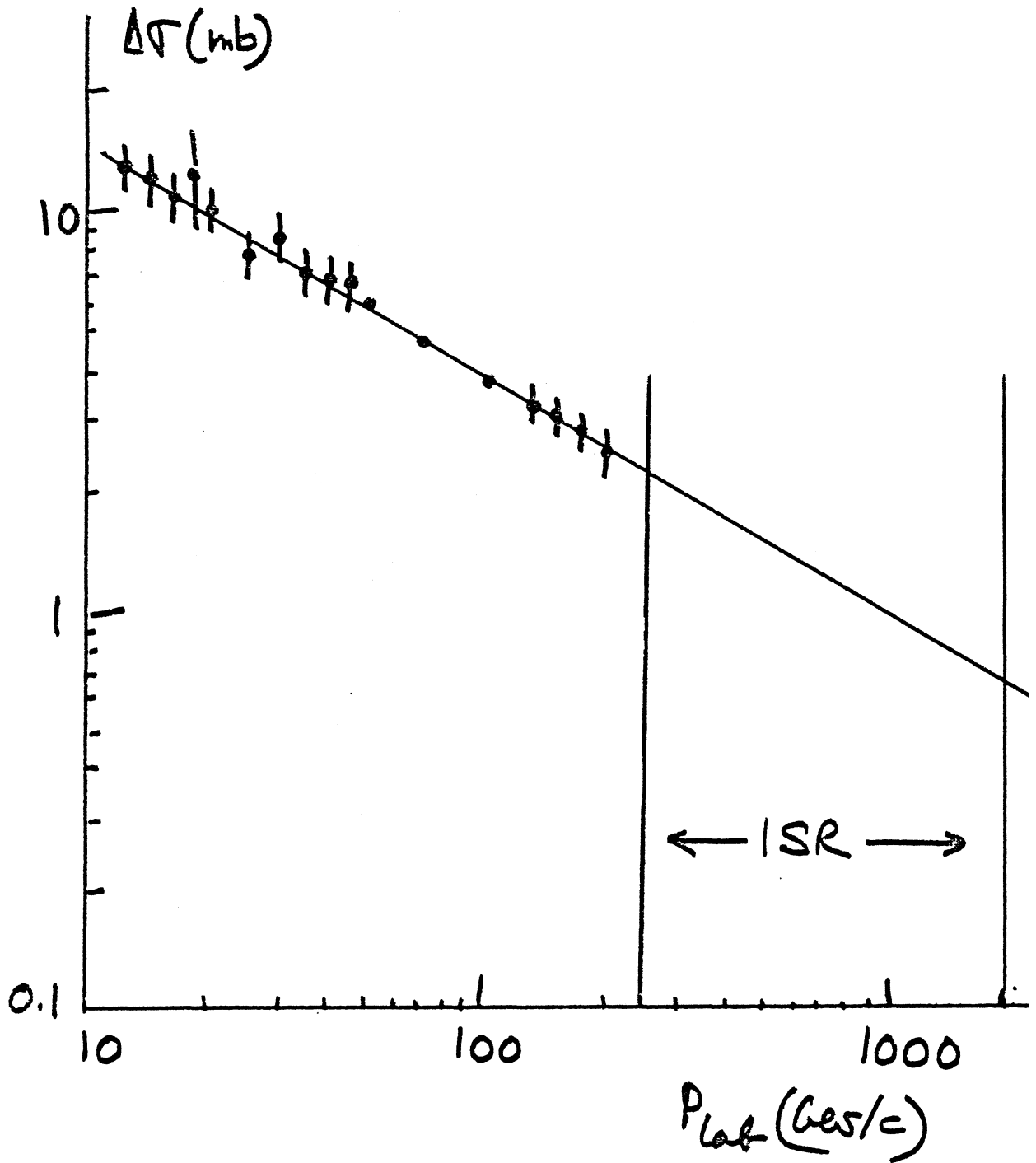
Figure 2

Difference between the p̄p and pp total cross-sections, and its Regge extrapolation through the ISR energy range.
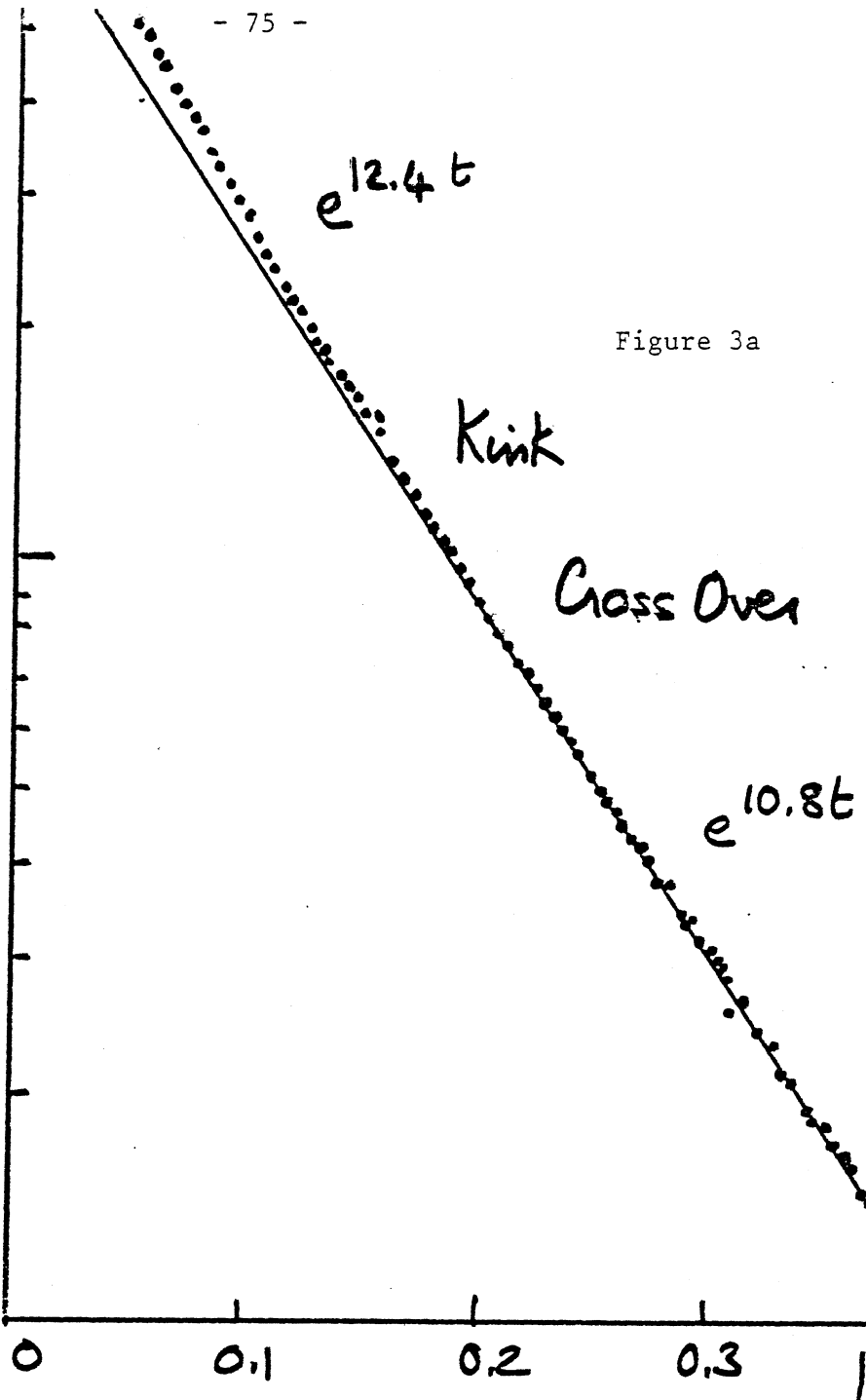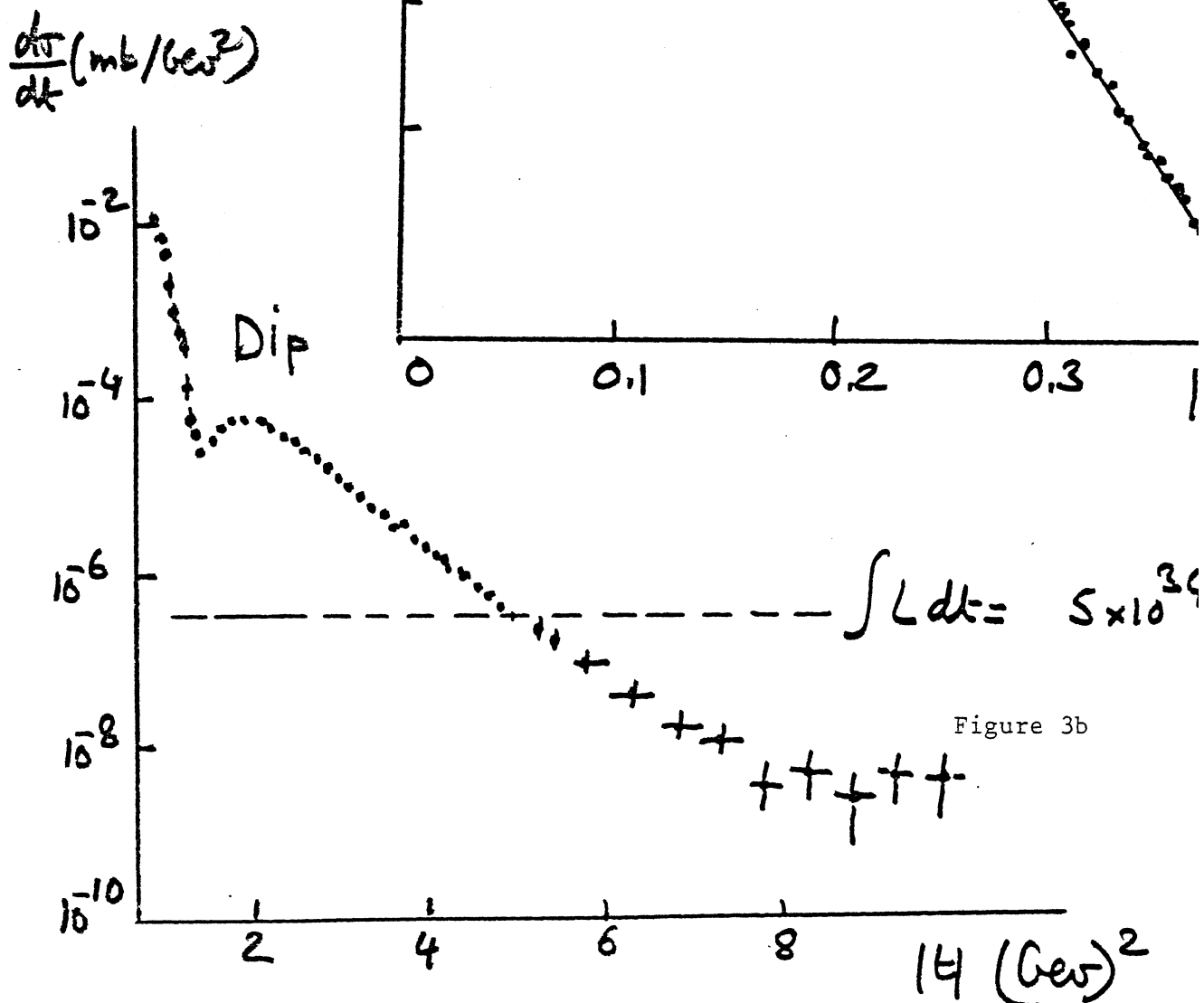
The pp differential cross-section in the Kink (a) and Dip (b) regions. Experimentation with p̄ could easily reach |t| = 5(GeV/c)² granting a
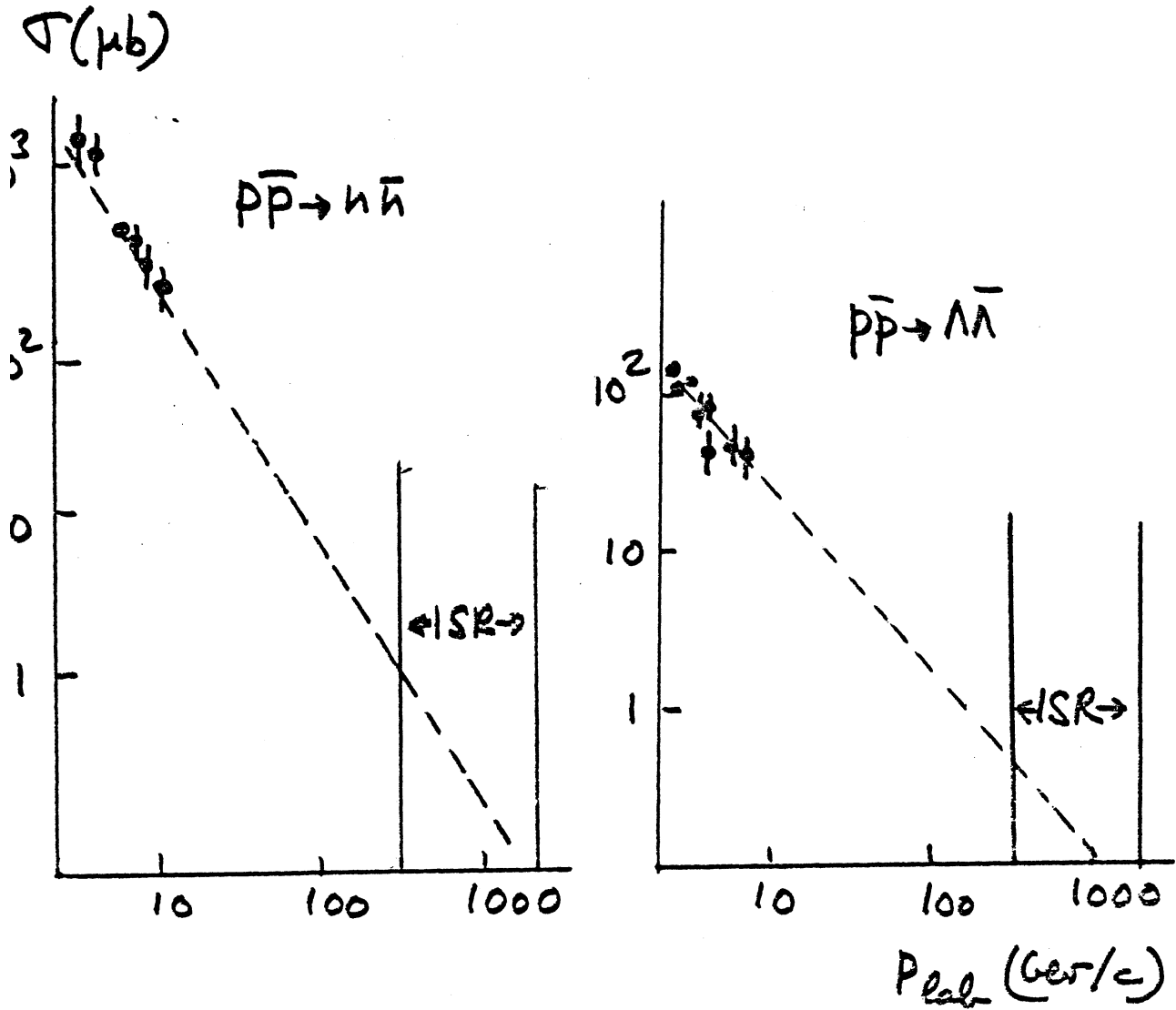
Naive extrapolation of two exclusive reactions. One expects
the leading trajectory to take over with a more gentle fall off,
in particular in the former case, where pion exchange appears to
dominate up to SPS energies.

Figure 4

$$\frac{d\sigma}{dM} \ (cm^2/GeV)$$

$$\sqrt{s} = 53 \ GeV$$

$$L = 10^{29}$$

$$L = 10^{30}$$

One event / day GeV

$\overline{P}P$

PP

$M \ (GeV)$

Figure 5

Differential cross-sections for lepton pair production in pp and p̄p induced reactions.
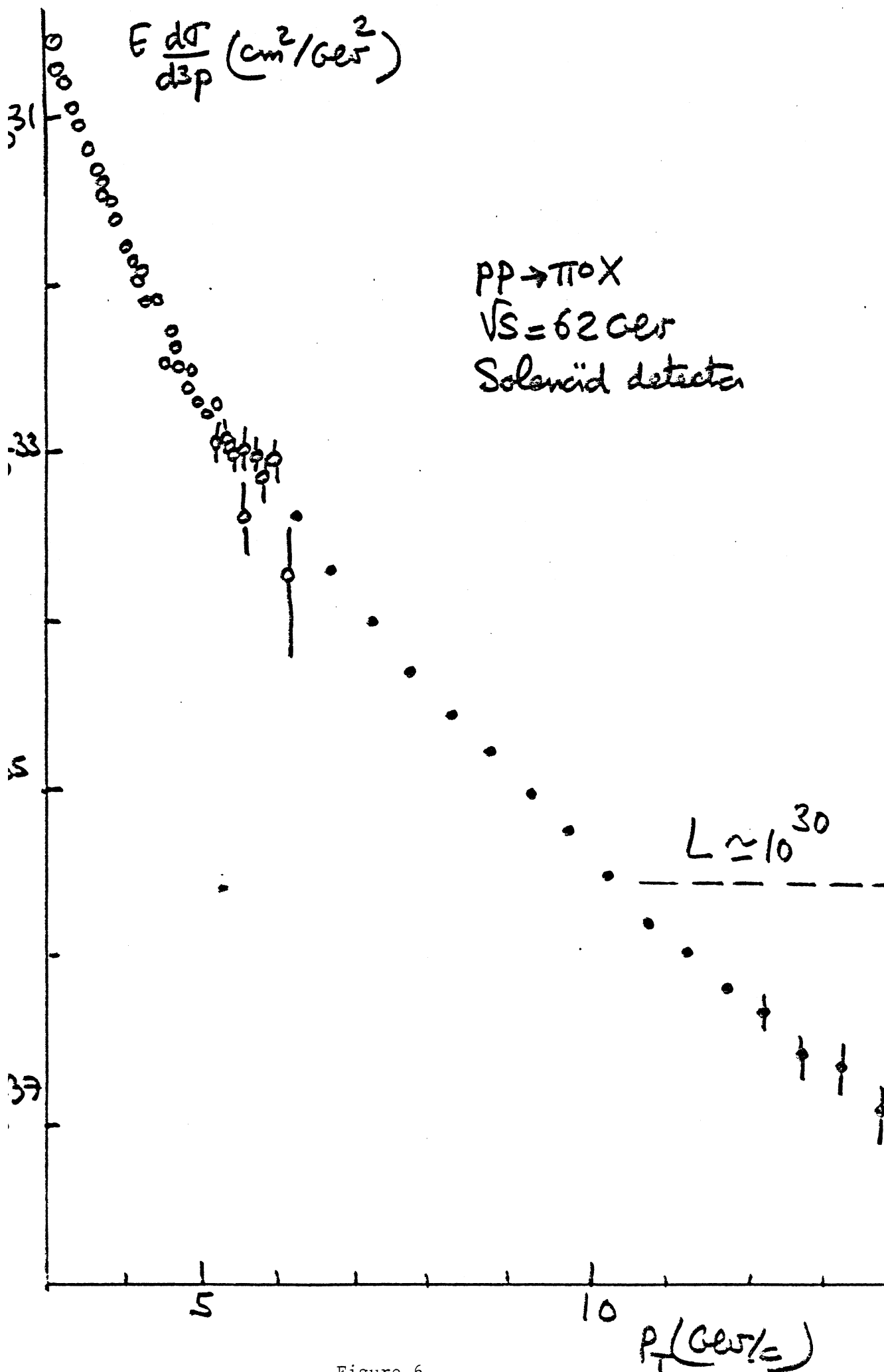
Figure 6

Inclusive destribution of π^o in pp reactions. With the expected luminosity

VI. EXPECTED ISR PERFORMANCE WITH ANTIPROTONS

ISR DIVISION p̄p STUDY

(Presented by P. Bryant - CERN-ISR)

1. Injection Scheme

In previous reports[1] two schemes for the transfer of antiprotons from the Antiproton Accumulator (AA) have been described and discussed. It has now been decided[2] that the 3.5 GeV antiprotons from the accumulator will be reinjected into the PS and accelerated to 26 GeV before being transferred to the ISR. In the PS the antiprotons will circulate in the opposite direction to the normal protons, hence a new transfer line will be needed from the PS extraction system, whic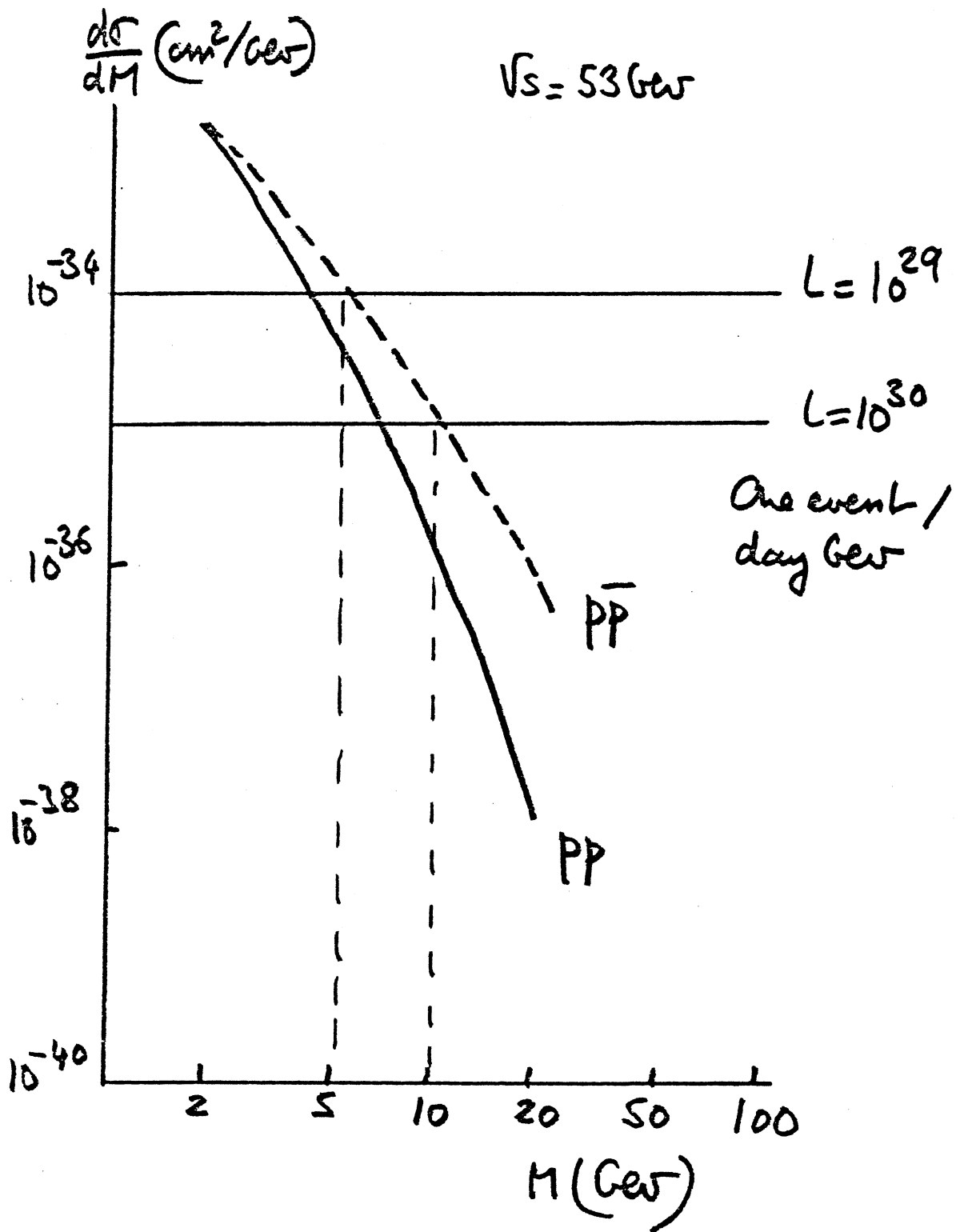h is being built for the SPS collider, to the injection channel TT1 of the ISR. The proposed layout of transfer lines between the accumulator, PS and ISR is shown in Fig. 1. The new line, TT6, which will bring antiprotons into ring 2 of the ISR, is expected to be completed early in 1981.

2. Estimated p̄p luminosities

This injection scheme will allow stacking to be performed in the ISR. Since the operating energy (11-26 GeV) will be the same as the injection energy each time a pulse of antiprotons is available in the AA-ring, it will be transferred to the ISR and added to the existing circulating antiprotons. For the following estimates an operations cycle of five pulses injected over four days followed by a six day stable beam run has been somewhat arbitrarily assumed.

The antiproton intensity available has been taken as 6×10^{11} antiprotons every 24 hours arriving in the ISR with normalized emittances $\varepsilon_h = 5.2\pi$ mm.mrad, $\varepsilon_v = 3.7\pi$ The stacking scheme already described is shown schematically in Fig. 2 and the estimated values for the peak and integrated luminosity with this scheme, for the three types of intersections, standard, steel low-β and superconducting low-β are given in Table I.

Table I refers to 26 GeV but operation at lower energies will be possible using the same operations cycle. The estimated peak luminosities in each case are given in Table II. Integrated luminosities are expected to approximately scale. Also given in Table II is an estimate of the maximum luminosity at 31.4 GeV but at this energy the operations cycle will be slightly different; stacking for the first four days will be at 26 GeV, followed by phase displacement acceleration.

Hence, in each ten day operations cycle, four days will be at 26 GeV and six days at 31.4 GeV.

3. Cooling in the ISR

The above estimates of integrated luminosity have been made assuming no stochastic cooling on either the antiproton or proton beams. Whereas the very low intensity antiproton beam will be relatively easy to cool with an existing scheme, it is not expected to be possible to cool the high intensity (30 A) proton beam but because of the very long operating times it may be interesting to use lower intensity beams with stochastic cooling such that the increase in beam height and hence luminosity loss rate is zero. A conservative estimate suggests that these conditions might be achievable for a 7 A beam. The resulting estimated luminosities for the same operating cycle are given in Table III. Compared with Table I the integrated luminosities are lower by about a factor of 2 but this mode of running may be preferable in view of the anticipated improvement in background conditions. It may prove difficult to provide good conditions for physics at the end of a ten day run and cooling will certainly help.

4. Operation of Experimental Magnets

At present there are three experimental magnets operating at the ISR which put a substantial magnetic field on the circulating beams and hence require compensation. These are the Open Axial Field Magnet (OAFM) of experiment R 807, the Superconducting Solenoid (SCS) of R 108 and the Split Field Magnet (SFM). In all three cases operation with antiprotons will require a new compensation scheme. For the OAFM this will be possible using the existing compensation magnets, for the SCS a beam separation of 17 mm must be compensated and this will require new dipole correction magnets and a vertical aperture restriction will still exist. However, tests have recently been carried out which suggest that this will not be a serious problem.

The antiproton beam orbit through the SFM will be so far displaced from the proton orbit that with the existing vacuum chamber the horizontal aperture will be reduced to zero. However, a scheme has been worked out which will provide an acceptable horizontal aperture for the antiproton beam (85 mm) with the existing intersection vacuum chamber displaced radially and the SFM operating field reduced to 0.85 T instead of 1 T at 26 GeV. This solution has been judged preferable to the only alternative of a larger and hence thicker central vacuum chamber. Part of the vacuum chamber within the detector region will have to be moved between periods of p̄p and pp operation; this is presently being studied together with its implications for the detector system.

5. Terwilliger Scheme

The possibility of making available the 'Terwilliger scheme' which reduces the momentum dispersion to zero in the even intersections, is being studied and is expected to be feasible. The original scheme will be disturbed when the superconducting low-β insertion is installed in intersection 8 in 1980.

References

1) ISR Operation with Antiprotons, CERN-ISR-BOM/78-18, compiled by P.J. Bryant.

2) The project was confirmed and funds allotted at the meeting of the CERN Executive Board of 25th January 1979.
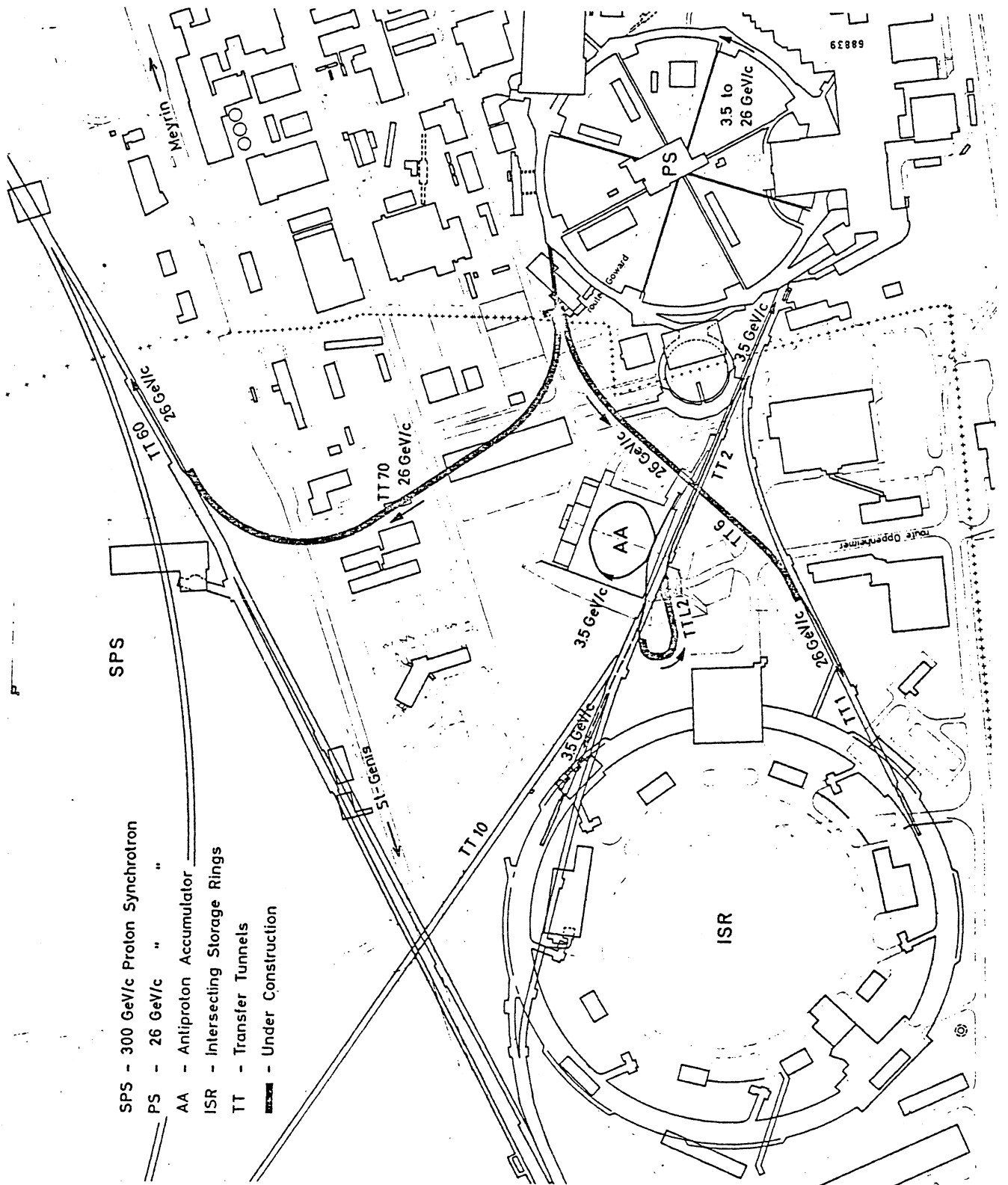
- 82 -

Table I

ISR Performance at 26.6 GeV/c

Conditions $I_p = 30$ A $I_{\bar{p}(max)} = 0.15$ A	σ_p (mm)	$\sigma_{\bar{p}}$ (mm)	h_{eff} (mm)	L_{max} (cm^{-2} s^{-1})	$\frac{1}{L}\frac{dL}{dt}$ (s^{-1})	$\int Ldt$ (cm^{-2})(10 days)
Standard Intersection β_v=14m	1.18	0.68	3.4	1.3×10^{29}	1.4×10^{-6}	5.7×10^{34}
Steel low-β β_v = 3m	0.55	0.31	1.6	2.8×10^{29}	1.4×10^{-6}	1.2×10^{35}
S.C. low-β β_v = 0.3m	0.17	0.10	0.5	9.2×10^{29}	1.4×10^{-6}	4.0×10^{35}

Table II

Peak Luminosities at other energies

Conditions	11.8 GeV/c I_p = 12 A L_{max}(cm^{-2} s^{-1})	15.4 GeV/c I_p = 20 A L_{max}(cm^{-2} s^{-1})	22.5 GeV/c I_p = 25 A L_{max}(cm^{-2} s^{-1})	31.4 GeV/c I_p = 30 A L_{max}(cm^{-2} s^{-1})
Standard Intersection β_v=14m	3×10^{28}	6×10^{28}	1×10^{29}	1×10^{29}
Steel low-β β_v = 3m	7×10^{28}	1×10^{29}	2×10^{29}	2×10^{29}
S.C. low-β β_v = 0.3m	2×10^{29}	4×10^{29}	7×10^{29}	9×10^{29}

Table III

Estimated 26 GeV/c Performance with Cooled Beams

Conditions $I_p = 7.25$ A $I_{\bar{p}(max)} = 0.15$ A with stochastic cooling	σ_p (mm)	$\sigma_{\bar{p}}$ (mm)	h_{eff} (mm)	L_{max} (cm^{-2} s^{-1})	$\frac{1}{L}\frac{dL}{dt}$ (s^{-1})	$\int Ldt$ (cm^{-2})(10 days)
Standard Intersection β_v= 14m	0.68	0.68	2.4	4.5×10^{28}	0	3.1×10^{34}
Steel low-β β_v = 3m	0.31	0.31	1.1	9.9×10^{28}	0	6.8×10^{34}
S.C. low-β β_v = 0.3m	0.10	0.10	0.35	3.1×10^{29}	0	2.1×10^{35}

Fig. 1

Fig. 2

VII. PHYSICS WITH PROTONS AND ANTIPROTONS AT THE SFM

CERN-Heidelberg-Warsaw Collaboration

(Presented by H.G. Fischer - CERN-EP)

The physics activities around the Split Field Magnet facility during the past years can be grouped into the following main categories:

- elastic scattering /1/

- double Pomeron exchange /2/

- diffraction /3/

- high p_T physics /4/.

Due to some problems with the original SFM detector and software analysis chain, this first generation of experiments missed some important topics like the study of general inelastic events (which should be a unique field of physics for the SFM due to its large acceptance) and the physics with leptons and lepton pairs.

These problems were mainly connected with acceptance and reconstruction losses, with a rather voluminous and thickwalled vacuum chamber and with missing particle identification.
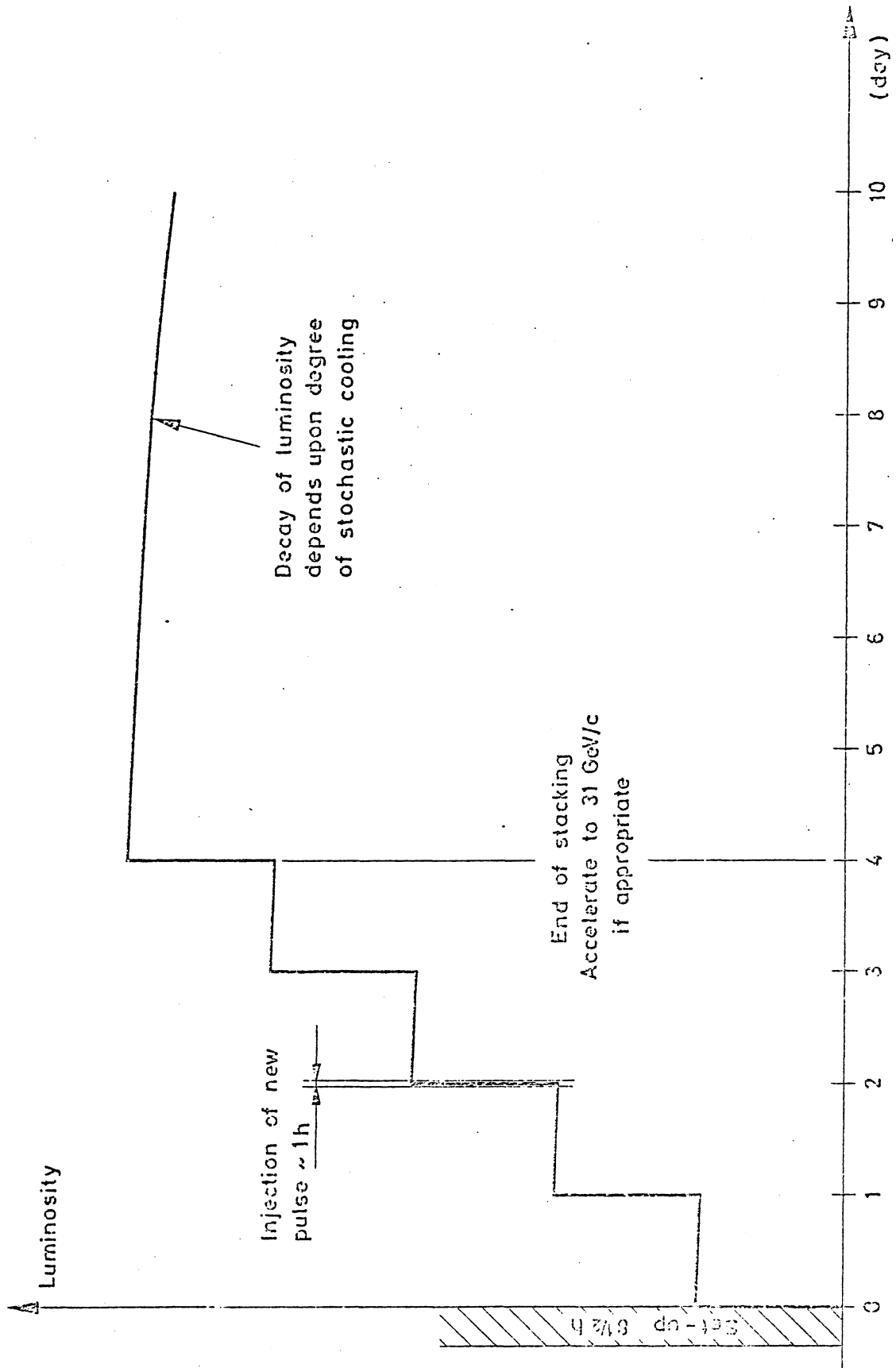
The SFM improvement program, which was carried out in 1976 and 1977, removed a large part of these shortcomings.

Particle identification via time-of-flight, Cerenkov counters and dE/dx techniques was introduced.

The acceptance for charged tracks was drastically improved. This is demonstrated in fig.1, which shows the measured, uncorrected charged multiplicity distribution with the old and the improved SFM detector.

Fig.2 shows a multiprong event in the new detector. Preliminary results on corrected multiplicity distributions are in good agreement with data published by the streamer chamber experiment R701 /5/, see fig.3.

The track finding efficiency, which showed a decline with increasing multiplicity, has been improved and is now independent of multiplicity as shown in fig.4. The overall level of efficiency in the new detector will increase further once the software is completed.

Finally, the new vacuum chamber contributed an essential part to the improvements by a drastic reduction in the rate of secondary interactions, photon conversions and subsequent spiralling secondaries.

With the first measurement of hadronic production of charmed mesons /6/, it was demonstrated that the SFM can also contribute in the field of hadron spectroscopy. Indeed, its full event reconstruction capability is an essential help in identifying small signals in the presence of a large combinatorial background.

Figs.5 and 6 show different stages in the localization of, first, a K^* signal and, second, a D^+ signal in the decay channel $K^* \pi^+$ by kinematical and topological cuts.

For future experiments, both with proton-proton and proton-antiproton interactions, the list of physics activities given above can be enlarged to contain also

- general inelastic collisions ("minimum bias events")
- hadron spectroscopy
- physics with leptons and lepton pairs.

For $\bar{p}p$ physics, annihilation triggers as studied for instance by Rushbrooke /7/ become feasible.

In all these topics, the unique possibility to study
correlations over the full phase space and especially with lea-
ding particles, makes the SFM an attractive alternative to
existing or planned, more specialized experiments. The improved
SFM detector should therefore have an active future at the ISR.

References

The references 1 to 4 give a small extract from the many
publications on SFM physics. For more information consult e.g.
the list of ISR physics publications edited by L.Passardi and
K.Potter (ISR).

/1/ CHOV collaboration E.Nagy et al to appear in Nucl.Phys.B

/2/ CCHK collaboration D.Drijard et al Nucl.Phys. B143(1978)61

    CHOV collaboration H.deKerret et al Phys.Lett.68B(1977)385

/3/ CHOV collaboration H.deKerret et al Phys.Lett.63B(1976)477

    G.Goggi et al Phys.Lett.72B(1977)261

/4/ CCHK collaboration M.Della Negra et al Nucl.Phys.B127(1977)1

    BFS collaboration M.G.Albrow et al Nucl.Phys.B135(1978)461

/5/ ACHM collaboration H.Albrecht et al Nucl.Phys.B129(1977)365

/6/ CCHK collaboration D.Drijard et al submitted to Phys.Lett.B

/7/ J.G.Rushbrooke CERN/EF 78-7

Figure captions

Fig. 1 : Uncorrected charged multiplicity distributions for the old
           and improved SFM detector.

Fig. 2 : A multiprong event as seen in the new detector

           (a) plan view

           (b) view along the beam axis.

Fig. 3 : Preliminary data from experiment R 416, corrected charged
           multiplicity distribution compared to the results of
           experiment R 701.

Fig. 4 : Track finding efficiency as a function of particle
           multiplicity for the old and new detectors.

Fig. 5 : A $K^-\pi^+$ mass spectrum from experiment R 416 showing a K^* peak.

Fig. 6 : Emergence of a D^+ signal in $K^-\pi^+\pi^+$, $K^-\pi^+$ in K^*, with different
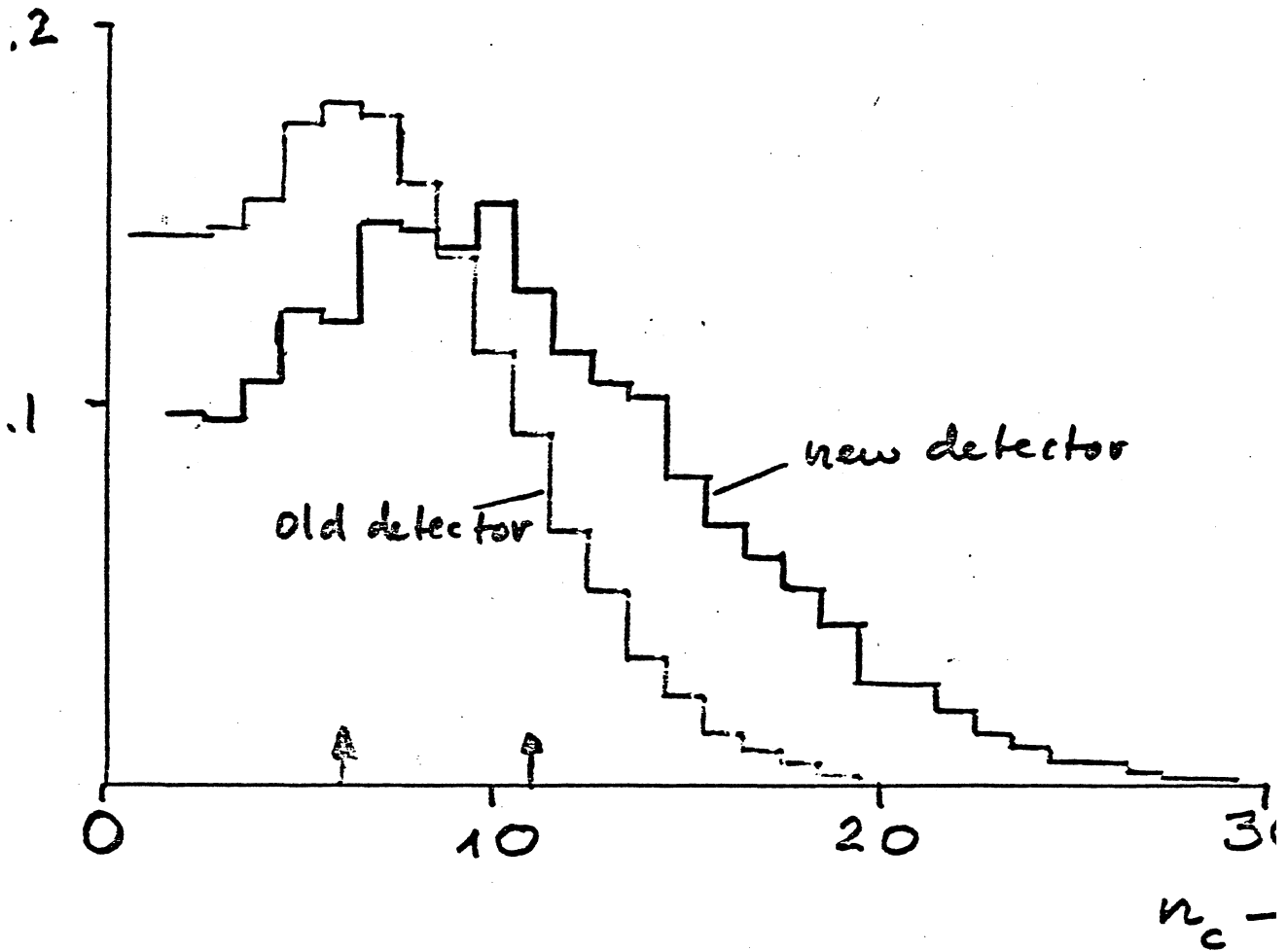   kinematical and topological cuts.
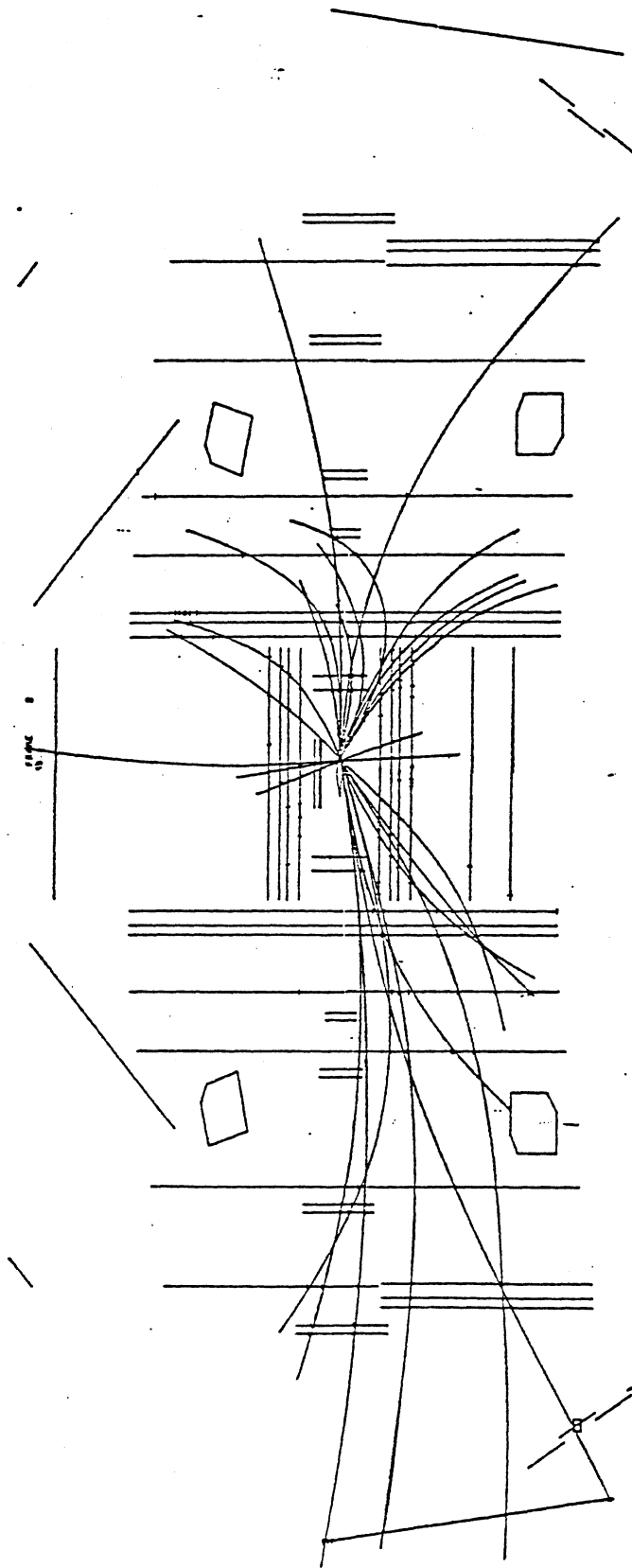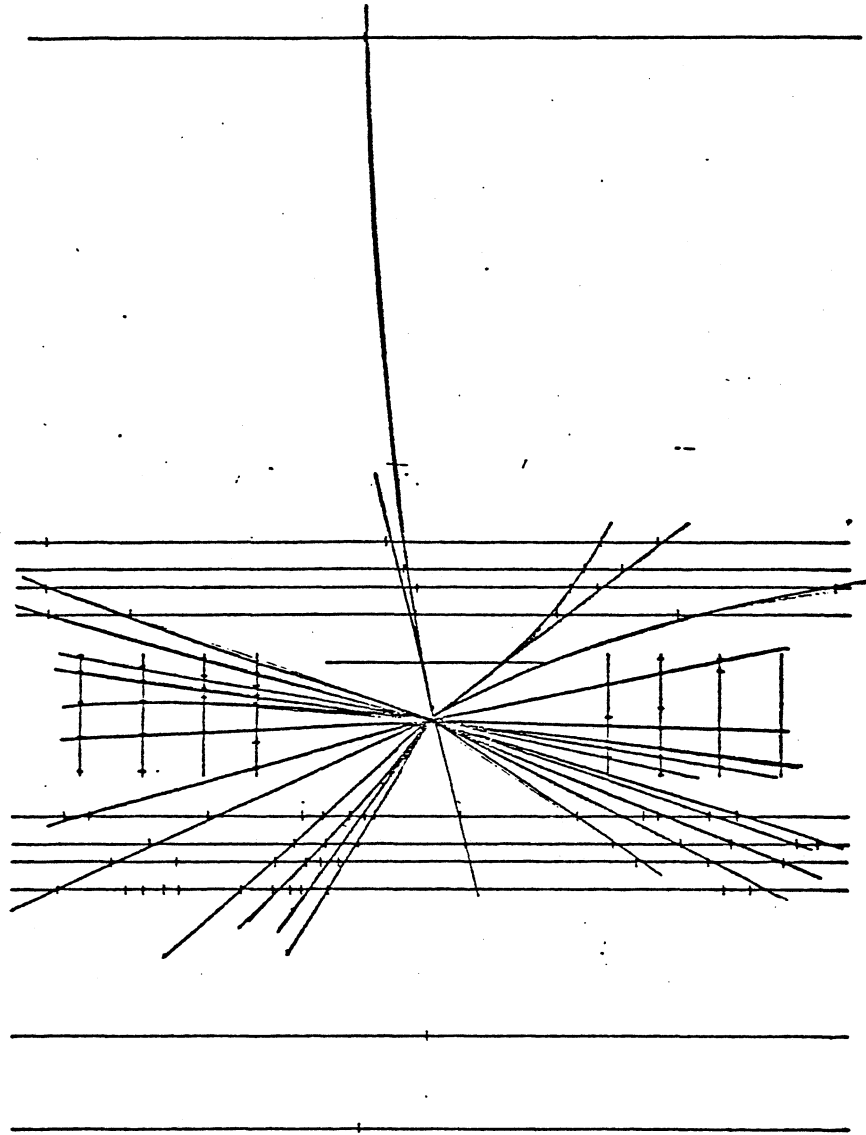
SFM

charged multiplicity

raw data

Fig. 1
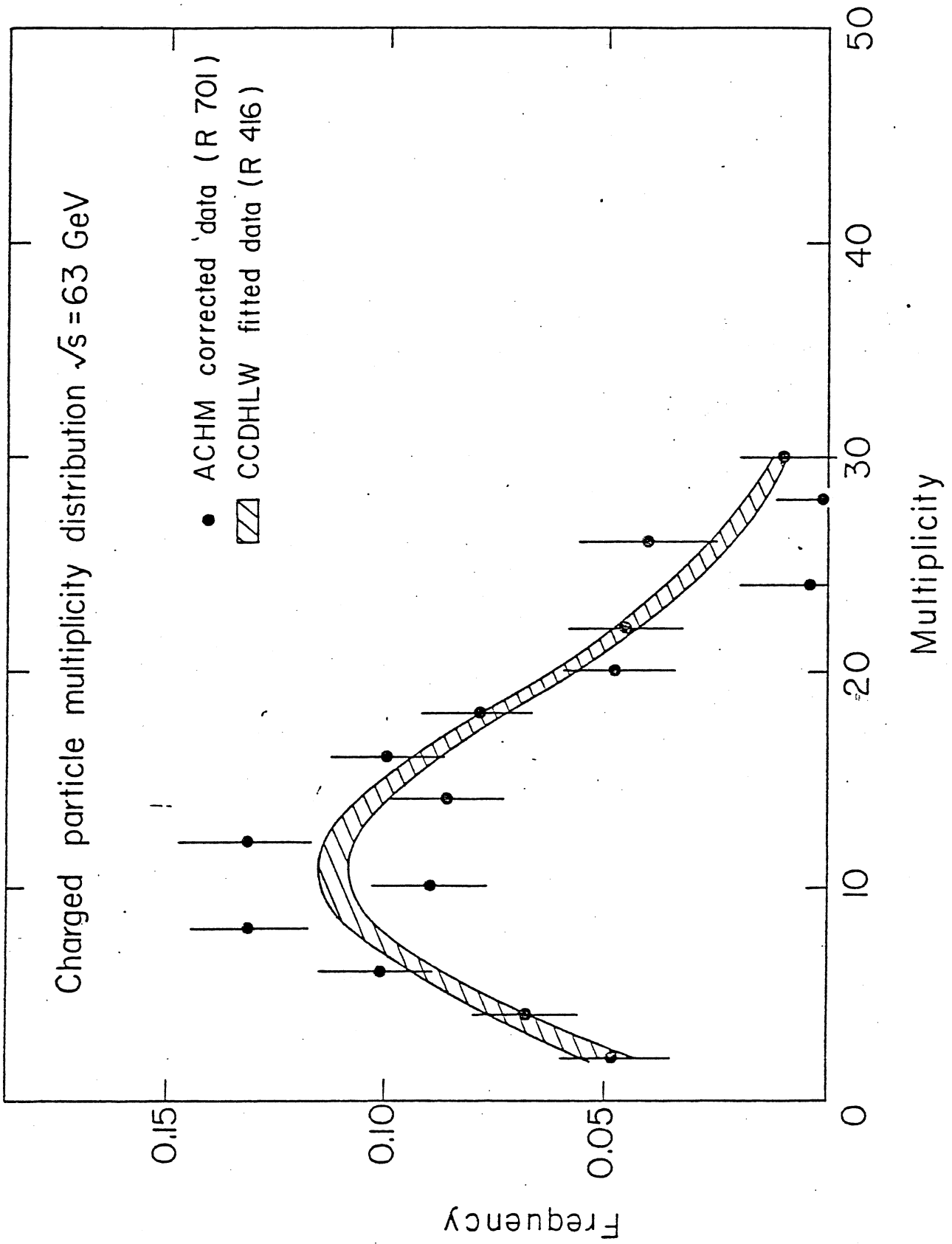
38 prong event
top view

Fig. 2a

View along beam axis

Fig. 2b

Fig. 3

Fig. 4

Fig. 5

$K^- \pi^+ \pi^+$ mass spectrum with $(K^- \pi^+)$ in K^*

(A)*(B)
(A)*(B)*(C)
(A)*(B)*(C)*(D)

Number of combinations / 80.MeV

300

200

100

0

1.0   2.0   3.0   4.0

M ($K^- \pi^+ \pi^+$) , GeV
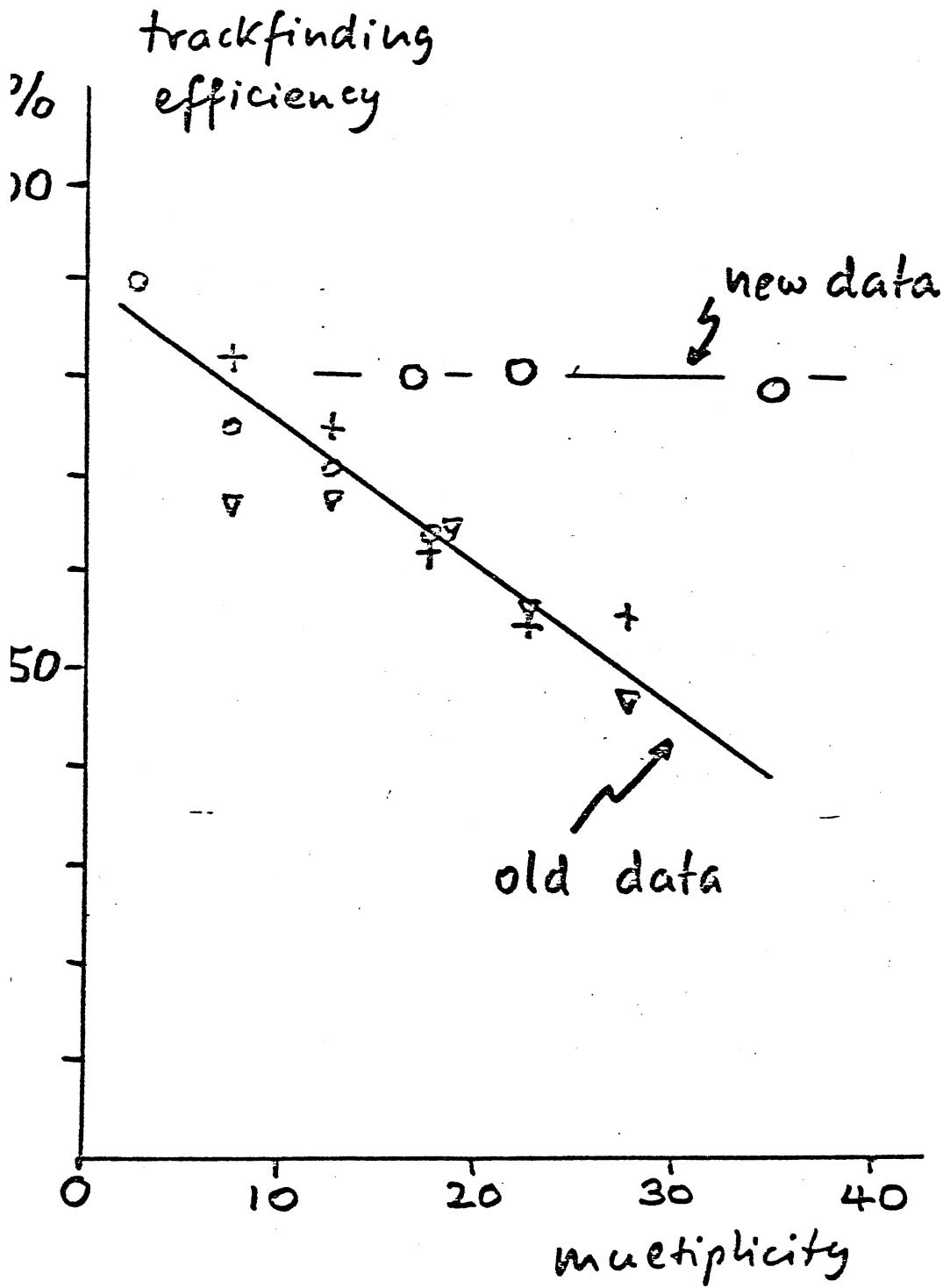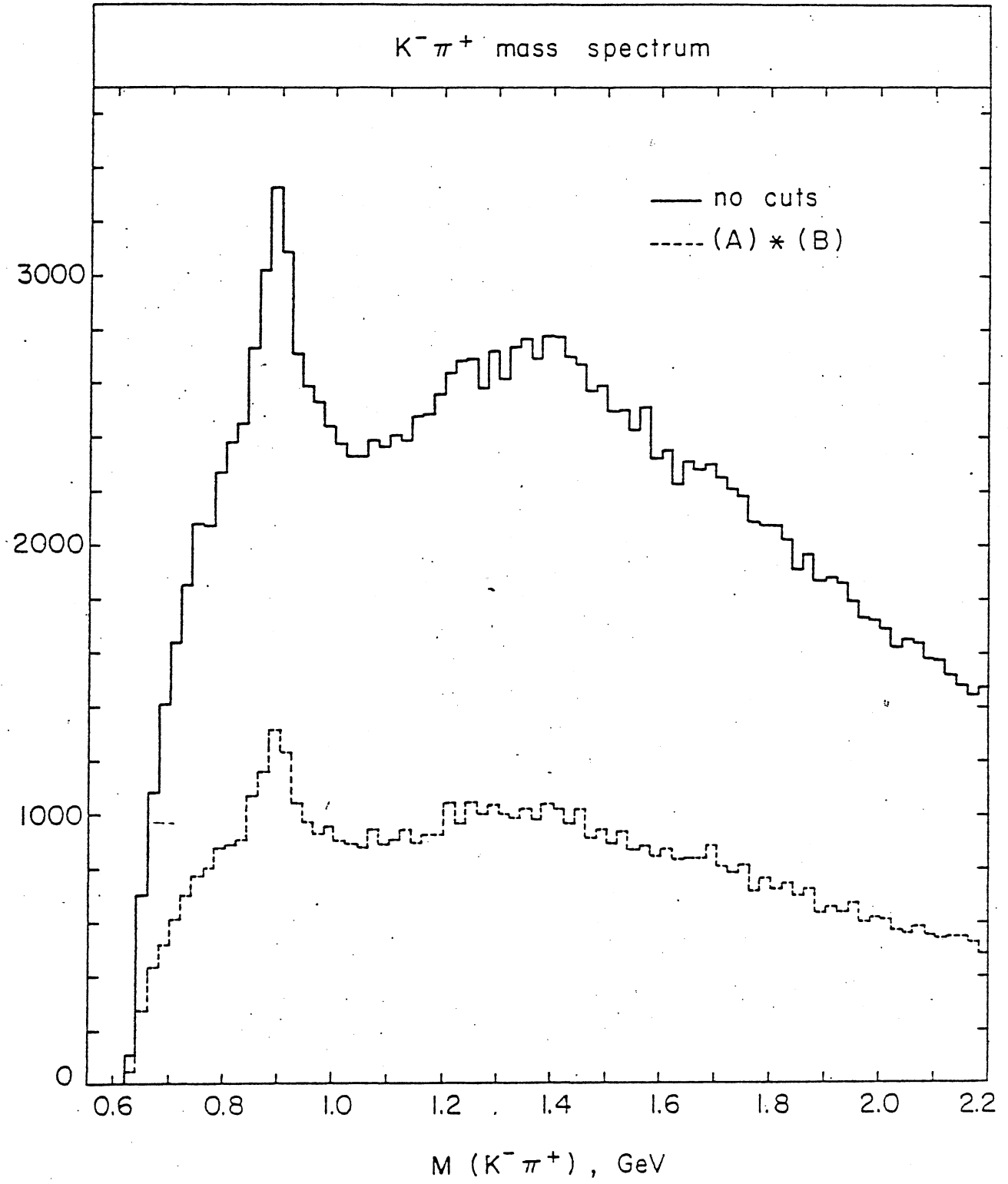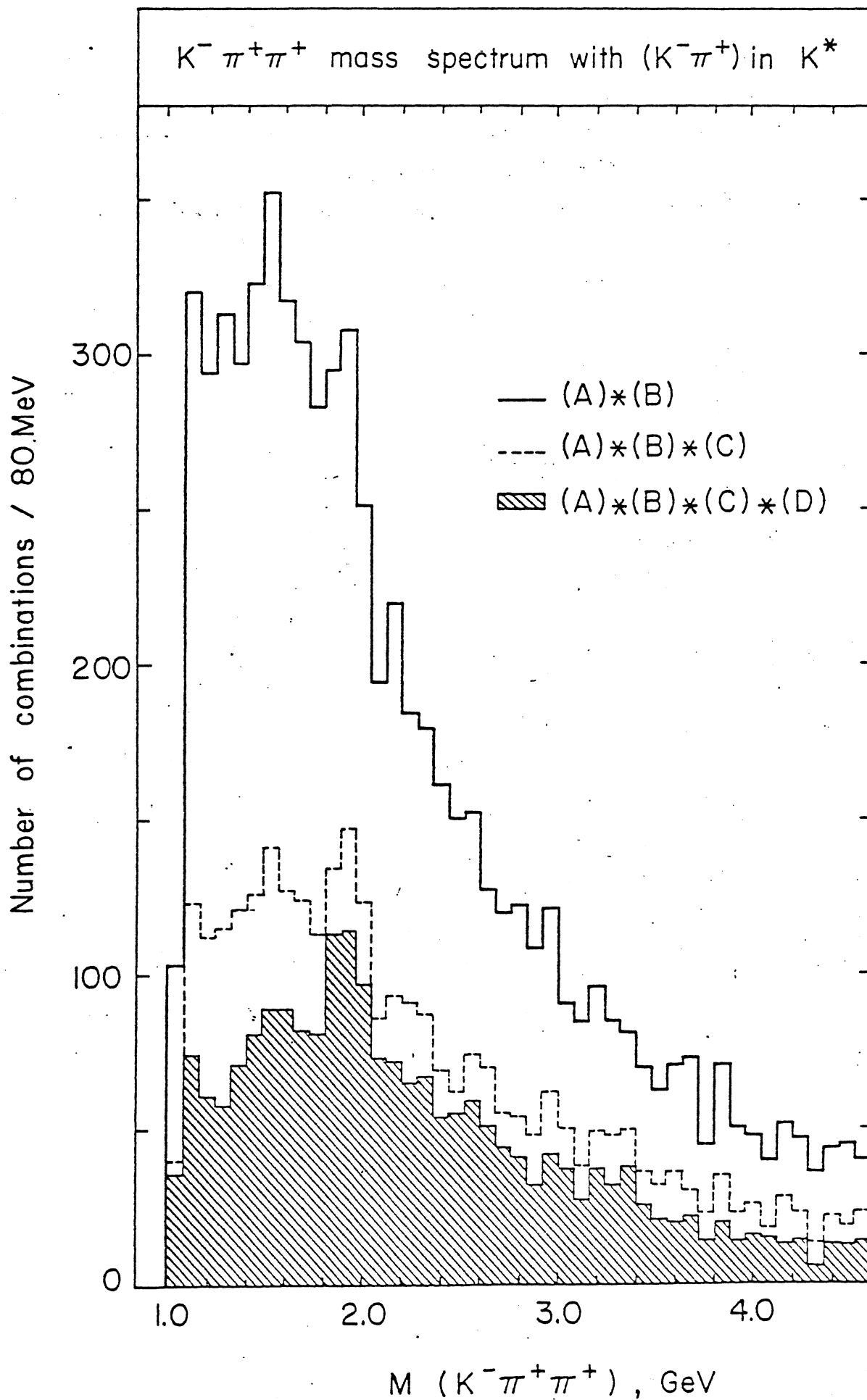
VIII. <u>PHYSICS WITH $\bar{p}p$ COLLISIONS IN EXPT. R 807</u>

M.G. Albrow - Rutherford Laboratory (CERN-EP)

Experiment R 807 is the Axial Field Spectrometer, currently being installed in Intersection 8 at the ISR by the CERN-Copenhagen-Lund-Rutherford Collaboration. The next six months will see a build up of the apparatus towards its final form in parallel with a commissioning programme so that hopefully by the summer/autumn of this year we might take some good data. The calorimeter, however, will be later and not complete before 1980. It is an experiment to study in as much detail as possible the 'deep region' : large angles $\theta_{cm} > 20^{o}$ and large p_T (> 5 GeV/c). The experiment will run in two configurations or phases by reshuffling the equipment. The first phase is shown in Figure 1. The Open Axial Field Magnet, designed by T. Taylor (ISR) provides a 5 kG field with azimuthal symmetry, parallel to the beams. The magnet may be thought of as a pair of Helmholtz Coils with a return yoke on the floor beneath. Between the poles will be a central drift chamber with 42 layers of wires parallel to the beams, arranged in (82) 4° ϕ sectors. The precise (drift) measurement is the transverse coordinate x,y, i.e. in the bending plane, with a $\sigma \simeq 200$ μ which will give $\Delta p/p \simeq 1.5$ p (GeV)%. Alternate wires are displaced slightly right and left of a radius vector to resolve the left/right ambiguity. Each wire end is equipped with an ADC, thus charge division will be used to determine the longitudinal coordinate (Z) with $\sigma_Z \simeq 6 - 8$ mm. The resulting charge signals will also be used to measure $\partial E/\partial x$ for each track. With a fractional energy loss measurement to $\simeq 16\%$ particle identification will be possible for $\pi/k/p$ up to $\simeq 1$ GeV/c and for electrons over most of the range up to $\simeq 10$ GeV/c. This would, however, only be achieved when the full chamber depth is traversed, $\theta \geq 40^{o}$. A hardware processor (ESOP) is being built to be able to use the D.C. information in a fast on-line filter, for example by looking for straight tracks in the transverse plane.

The calorimeter in phase I covers 270° of azimuth and is made of uranium-scintillator sandwich, read out via wavelength shifter plates with $\simeq 2000$ p.m.t's. The front section (5 radiation lengths) and the back section (3 interaction lengths) are separately read out to provide electromagnetic/hadronic identification capability. Thus, in conjunction with $\partial E/\partial x$ measurements on tracks, electrons can be identified over $\simeq 6$ srad. The calorimeter will have a resolution $\simeq \frac{14\%}{\sqrt{E}}$ for electromagnetic showers and $\simeq \frac{30\%}{\sqrt{E}}$ for hadronic showers, and the shower centre-of-gravities can be located to within a few centimetres by light-sharing techniques. A system of triggers is being developed to allow triggering on various energy

deposition configurations, e.g. (a) Total Energy ($\theta > 45^{\circ}$) above a threshold, (b) one high energy localised cluster above a threshold, (c) two clusters, etc. The calorimeter has several purposes - the main one being the study of high p_T jets by triggering, the second being detection of neutral particles (π^{0}, K^{0}_{L}, n, etc over a large solid angle, the third identification of electrons, etc.

Finally, in this phase 45° of azimuth, $45^{\circ} < \theta < 135^{\circ}$ (which is 1 steradian) consists of a hadron identification sector. Three successive hodoscopes, (i) aerogel, 88 cells, n = 1.05, (ii) high pressure freon, 24 cells, (iii) atmospheric freon, 18 cells, have the capability of identifying π, k, p up to $\simeq$ 12 GeV/c apart from a small region of ambiguity (which can be moved in momentum if required). Two layers of proportional chambers in this sector are used both for following the tracks determined in the drift chamber to ensure continuity (no interactions or decays) and for providing a high p_T single particle trigger.

That is basically the phase I set-up, best suited to high p_T particle identification, and probably the one that will mostly be used with $\bar{p}p$ in the ISR. It should be noted that I8 will be equipped with the superconducting low-β insertion which increases the luminosity to values $\simeq$ 10^{30} cm^{-2} sec^{-1}.

The phase II set-up which will be used for some of the time has an extra calorimeter wall in place of the Cerenkov sector, thus providing full azimuthal coverage for $45^{\circ} < \theta < 135^{\circ}$. This is shown in Figure 2. It is better suited for topology studies (2 jets, > 3 jets, non jet events, etc.) as the trigger can be on large total transverse energy without bias as to its azimuthal configuration. In addition, muons can be triggered on and identified in the following way : the high pressure and atmospheric Cerenkov counters are placed behind the calorimeter at opposite azimuth, along with proportional chambers and extra hadron absorber. High p_T muons can be triggered by the p.c.'s as tracks apparently originating from the diamond despite passage through the calorimeter and extra absorber. The Cerenkovs can be set to count muons, and in addition a minimum ionizing signal can be required in the calorimeter. The momentum is of course well measured in the upstream drift chamber. This configuration is then good for jets, e pairs and over a more restricted solid angle for μ pairs. In addition of course one may look for μe, μ-jet, e-jet types of events.

- - - - -

I now turn to a summary of the physics interest for us of $\bar{p}p$ collisions, not forgetting that we can very directly compare $\bar{p}p$ with pp in the same apparatus, a very nice feature of the ISR project. Figure 3 shows the phase space of the collisions, the dashed line showing roughly the coverage of R 807, $\gtrsim 20-30^{\circ}$ for tracks in the inner drift chamber, $> 45^{\circ}$ for jets in the calorimeter and for identification in the Cerenkov arm. The fragmentation regions are not studied. Low p_T central region particles can and will easily be studied from a minimum bias type trigger - this is very quick and easy and although we do not emphasize it, no doubt we shall get data of this type to look at general particle/ resonance production. It is the deep region, $\theta > 45^{\circ}$, $p_T \gtrsim 5$ GeV/c that is really of interest to us. One would include under the same heading the study of high mass dileptons, e.g. Υ, and continuum production. In our present understanding this is the physics dominated by large Q^2 parton-parton collisions, and as p_T or $x_T = \frac{2p_T}{\sqrt{s}}$ goes up so does both Q^2 and the x-region of the proton/antiproton which is probed. It is mainly in this region that one might expect big differences between $\bar{p}p$ and pp collisions, depending on how dominant the valence quarks are compared to gluons (and sea) as x increases byeond $\simeq 0.2$. For valence-valence collisions in pp only t and u channel scattering are allowed. For $\bar{p}p$ one has in addition the s-channel annihilation diagram, and it is a safe prediction that $\sigma(\bar{p}p) > \sigma(pp)$ for production of high p_T jets, for example.

Taking this further, assume that both p and $\bar{p}$ have three types of constituents : gluons, sea quarks and antiquarks, and valence quarks. All but the last should be identical for p and $\bar{p}$, and the last (v) should be the C-reflection $q \rightarrow \bar{q}$. There are, of course, many types of constituent-constituent collisions possible, and for many of the types either t/u channel scattering or annihilation is possible. $\bar{p}p$ is essentially identical to pp except for the valence-valence annihilation term, which can be statistically measured by subtraction.

Thus for high p_T jets

$$\frac{d^2\sigma}{dEd\Omega}\bigg|_{\bar{p}p} - \frac{d^2\sigma}{dEd\Omega}\bigg|_{pp} = \frac{d^2\sigma}{dEd\Omega}\bigg|_{v\bar{v} \text{ ann.}}$$

or for lepton pairs

$$\frac{d\sigma}{dMdy}\bigg|_{\bar{p}p} - \frac{d\sigma}{dMdy}\bigg|_{pp} = \frac{d\sigma}{dMdy}\bigg|_{v\bar{v}}$$

Now the valence quark distributions are rather well known and thus we may expect

that we will learn rather directly about

$$\frac{d\sigma}{d\hat{t}} \ (\hat{s},\hat{t}) \ \text{for} \ q\bar{q} \ \rightarrow \begin{pmatrix} g \\ \gamma \end{pmatrix} \ \rightarrow q\bar{q}, \ell\bar{\ell}$$

This would be a very important study for many reasons :

1. It is calculable in QCD :
   photonic annihilation and weak annihilation are present at some
   low but calculable level. ·

2. A massive gluon, from the annihilation, has all kinematically possible
   $q_i\bar{q}_i$ decay channels open to it. Thus $c\bar{c}$, $b\bar{b}$ can be produced, and charmed
   and other exotic particles may be relatively abundant.

Before getting too optimistic, we should look a little at possible rates given
our luminosity and acceptance. With the superconducting low-β insertion we can
hope for $L \simeq 10^{30} \ cm^{-2} \ sec^{-1}$. Not knowing the cross-sections we can take pp
as a lower limit, where the ISR data on π^0 extend to $\simeq$ 15 GeV/c in p_T. We take
a factor 3 for $\frac{\text{all hadrons}}{\pi^0}$ assuming $\pi^+ + \pi^- = 2 \ \pi^0$ and $k^+ + k^- + p + \bar{p} = \pi^0$.
Our Cerenkov arm is 1 sterad of solid angle and will be equipped with a trigger
for single high p_T particles. The rates/hour and per month, given 25%
efficiency, are shown in table 1. Clearly, the single particle spectra are
petering out by $\simeq$ 10 GeV/c. However, (a) these, being pp, are lower limits,
(b) the cross-sections for jets are probably a factor of $10^2 - 10^3$ higher.
Thus, in $\bar{p}p \rightarrow$ jet + X, 15 GeV may be within reach. Note that for jets we have
a solid angle up to $\simeq$ 8 times larger than the Cerenkov arm.

To what extent are valence-valence collisions going to dominate?
This is still a very open question. Some important data from FNAL
(Chicago-Princeton) show that in pp collision the π^+/π^- ratio begins to take
off for $x_T \gtrsim 0.3$ (see Figure 4). Remembering that gluons and sea quarks
should give equal numbers of π^+ and π^-, this hints that one has to go to
$x_T \gtrsim 0.3$, $p_T \gtrsim 8$ GeV at $\sqrt{s} = 53$ GeV, before vv becomes important relative to
other terms. Incidentally, this rise has not yet been seen at the ISR; it will
be an early thing for R 807 to look for.

Some of our theoretical colleagues agree that this is where vv collisions
begin to dominate high p_T production. Owens, Reya and Gluck for example have
shown a QCD calculation of π production at the ISR. For $pp \rightarrow \pi^0 + X$ the
calculated $qq \rightarrow qq$ term is almost as large as the data for $p_T \gtrsim 8$ GeV and much
larger than other terms (see Figure 5).

But this dominance or otherwise must depend rather crucially on the gluon structure functions. All we really know is that the gluons carry $\simeq$ 50% of the hadrons momentum : $\int xg(x) \, dx \simeq 0.5$. I shall demonstrate this ignorance by showing two examples of theorists 'guesses'. The first is from a paper by Buras and Gaemers (CERN-TH-2322) who were especially concerned with the Q^2- dependence or scaling violation. At small Q^2 both the gluons and sea are relatively small by $x \simeq 0.3$ and by $Q^2 \geq 70$ GeV^2 which is the region we shall be studying they have become negligible $-$ (see Figure 6). Thus in this extreme case valence-valence are completely dominant for producing a pair of high p_T jets, $p_T \geq 8$ GeV/c.

On the other hand, g(x) may be almost as flat as the valence quark distribution $-$ Figure 7 shows a $(1-x)^4$ distribution used by Feynman, Field and Fox. In this opposite extreme, vv will never completely dominate.

We can obtain information on this, of course, by comparing the $q\bar{q}$ annihilation $\rightarrow$ jet cross section with the total jet cross section, the latter including gg and gv as well.

The next important question is this : even if vv collisions dominate, how large is the annihilation term compared with ordinary t and u channel scattering, given a $u\bar{u}$ collision, say.

This can be calculated in QCD in the Born Approximation, and is a well defined function of $\hat{s}$, $\hat{t}$, $\hat{u}$ and hence of θ, the cm scattering angle. The annihilation term goes like $(1 + \cos^2\theta)$; the t/u scattering terms are much more forward peaked and thus relatively speaking the annihilation/scattering is maximum at $\theta \simeq 90^\circ$ where it is $\simeq$ 40%. This is for $q\bar{q} \rightarrow q\bar{q}$; in addition there is $q\bar{q} \rightarrow$ gg which is comparable.

Another way of looking at the 1 gluon annihilation term is to compare it with Drell-Yan 1 photon annihilation $-$ which can be measured with lepton pairs. The relative cross sections are $\simeq (\alpha_s/\alpha_{cm})^2$ higher which will be perhaps 10^3. A direct comparison of vv annihilation to jet pairs or to lepton pairs would clearly be exciting.

There is another calculation by Peierls, Trueman and Wang, comparing jet production in $\bar{p}p$ and pp collisions, actually at Isabelle energies but the results seem to be essentially dependent only on x_T. The relative difference

$$\Delta(x_T) = \frac{\frac{d\sigma}{dpd\Omega}\Big|_{\bar{p}p} - \frac{d\sigma}{dpd\Omega}\Big|_{pp}}{\frac{d\sigma}{dpd\Omega}\Big|_{pp}} \quad \text{is then a measure of} \quad \left(\frac{\text{annihilation of } \bar{q}q}{\text{scattering of anything}}\right)$$

and reaches $\simeq$ 20% by $x_T \simeq 0.4$ (see Fig. 8) which for jets we can certainly reach. Th is not a large percentage; so the questions are :

1. Can one separate out the annihilation term by subtraction?

2. If so, does it go like $1/p_T^4$? Can one measure the $\hat{t}$ and $\hat{s}$ dependence?

3. How democratic is it, i.e. how good at producing $c\bar{c}$ or $b\bar{b}$ compared with $u\bar{u}$ or $d\bar{d}$ primary quarks?

Finally, I come on to lepton pair physics, which these days hardly needs any justification. Among others, Berger has calculated relative production cross sections. The supposedly scaling quantities (pre QCD!) $M^3 \frac{\partial\sigma}{dMdy}$ is much flatter for $\bar{p}p$ than for pp as you would expect (Figure 9). The ratio could get very large at large mass. This calculation is, of course, very uncertain, as it depends strongly on assumed gluon (and sea) distributions at large Q^2. Therefore a measurement is of great importance.

In R 807 we might expect to measure Drell Yan with $\bar{p}p$ up to $\gtrsim$ 15 GeV, e^+e^- mass, if this estimate is not optimistic. In the calculation the dominant diagram has a gluon jet emitted to balance the p_T of the lepton pair - which may not be large but is an interesting measurement to make. Of course, the same diagram gives on-mass shell (real) photons, balancing a gluon jet. This is another very important piece of physics. The direct $\gamma : \pi^0$ ratio is expected in QCD to be rising with p_T and perhaps even comparable to 1 for $p_T \simeq$ 10 GeV/c. There are preliminary indications that this might be happening at the ISR. In pp the dominant diagram is probably $qg \to q \to q\gamma$, and a high p_T photon will be balanced by a quark jet. In $\bar{p}p$ maybe (g(x)?) an alternative annihilation diagram dominates, with the $p_T(\gamma)$ balanced by a gluon jet. This could give a clean sample of gluon jets to study, but is difficult physics. In R 807 it would need a special photon detector in front of the calorimeter which is presently being thought about.

To summarize :

1. We believe that it is in the deep (large p_T, high mass) region that differences between $\bar{p}p$ and pp will be largest and most interesting.

2. A direct comparison between $\bar{p}p$ and pp in the same detector is needed to isolate valence-valence annihilation.

3. The study of high p_T jets and single identified particles, and of high mass lepton pairs (continuum and J/Ψ, T) will teach us much
    - gluon distributions
    - QCD terms
    - gluon + quark decay functions

4. We'll want all the luminosity we can get!

Table 1

Rates in Cerenkov Sector, $\Delta\Omega = 1$ sr, $L = 10^{30}$, $\sqrt{s} = 63$ GeV

Lower limits, using pp data on Π° production, and charged hadrons = 3 Π°

p_T (GeV/c)	Rate/hour	Rate/month (400 hours eff. = 0.25)
5 - 6	67	6700
6 - 7	18	1800
7 - 8	5.5	550
8 - 9	1.8	180
9 - 10	0.6	60
10 - 11	0.23	23

Figure captions

Fig. 1   : Layout of experimental equipment of experiment R 807 (Phase I).

Fig. 2   : Experiment R 807 (Phase II).

Fig. 3   : Coverage in phase space of the R 807 detectors.
                 Dashed line limit of inner drift chamber $\geq 20 - 30^\circ$,
                 $> 45^\circ$ for jets in the calorimeter and Cerenkov arm.

Fig. 4   : Π^+/Π^- ratio in pp $\rightarrow \Pi + X$ versus X_T, data from FNAL
                 (Chicago-Princeton)

Fig. 5   : QCD predictions for high p_T Π production at the ISR
                 (Owens, Reya and Gluck)

Fig. 6   : Structure functions from Buras and Gaemers (CERN-TH-2322)
                 at $Q^2 = 70$ GeV^2 (R 807 region).

Fig. 7   : Structure functions $(1 - X)^4$ used by Feynmann, Field and Fox.

Fig. 8   : Jet production in $\bar{p}p$ and pp collisions

$$(X_T) = \frac{\frac{d\sigma}{dpd\Omega}\Big|_{\bar{p}p} - \frac{d\sigma}{dpd\Omega}\Big|_{pp}}{\frac{d\sigma}{dpd\Omega}\Big|_{pp}}$$ Peierls, Trueman & Wang.

Fig. 9   : Lepton pair production from pp and $\bar{p}p$
                 (E.L. Berger, ANL-HEP-PR-78-12).
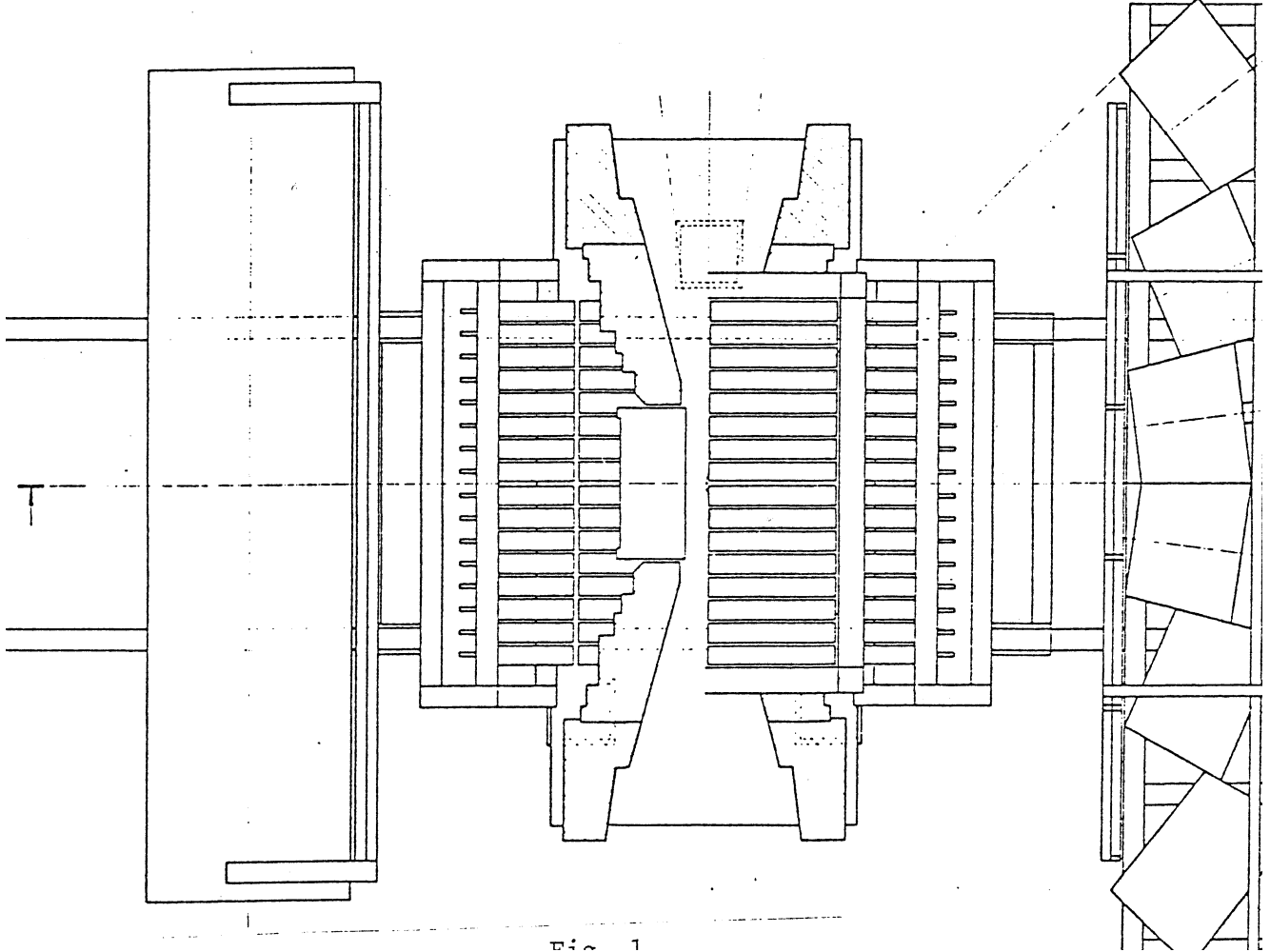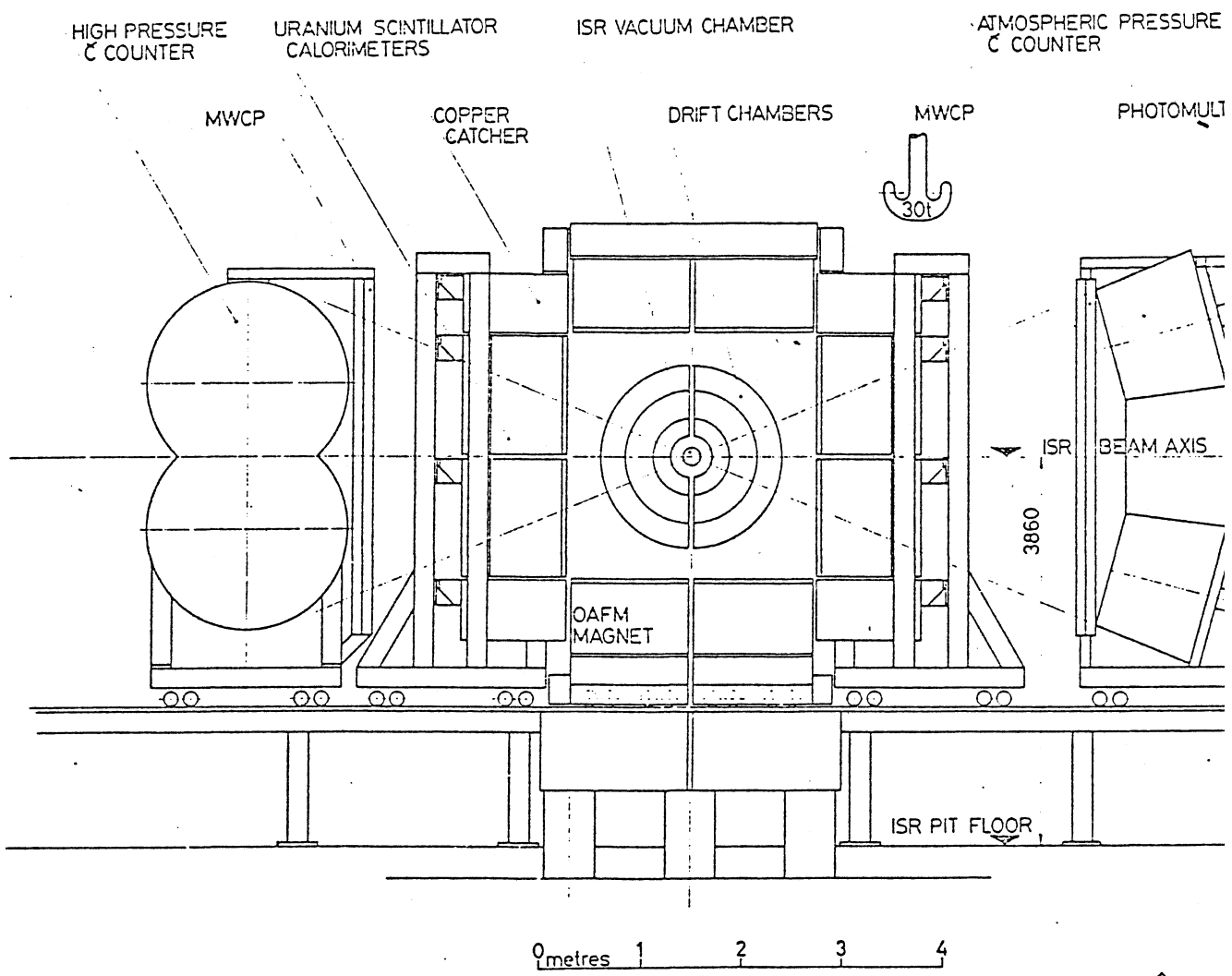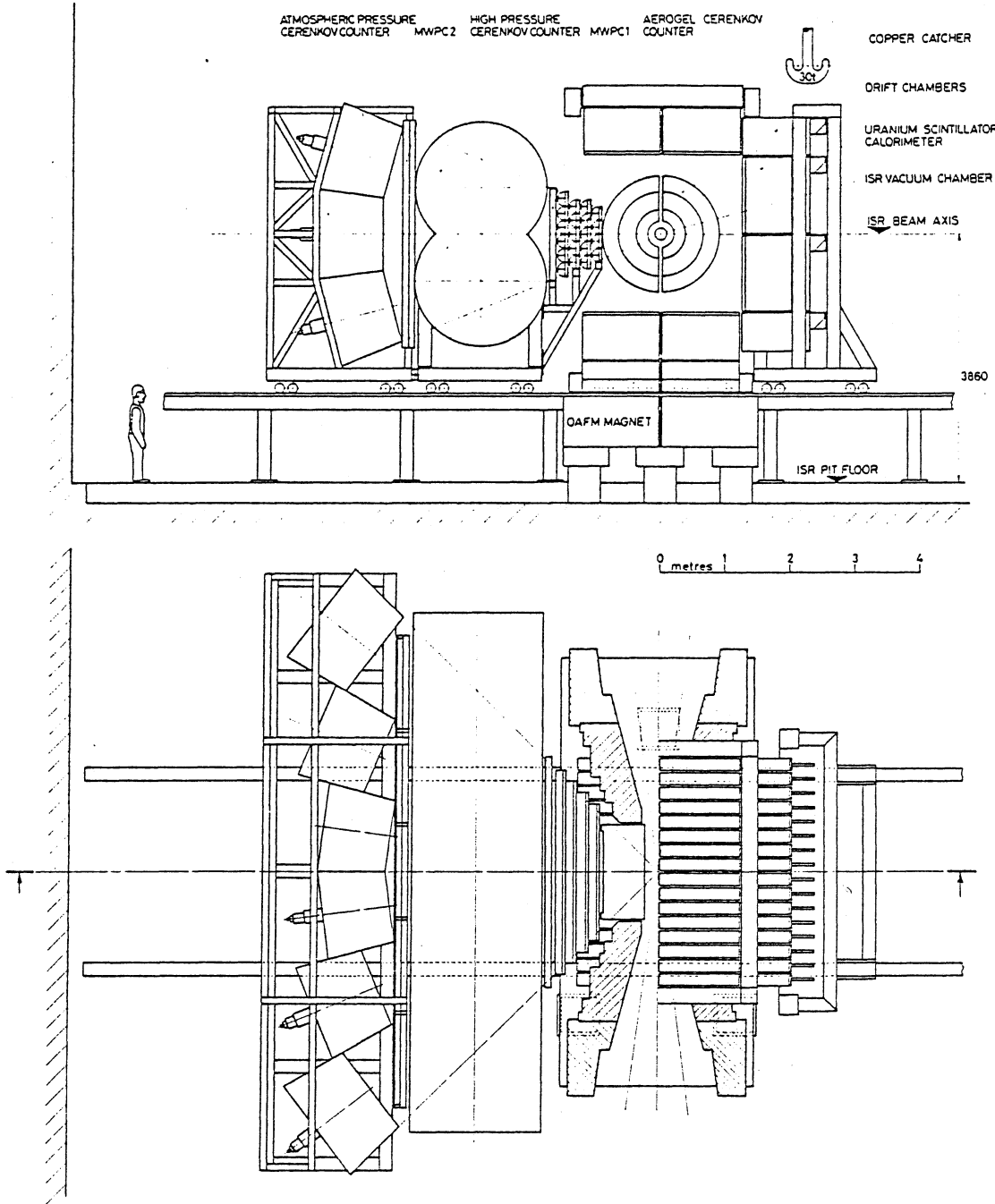
HIGH PRESSURE
Č COUNTER

URANIUM SCINTILLATOR
CALORIMETERS

ISR VACUUM CHAMBER

ATMOSPHERIC PRESSURE
Č COUNTER

MWCP

COPPER
CATCHER

DRIFT CHAMBERS

MWCP

PHOTOMULT

ISR   BEAM AXIS

3860

OAFM
MAGNET

ISR PIT FLOOR

0 metres   1   2   3   4

T

Fig. 1

ATMOSPHERIC PRESSURE
CERENKOV COUNTER   MWPC 2

HIGH PRESSURE
CERENKOV COUNTER MWPC 1

AEROGEL CERENKOV
COUNTER

COPPER CATCHER

DRIFT CHAMBERS

URANIUM SCINTILLATOR
CALORIMETER

ISR VACUUM CHAMBER

ISR BEAM AXIS

3860

OAFM MAGNET

ISR PIT FLOOR

0   metres   1   2   3   4

Fig. 2

fig.3

Fig.4
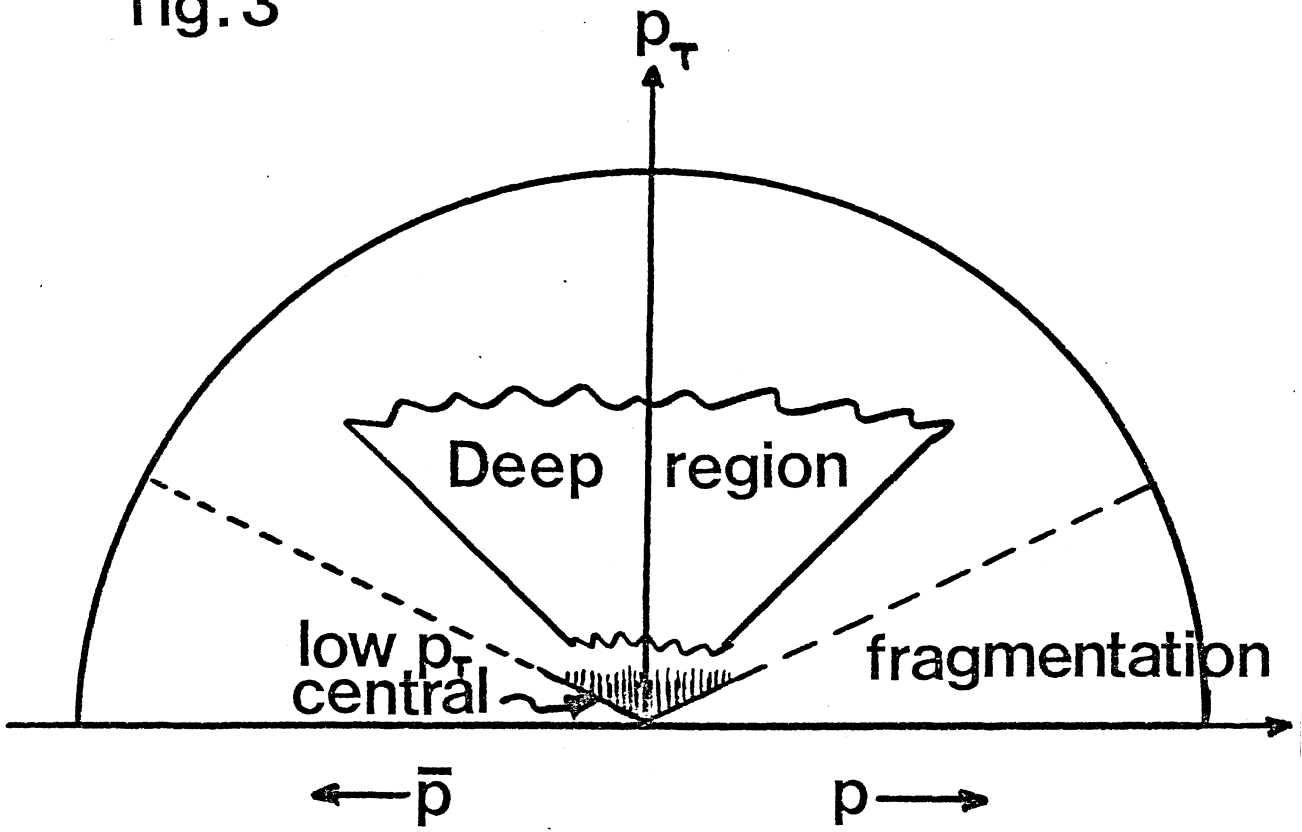

(a)

$p + p \rightarrow \pi + X$

π^+/π^-

∇ 200 GeV
$\square$ 300 GeV
$\circ$ 400 GeV

X_T

OWENS, REYA, GLÜCK   (QCD)

$pp \longrightarrow \pi + X$

$\sqrt{s} = 53$ GeV $(\theta = 90°)$

■
• π^0

○
□ $(\pi^+ + \pi^-)/2$

$gg \rightarrow gg$

$q\bar{q} \rightarrow q\bar{q}$

$E\, d^3\sigma/dp^3$ (cm^2 c^3/GeV^2)

total

$qq \rightarrow q$

$gq \rightarrow gq$

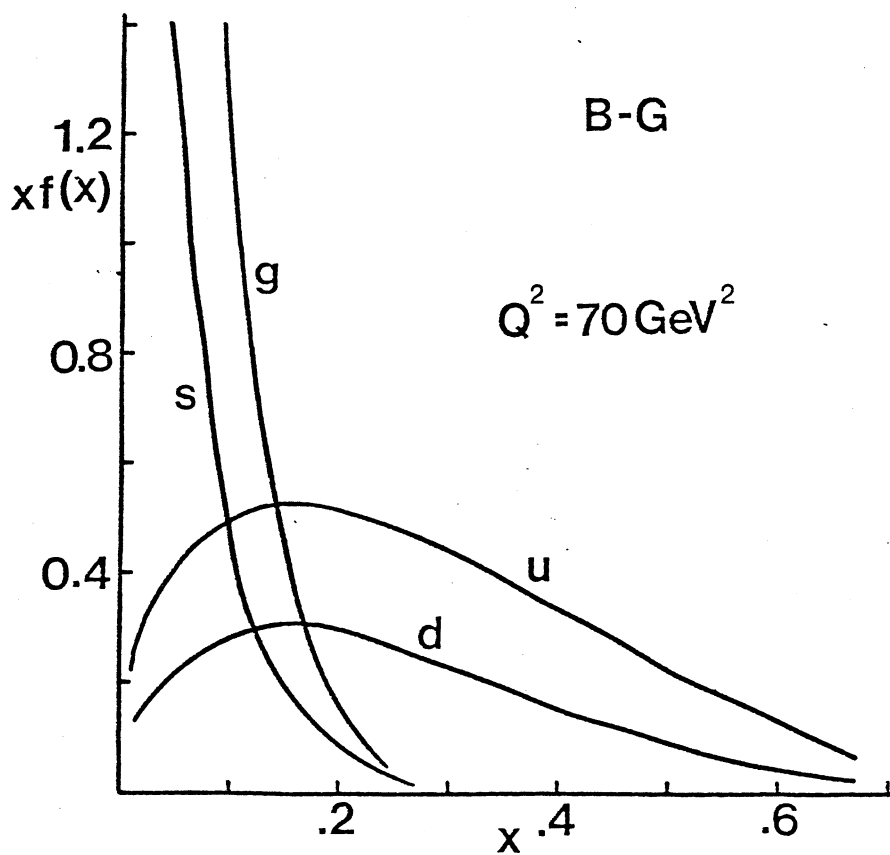$gg \rightarrow q\bar{q}$

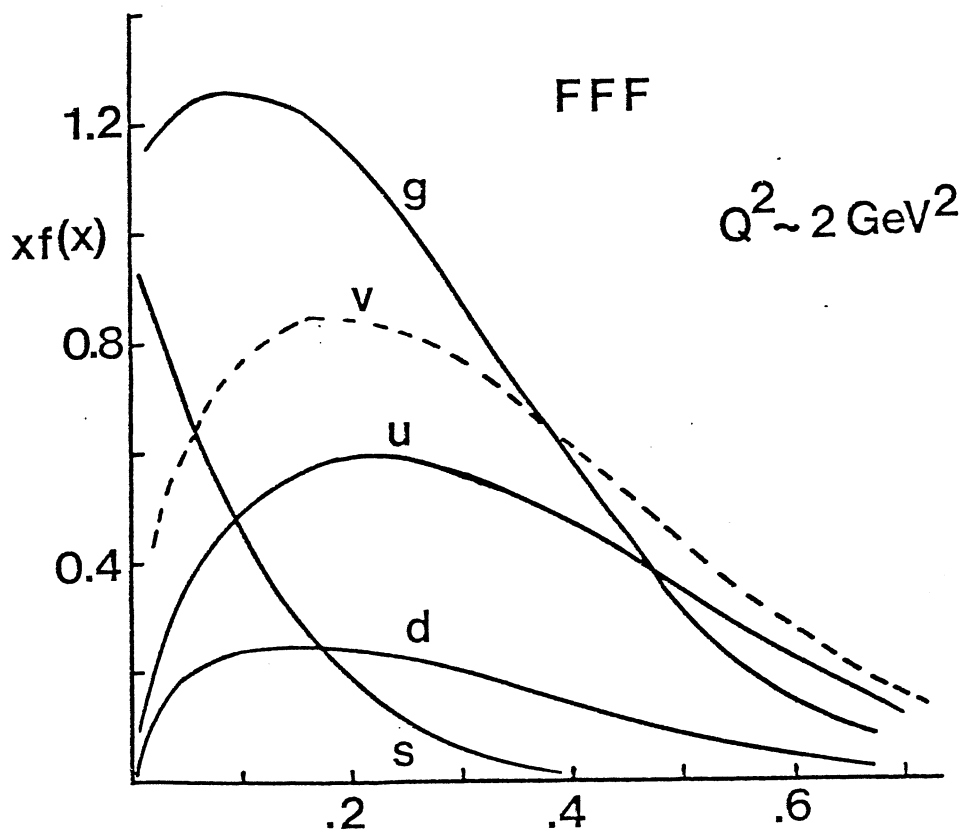$q\bar{q} \rightarrow gg$

P_T (GeV/c)
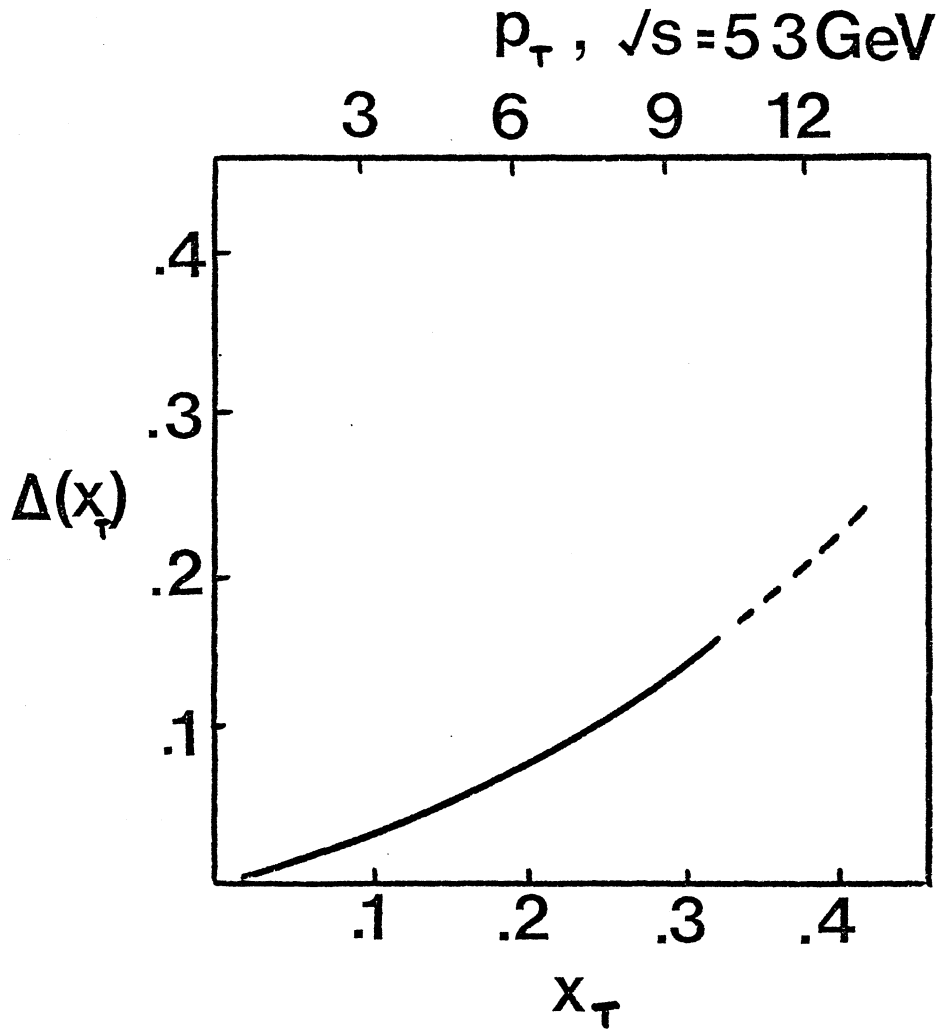
fig 6

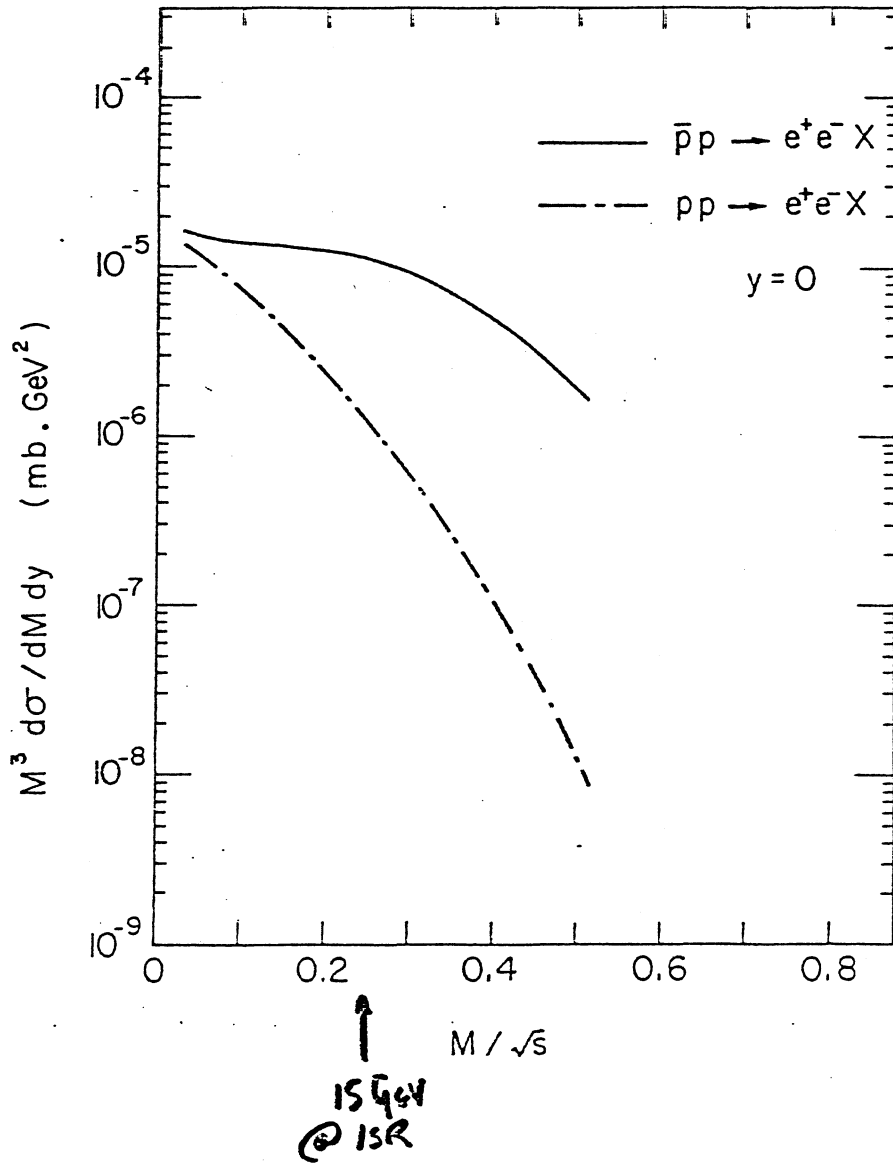
fig 7

fig 8

LEPTON PAIRS

Fig. 9

IX. A PRECISE MEASUREMENT OF PROTON-ANTIPROTON TOTAL CROSS SECTION AT THE CERN ISR

T. Del Prete - CERN-EP

It is not worth spending many words on the relevance of $\bar{p}p$ total cross-section measurement at the ISR. Measurements of $\sigma_T(\bar{p}p)$ at FNAL up to $\sqrt{s} \simeq 20$ GeV show a rate of decrease less pronounced than at lower energies (Figure 1). At the ISR one expects $\sigma_T(\bar{p}p)$ to go through a shallow minimum, start rising and approach $\sigma_T(pp)$. This is confirmed by the difference $\sigma_T(\bar{p}p) - \sigma_T(pp)$ as a function of p_{lab} (Figure 2) which is expected to range from $\simeq 2.0$ to 0.6 mb over ISR energies.

The relatively small increase of $\sigma_T(\bar{p}p)$ ($\simeq 1.5$ mb) and the limited differences $\sigma_T(\bar{p}p) - \sigma_T(pp)$ imply that the total cross-section measurement has to be done with high precision, i.e. a relative error $\Delta\sigma_T/\sigma_T \leq 1\%$.

1. Method

Similarly to R 801, the Pisa-Stony Brook Collaboration experiment, we shall propose measuring σ_T by its own definition :

$$\sigma_T = R_{tot}/L$$

where R_{tot} is the total interaction rate and L is the ISR luminosity.
The choice of this method is essentially suggested by :

i) it is the most direct measurement of the total cross section (no theory needed).

ii) it has provided precise results in two past experiments (R 801 experiment[1,2] performed in 1971/1972 and in 1974. The precision attained there was $\frac{\Delta\sigma}{\sigma} \simeq 1\%$ mostly due to uncertainties of the luminosity calibration.

iii) most of the equipment used in R 801 is still operational and is now installed in the I2 intersection region, providing a 'minimum bias trigger' in the R 209 experiment.

We foresee using the same experimental apparatus (Figure 3) which comprises large scintillation counter hodoscopes surrounding the downstream pipes covering a polar angle down to 3 mrad and an L hodoscope covering the central region of

polar angles $40°-90°$. The azimuthal angle coverage is complete. The hodoscopes are finely divided in θ (polar) and ϕ (azimuthal) bins.

The basic trigger requires at least one charged particle in both L (left) and R (right) hemispheres, the large-angle hodoscope L being a logical part of one of the two hemispheres.

The live-time of each event is part of the information recorded together with the time of flight (TOF) measurement between any pair of hodoscopes and the pattern of fired counters.

The luminosity L is measured by the Van Der Meer (VDM) method.

2. Analysis and Corrections

Let's use the parent experiment R 801 as a basis for the estimate of the typical limitations present in this method for a σ_T measurement of proton-proton interactions.

$$\sigma_T = \frac{1}{L} R_{meas} \times \eta_{extr} \times \varepsilon$$

The measured rate (R_{meas}) had to be corrected (η_{extr}) for the loss of elastic and single diffractive events with one proton scattered off at angles $\leq$ 5 mrad. Another correction (ε) accounted for dead time losses, dead spaces, trigger inefficiencies, randoms in the trigger and TOF chain.

TOF measurements between signals of any pair of hodoscopes and an accurate off-line analysis, allowed the counting of good beam-beam events with a systematic error $\leq$ .3%, essentially independent of the ISR energy and with a negligible statistical error.

Elastic extrapolation was made by integrating over the uncovered solid angle the known $\frac{d\sigma}{dt}$ elastic cross section. Inelastic losses at small angles were similarly determined by empirical extrapolation of the measured angular distributions[2].

η_{extr} ranges from 1.009 $\pm$ .0008 to 1.0681 $\pm$ .004 depending on ISR beam energy.

ε was continuously monitored using LED (light emitting diodes) attached to each counter, simulating real events. Moreover, dead space losses were measured in special runs in which one arm hodoscopes were run in OR. ε is independent of energy and is $\approx$ 1.012 $\pm$ .002 (table I is a summary of rates and corrections).

The ISR luminosity was measured by the VDM method with part of our hodoscope system. This guaranteed a :

i) highly inclusive monitor ($\sigma_{mon} \gtrsim 1/2 \ \sigma_{tot}$)

ii) high counting rate so that the measurement could be done fast to avoid the effects of blowing up of the beams

iii) high stability over months of working time

iv) independence of variations of stacked beams (radial position of source).

v) good handling of background and randoms, by the TOF chains.

The summary of errors on R 801 was as follows :

$$\Delta L/L = \pm \ .5\% \quad \text{point to point}$$

$$\pm \ 1\% \quad \text{scale error}$$

$$\Delta R_{meas}/R_{meas} = \pm \ .3\% \quad \text{systematic, due to single beam subtraction}$$

$$\Delta \eta_{extr}/\eta_{extr} = \pm \ .3\% \quad \text{from elastic and inelastic extrapolations at small angle.}$$

$$\Delta \varepsilon/\varepsilon = \pm \ .15\% \quad \text{statistical error.}$$

We can conclude by saying that the final error was dominated by the luminosity calibration.

3. Improvements

The most important improvement necessary if we want to gain in precision is to reduce the error on the luminosity calibration. This is possible because :

i) a better understanding of systematic effects, like magnet hysteresis, has been obtained by the use of precise scrapers in I5 and I7 (1975)

ii) a precise magnetic beam position detector[3] has been developed tested and run giving a direct measure of beam position with errors $\simeq \pm$ 10 μm.

iii) the background has gone down by a factor of $\simeq$ 10 due to improved ISR operations. This is a general benefit, in particular for the tails of VDM calibration curves.

Thus, we expect, with a correct handling of an inclusive monitor:

$$\Delta L/L \simeq \pm .5\% \quad \text{or better and } \underline{no} \text{ scale error.}$$

It must be stressed that the background reduction will also reduce the systematic error on measured rate to $\Delta R_{meas}/\dot{R}_{meas} \simeq 0\%$.

4. Differences between pp and p̄p Rate Measurements

There is one main disturbing difference between the two reactions: the total charge of final states of p̄p is zero, while for pp it is two. This may imply larger trigger losses. FNAL measurement on pp reactions can shed light on this problem.

Topological cross-sections (Figure 4) are different mainly in the zero prong channel (which cannot exist in pp reactions). This channel is expected to be negligible at ISR energies ($\simeq 10$ µbarns); it is in fact quite small ($\sigma_0 \simeq .07$ mb) at 100 GeV/c and drops as a power of equivalent laboratory momentum. The multiparticle inclusive reactions for pp and p̄p are quite similar at FNAL energies[4], the difference being attributed to annihilation processes. The annihilation processes show a clear leading hadron effect ($\pi^{\pm}$ follows $p^{\pm}$ taking over most of its momentum) and so even these relatively rare channels should not be missed by the trigger.

Exclusive channels like p̄p → n̄n or charge exchange diffraction have all died out. We have an idea of their possible contribution from the measurement of pp → nΔ^{++} performed at the ISR[5] giving a $\sigma_{tot} = (1.2 \div .2)$µb.

As a conclusion there is no evidence that the trigger should be less inclusive in the p̄p case than in pp.

We have already pointed out that the basic Left arm * Right arm trigger detects from 98% to 93% of total rate at the two extreme ISR energies. We are, anyway, considering two main extensions of the trigger in order to avoid even the unlikely probability of missing strange topologies.

A.   Insertion of lead converters in front of the main hodoscopes during special runs.
     In this way the system will become more inclusive, detecting also π^0's.

B.   The use of a 'ONE ARM only' trigger in special runs.
     The rejection of background becomes a major problem and tracking of charged particles with vertex reconstruction will be needed. This extension

of the system is an important one, but not unreasonable since a drift chamber system, built in Pisa and covering almost the full solid angle, is in operation together with the hodoscope system in I2 (R 209) and might be used for this task. In such a way we would gain :

- reduction of extrapolation corrections (rescuing of single diffractive events)

- more safety in triggering on low multiplicity channels

- correlation physics

We end this section on differences between proton and antiproton with the remark that the $\bar{p}p$ elastic scattering cross section is not known at ISR energies. The problem will not be there as soon as data is available from ISR experiments. However, this fact does not make it impossible to correct for elastic losses in a quite reliable way. Elastic events are, in fact, detected by our system and their angular distributions can be integrated over the uncovered small angle region. Another approach is to extrapolate FNAL elastic cross section data to the ISR energy region. In fact, the slope and integrated elastic cross section are approaching the pp ones even at 150 GeV/c and are expected to become equal over the ISR energy range (Figure 5). A quite conservative estimate of the errors on the extrapolation factor gives, for these temporary solutions $\Delta\eta_{extr}/\eta_{extr} \simeq .5\%$ at the highest ISR energy.

5. Conclusions

The total cross section for $\bar{p}p$ (as well as for pp) can be measured with a precision essentially limited only by the luminosity calibration. The method of beam position measurement should be tested and modified for low current beams (.150 Amps), but we can anyway expect, in the worst case :

$$\frac{\Delta\sigma_T}{\sigma_T} \simeq .5\%$$

6. Running of the Experiment

The measurement is based on the following assumptions concerning the ISR :

1. The experiment is installed on an even numbered intersection to exploit as well as possible the small angle region, preferably I2 where the equipment is already installed.

2. Low current proton beam. However, the optimized background conditions should be found empirically.

3. Alternate p̄p and pp runs at similar intensities to reduce any possible systematic effect.

4. The running will be done at the 5 standard ISR energies.

5. Special runs for luminosity calibration are required.

To conclude :

Most of the equipment we have referred to is installed, cabled and fully operational in I2; data acquisition and off-line programmes exist. The running of the experiment, once the 2μ MIT spectrometer has been removed, is fast if we stay in I2. We would consider remeasuring the $\sigma_T(pp)$ during 1980 in order to be confident of the system and to be fully ready, in early 1981, for the beginning of p̄ operations.

References

1) S.R. Amendolia et al. Il Nuovo Cimento, 17A (1973) 735

2) U. Amaldi et al., to be published in Nuclear Physics

3) K. Brand and J-P. Gourber, CERN-ISR-BOM/77-3

4) J. Whitmore, Physics Reports 27C 1976

5) H. de Kerret et al., Phys. Lett. 69B (1977) 372.

TABLE 1

SUMMARY OF RATES AND CORRECTIONS (R 801 - 1974)

$\sqrt{s}$ (GeV)	23.5	30.6	44.7	52.8	62.7
Elastic extrapolation factor	1.0063 ± .0008	1.0131 ± .001	1.0306 ± .002	1.0408 ± .0022	1.0542 ± .0030
Inelastic extrapolation factor	1.0027 ± .0005	1.005 ± .001	1.0096 ± .002	1.012 ± .0025	1.014 ± .003
η_{extr}	1.009 ± .0008	1.018 ± .0014	1.040 ± .003	1.053 ± .003	1.068 ± .004
ϵ	1.015 ± .002	1.013 ± .002	1.012 ± .001	1.010 ± .001	1.010 ± .001
R_{meas}/R_{tot}	0.98 ± .003	0.97 ± .003	0.95 ± .003	0.94 ± .003	0.93 ± .003

Figure captions

Fig. 1   : Total cross-section data for p, $\bar{p}$, π^+, π^-, K^+, K^- at laboratory momenta p_{lab} between 10 and 2000 GeV/c.

Fig. 2   : Difference between $\sigma(\bar{p}p)$ and $\sigma(pp)$ as a function of laboratory momentum p_{lab} between 2 and 300 GeV/c.

Fig. 3   : Schematic layout of the experimental apparatus.

Fig. 4   : $\bar{p}p$ topological cross-sections as a function of laboratory momentum p_{lab} between 2 and 100 GeV/c. The dashed curve is an extrapolation of zero-prong data in the ISR energy region.

Fig. 5   : Total elastic cross-section (upper side) and elastic slope b parameter for $\bar{p}p$ interaction (triangles) and pp interaction (open points) as a function of the laboratory momentum p_{lab} between 10 and 2000 GeV/c.
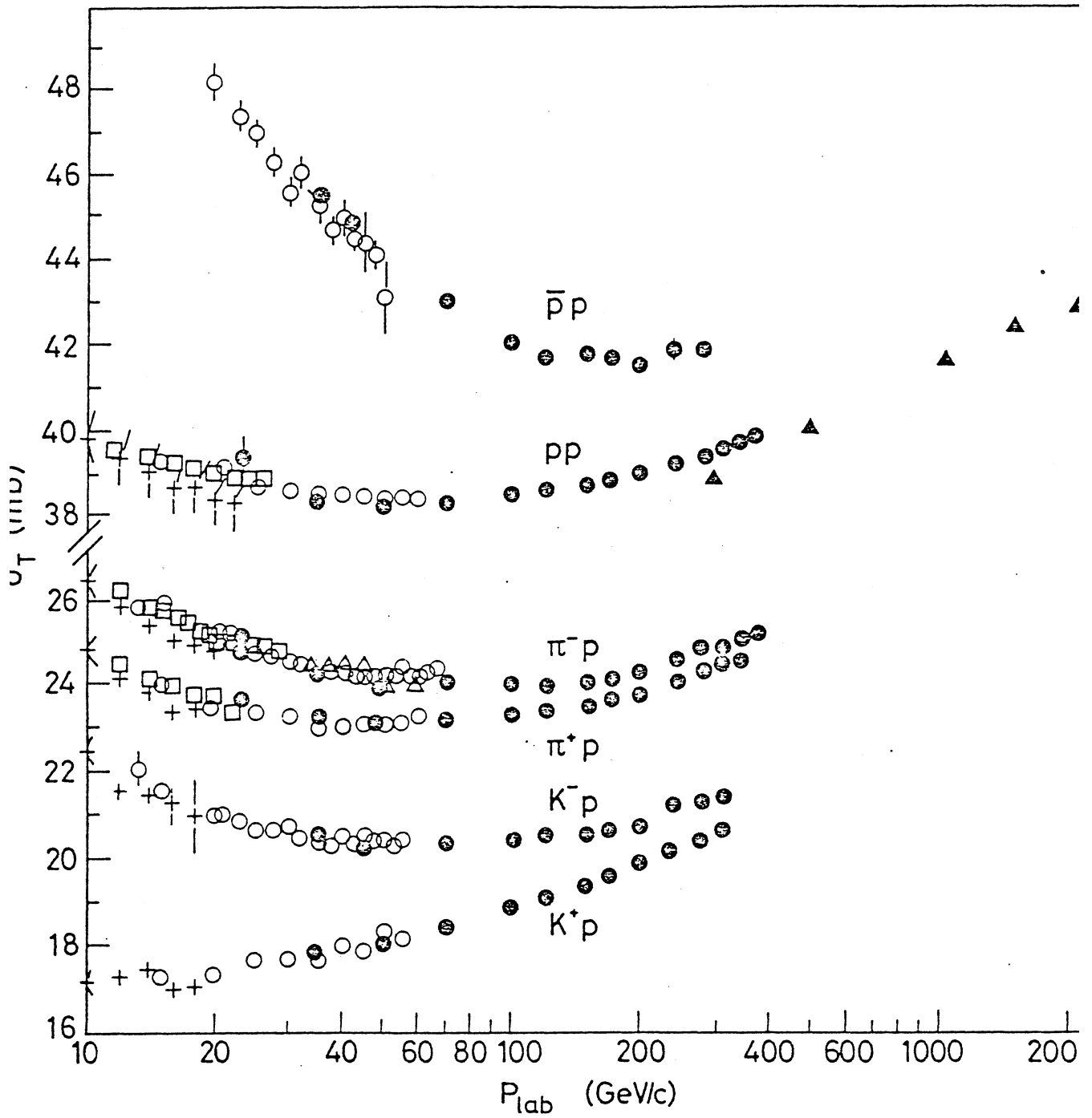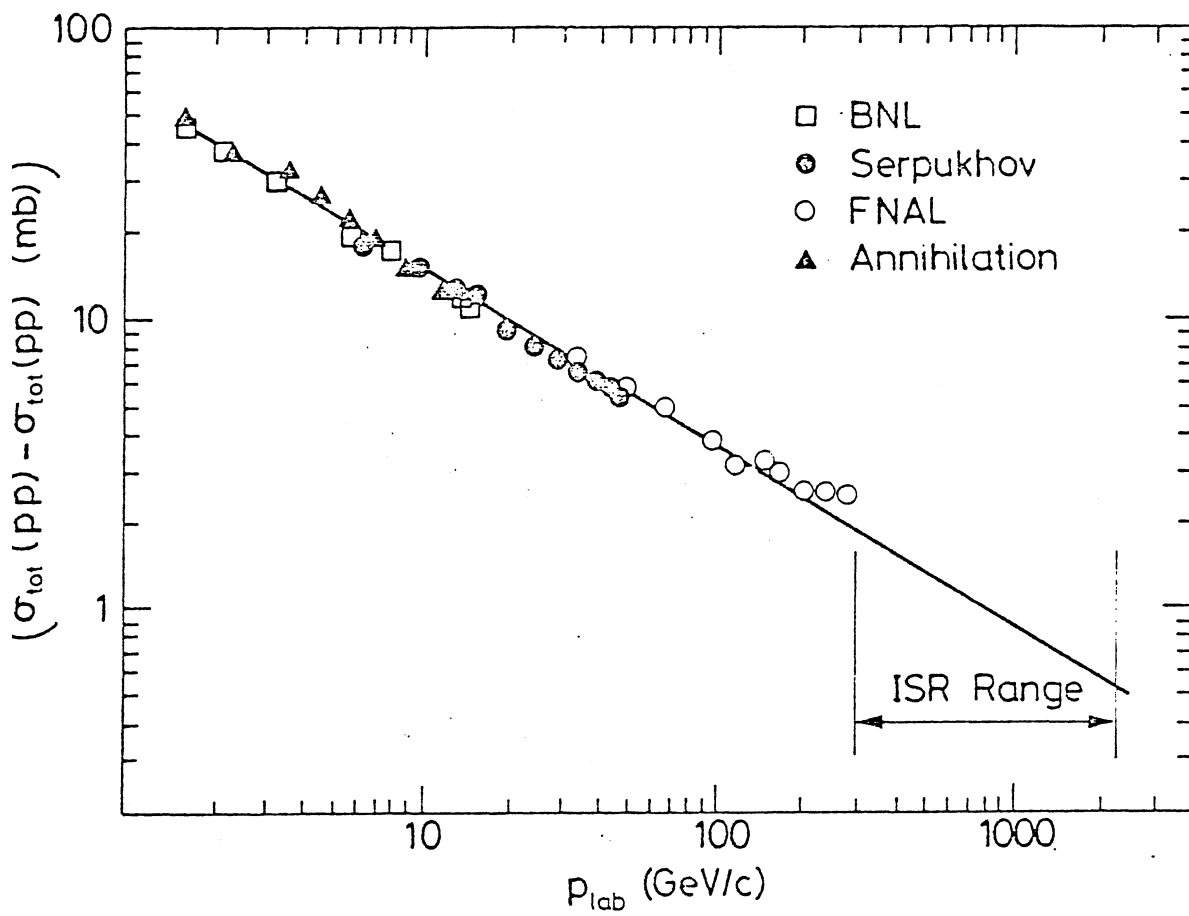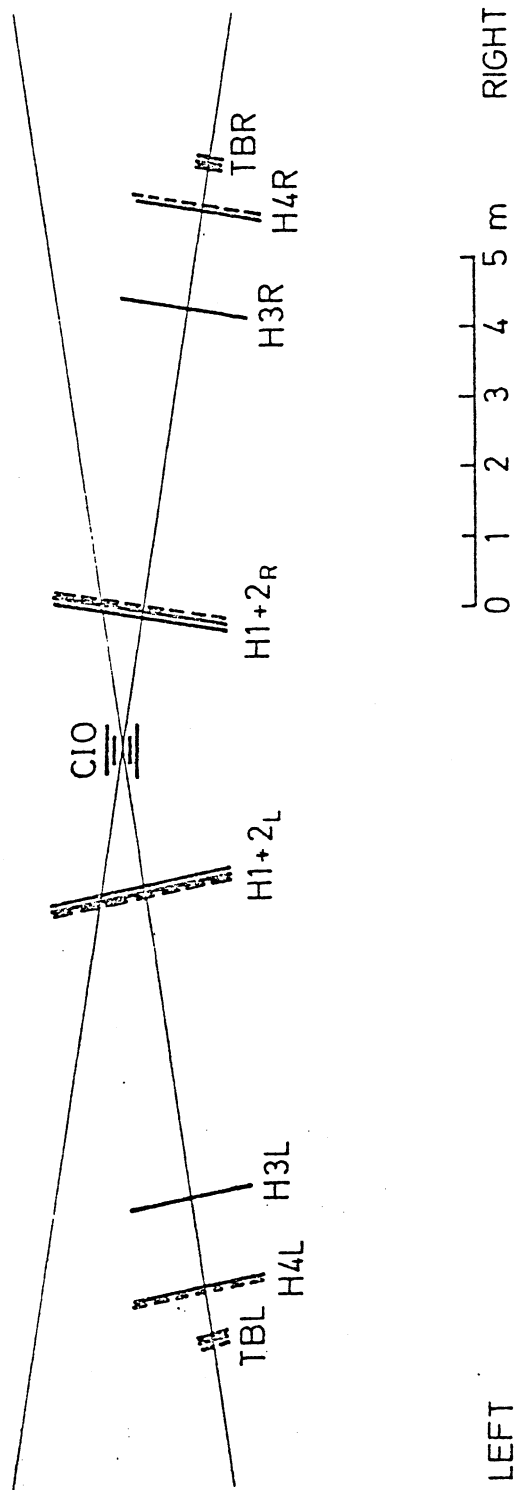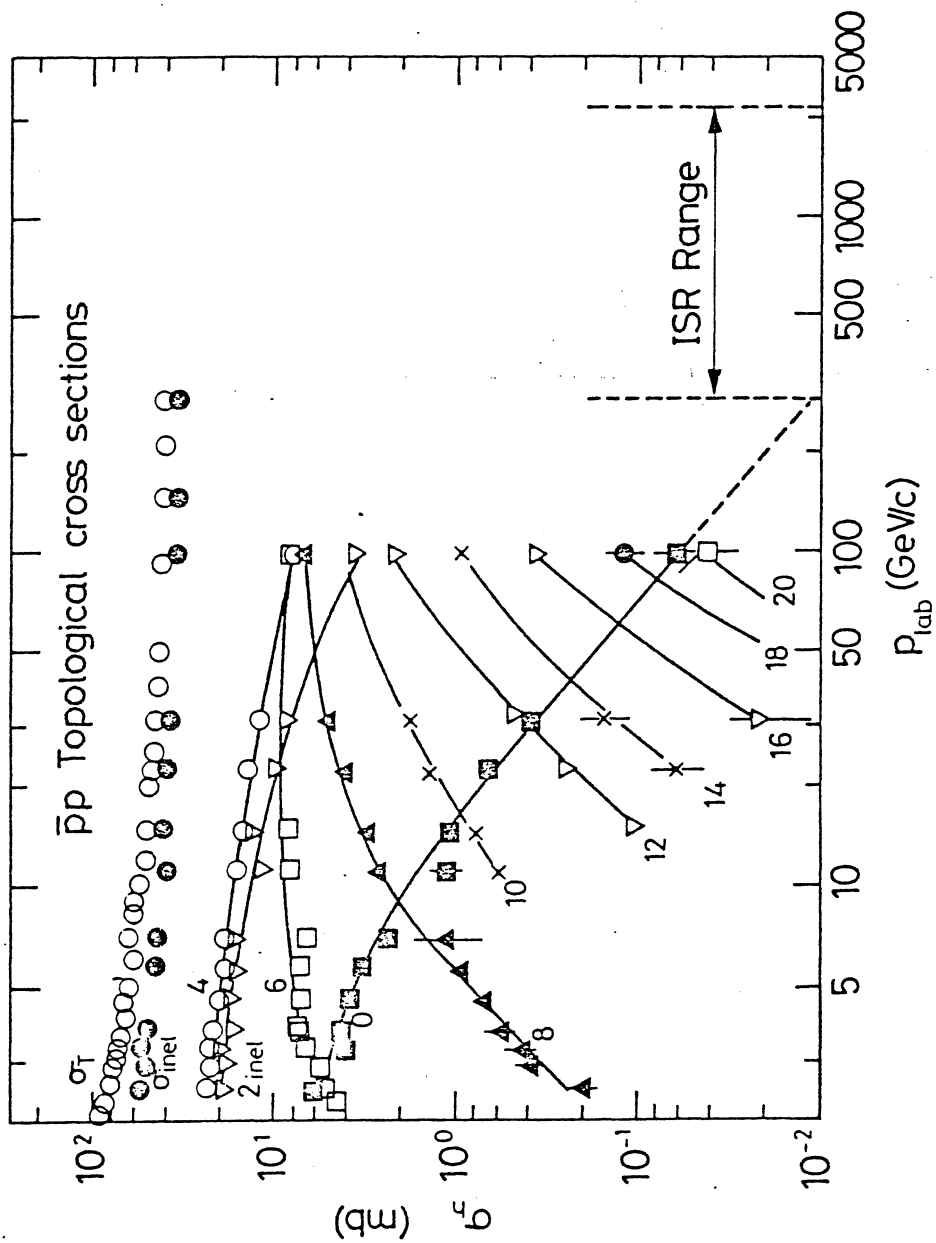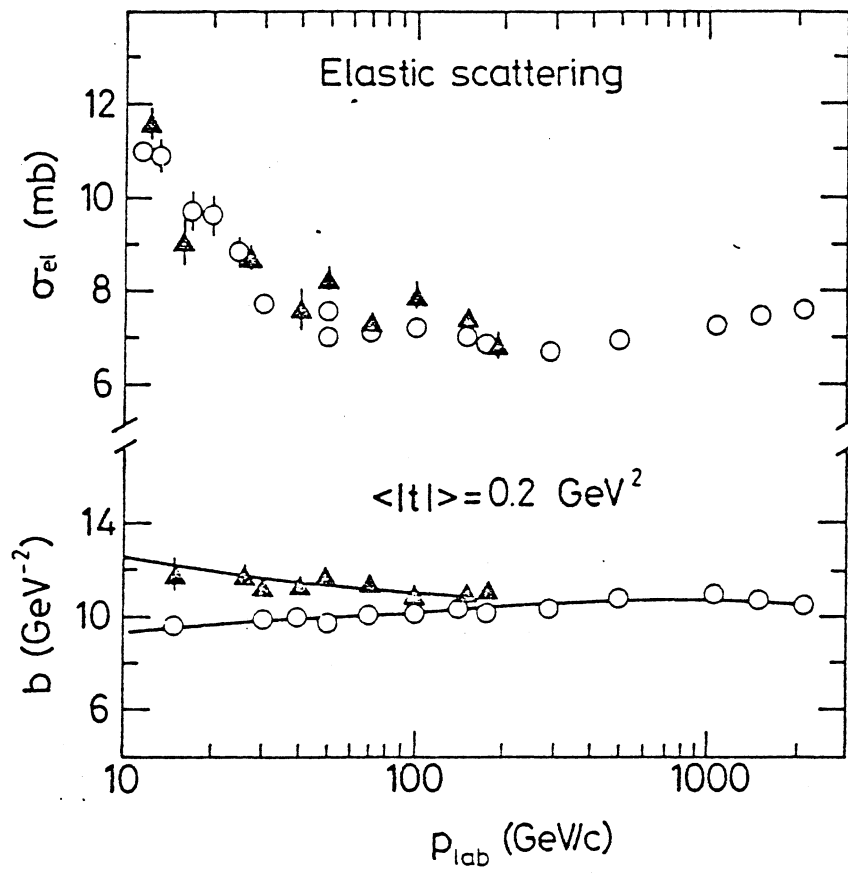
Fig. 1

Fig. 2

Fig. 3

Fig. 4

Fig. 5

X. $\bar{p}p$ TOTAL CROSS SECTION

Amsterdam-Louvain-North-Western Collaboration[1]

(presented by J-C. Sens - CERN-EP)

1. Precision required

The expected behaviour of the $\bar{p}p$ total cross-section in the ISR energy range is shown in Figure 1 where the pp total cross-section has been parameterized as :

$$\sigma(pp) = 25.4 + 4.29 \ \ell n \ \frac{\sqrt{s}}{GeV} \qquad 23.5 < \sqrt{s} < 62.7$$

then if

$$\sigma(pp) = \sigma(pp) \ \text{at S large}$$

$$\sigma(pp) = \sigma_o + \sigma_+ \qquad \sigma(\bar{p}p) = \sigma_o + \sigma_-$$

$$\sigma_o = A + B(\ell ns)^\alpha \qquad \sigma_\pm = C \ exp(A\ell n \ p_{lab}) \ \mp \ D \ exp(B\ell n \ p_{lab})$$

The differences $\sigma(\bar{p}p) - \sigma(pp)$ at the extreme ISR energies are then :

	$\sigma(\bar{p}p) - \sigma(pp)$ (asympt. equal)	$\sigma(\bar{p}p) - \sigma(pp)$ Linear contiuation of $\bar{p}p$
11.8/11.8	+ 2.1 mb	+ 2 mb
31.4/31.4	+ 0.7 mb	- 2.5 mb

Hence a measurement of $\sigma(pp)$ must aim at a precision given by

$$\delta\sigma(\bar{p}p) \leq 0.5 \ mb$$

---

[1] Letter of Intent : Measurement of the $\bar{p}p$ Total Cross-section at the CERN-ISR *(CERN-ISRC/78-30)*.

2. Minimum Angle

The elastic cross-section of Figure 2 can be written as

$$\frac{1}{\pi}\ \frac{d\sigma}{dt} = \left|\frac{2\alpha}{t}\ e^{i'\alpha\phi} + \frac{\sigma_T}{4\pi}\ (i+\rho)\ e^{-\frac{1}{2}bt}\right|^2$$

$$= \left(\frac{2\alpha}{t}\right)^2 + \left(\frac{\sigma_T}{4\pi}\right)^2\ (1+\rho^2)\ e^{-bt} + \text{Interference}$$

or Coulomb term + Strong Interaction term + Interference.

The Coulomb and Strong Interaction terms are approximately equal when

$$t_c = \frac{0.074}{\sigma_T(\text{mb})}\ \text{GeV}^2$$

$$\simeq 0.0018\ \text{GeV}^2$$

The following table summarizes the situation at the ISR :

Minimum angles in mrad				
Type of data	t	11.8/11.8	15-4/15.4	31. 4/31.4
Coulomb	$\leqslant \frac{1}{2}\ t_c$	2.5	1.9	1.0
σ_T, b	$t \geqslant 3t_c$	6.2	4.8	2.4
Break	$\simeq 0.1\ \text{GeV}^2$	26.8	20.5	10.0
Dip	1.44	102	–	–
	1.42	–	77	–
	1.32	–	–	37

It is apparent that for a Coulomb and hence ρ measurement the scattering angles are very small and 'Roman Pot' type vacuum chambers are needed (Figures 5 and 6). They are not needed for measurements of σ_T and b.

3. Choice of Method

The σpp and $\bar{\sigma}$pp total cross-sections at the ISR can be obtained either by measuring the elastic cross-section and using the optical theorem (CERN-Rome method)[1] or by measuring total interactions and luminosity (Pisa-Stonybrook method)[2].

The cross-section obtained by the latter method can be written as

$$\sigma(PSB) = \frac{R_{INT}(1 + \epsilon)}{L} + \Delta\sigma_{EL}$$

where ϵ = correction for :

- diffractive events in vacuum pipe
- holes in 4π detector
- inefficiencies
- deadtimes, etc.

$\Delta\sigma_{EL}$ is the unobserved part of the elastic cross-section inside the beam pipe.

The observed and corrected cross-sections obtained in the Pisa-Stonybrook measurement can be summarized as :

	Observed $\sigma = R/L$	$\epsilon(\%)$	$\Delta\sigma_{EL}$	$\sigma(PSB)$
11.8/11.8	37.89	1.77	0.24	38.80 ± 0.25
15.4/15.4	38.86	1.80	0.52	40.08 ± 0.24
22.4/22.4	39.82	2.16	1.24	41.92 ± 0.25
26.6/26.6	40.16	2.27	1.66	42.73 ± 0.34
31.4/31.4	39.81	2.49	2.22	43.02 ± 0.40

Hence, the observed rise 11.8/11.8 to 31.4/31.4 was 5.2% while the real rise is 10.9%.

It should be noted that a knowledge of $\sigma_{(EL)}(0^o)$ is needed to obtain $\Delta\sigma_{EL}$ and also that there are some differences between pp and $\bar{p}$p since the $\bar{p}$p final state is neutral

$$pp \qquad \sum_{hemisphere} e = 1 \qquad \sum_{hemisphere} |e| = 1,3,5,7 \ \cdots$$

$$\bar{p}p \qquad \sum e = 0 \qquad \sum |e| = 0,2,4,6 \cdots$$
$$\uparrow \text{not seen in } R_{INT}$$

A similar analysis of the CERN-Rome method where

$$\sigma(CR) = \left[\frac{16\pi}{1+\rho^2} \ \frac{d\sigma}{dt}\bigg/_o \right]^{\frac{1}{2}}$$

$$= \left[\frac{16\pi}{1+\rho^2} \ \frac{\pi}{\rho^2} \ (1-\varepsilon_c) \ e^{b(t)} \ \frac{1}{\Delta\Omega} \ \frac{R_{EL}(t)}{L} \right]^{\frac{1}{2}} = \left[\frac{F(CR)}{L} \right]^{\frac{1}{2}}$$

leads to :

	ρ	ε_c	b	$\sigma(CR)$
11.8/11.8	0	0.0574	11.8 ± 0.3	39.01 ± 0.29
15.4/15.4	0.03	0.0141	12.3	40.35 ± 0.34
22.4/22.4	0.06	0.004	12.8	41.45 ± 0.26
26.6/26.6	0.07	0.006	13.1	42.38 ± 0.29
31.4/31.4	0.08	0.007	13.3	43.05 ± 0.33

Hence, we can conclude that :

- the precision of both methods is sufficient for $\sigma(\bar{p}p) - \sigma(pp)$ with $\delta\sigma(\bar{p}p) \leq 0.5$ mb,

but we note that :

- a measurement of $\sigma_{EL}(0^o)$ is necessary and <u>sufficient</u>,

- a measurement of $\rho(\bar{p}p)$ is not necessary since $\delta\rho(\bar{p}p) = 0.1$ is equivalent to $\delta\sigma(\bar{p}p) = 0.2$ mb.

A combined $\sigma_{EL}(0^o)$ and $\sigma_{(int)}$ carried out by CERN-Rome and Pisa-Stonybrook concluded that :

- the Optical Theorem is correct to $\pm$ 0.5%
- the Van Der Meer Luminosity measurement is correct to

We expect $b(\bar{p}p) \simeq b(pp)$ (see Figure 3) and $\rho(\bar{p}p) \simeq 0.05$ (see Figure 4).

Thus $\sigma(\bar{p}p)$ is best determined at the ISR by measuring small angle elastic scattering and using the optical theorem.

4. Wire chambers or hodoscopes at small angles ?

Elastic scattering in pp has been measured at the ISR by an ARCHGM collaboration using 32 multi-wire proportional chambers + 8 scintillators. They used 4 planes above and below the beam pipe 7 m from the interaction point and 4 similar planes at 9 m (1 mm wire spacing 100×100 mm^2) to cover the angular range 6-10 mrad (the CR hodoscopes covered 3-9 mrad).

The following features of the experiment are relevant for a comparison between hodoscopes and wire chambers :

1. The single plane efficiency was > 97% and single wire hits in $\geq$ 3 chambers occurred in 89.5% of the events.

2. They made a collinearity check and obtained a FWHM of $\simeq$ 0.3 mrad which has to be compared with an intrinsic spread due to the Lorentz transformation for tracks in the horizontal plane of $\leq$ 0.2 mrad. The CR hodoscope segments accepted $\simeq$ 0.25 mrad. Hence the quantisation of the angular distribution by the hodoscope method does not seem very important.

3. They obtained a closest distance of approach distribution with FWHM = 2.25 mm with horizontal beam width of 18 mm FWHM = 8 mm (Terwilliger scheme ON), the interaction region was 140 mm long and the beam height FWHM $\simeq$ 3.5 mm.

It is interesting to compare the final accuracy of this measurement with the CR measurement.

Final Accuracy :

	σ(ARCHGM)	σ(CR)
22/22	42.0 $\pm$ 0.3	41.45 $\pm$ 0.26
26/26	42.8 $\pm$ 0.3	42.38 $\pm$ 0.29
31/31	43.3 $\pm$ 0.4	43.05 $\pm$ 0.33

We conclude that :

- both chambers and counters can do the job

- no need for collinearity check if TW can be ON

- closest-distance of approach check only with chambers

It therefore seems reasonable to use hodoscopes and not chambers at small angles.

5. Counting Rates, ISR-Time

Assume :

i) the layout is similar to that used for the CR measurement shown in Figures 5 and 6. With hodoscopes of 54×88 mm^2 at 9 m covering an angular range of 3-9 mrad

ii) the beams are 30 mA of $\bar{p}$ against 1 A p with 1 cooled $\bar{p}$ pulse per day giving a luminosity of $L = 1.5 \times 10^{27}$/cm^2/sec.

We then calculate the following rates :

	t_{min}	Δt	rate/sec	measuring time for $\frac{1}{4}\%$ stat. acc. (days)
11.8/11.8	0.00125	0.0100	0.2	8
15.4/15.4	0.00208	0.0166	0.4	$4\frac{1}{2}$
22.4/22.4	0.00455	0.0365	0.8	$2\frac{1}{2}$
26.6/26.6	0.00637	0.0509	1.0	2
31.4/31.4	0.00876	0.0701	1.3	$1\frac{1}{2}$

It seems of little value to make a measurement at 11.8/11.8 where it is a long measurement, probably with poor beams. Hence with no measurement at 11.8 but repeating the other energies 3 times, the experiment can be completed in 30 days. The requirements are 12 fills of 1 $\bar{p}$ pulse each with the Terwilliger scheme on, the low-β off and possibly the SFM off.

As a final note on the differential cross-section, although the structure of $\frac{d\sigma}{dt}$ at low s for $\bar{p}p$ is different from pp, at the ISR it is expected to be the same (see Figure 7).

References

1) ISR Experiments R 601 and R 805, CERN-Rome Collaboration

2) ISR Experiment R 801, Pisa-Stonybrook Collaboration

3) Nucl. Phys. B, 141 (1978), 1.

Figure captions

Fig. 1 : $\bar{p}p$ and pp total cross sections in the ISR energy range.

Fig. 2 : small angle pp elastic scattering

Fig. 3 : slope parameter b in elastic scattering as a function of s (GeV^2).

Fig. 4 : $\rho(pp)$ and $\rho(\bar{p}p)$ in the ISR energy range.

Fig. 5 : Schematic layout of counter hodoscopes in the reentrant vacuum chambers ('Roman Pots') downstream of the interaction region.

Fig. 6 : The reentrant vacuum chamber used in experiment R 805 to make measurements at angles down to 1 mrad. The central window is 0.15 mm of stainless steel.

Fig. 7 : The differential cross section $\bar{p}p \rightarrow \bar{p}p$ at low s compared to pp at low s and ISR energies.

Fig. 1

Fig. 2

Fig. 3

Fig. 4

TOP VIEW

9 m

SIDE VIEW

A   C   B   D

Fig. 5
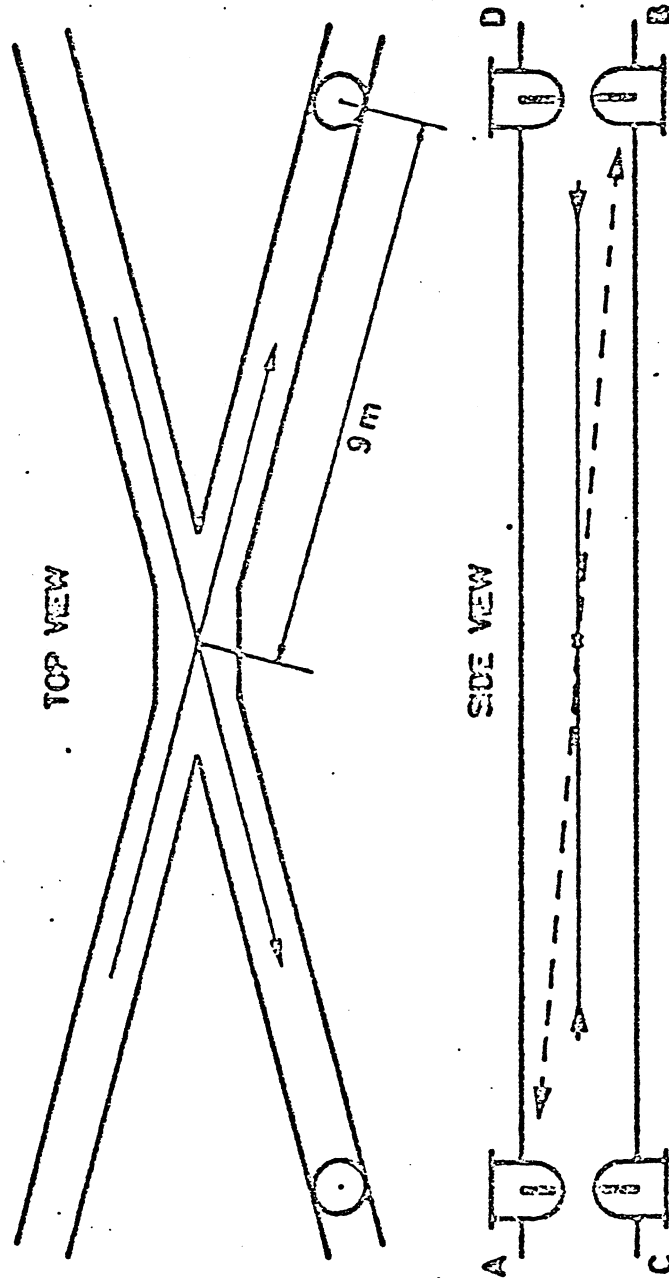
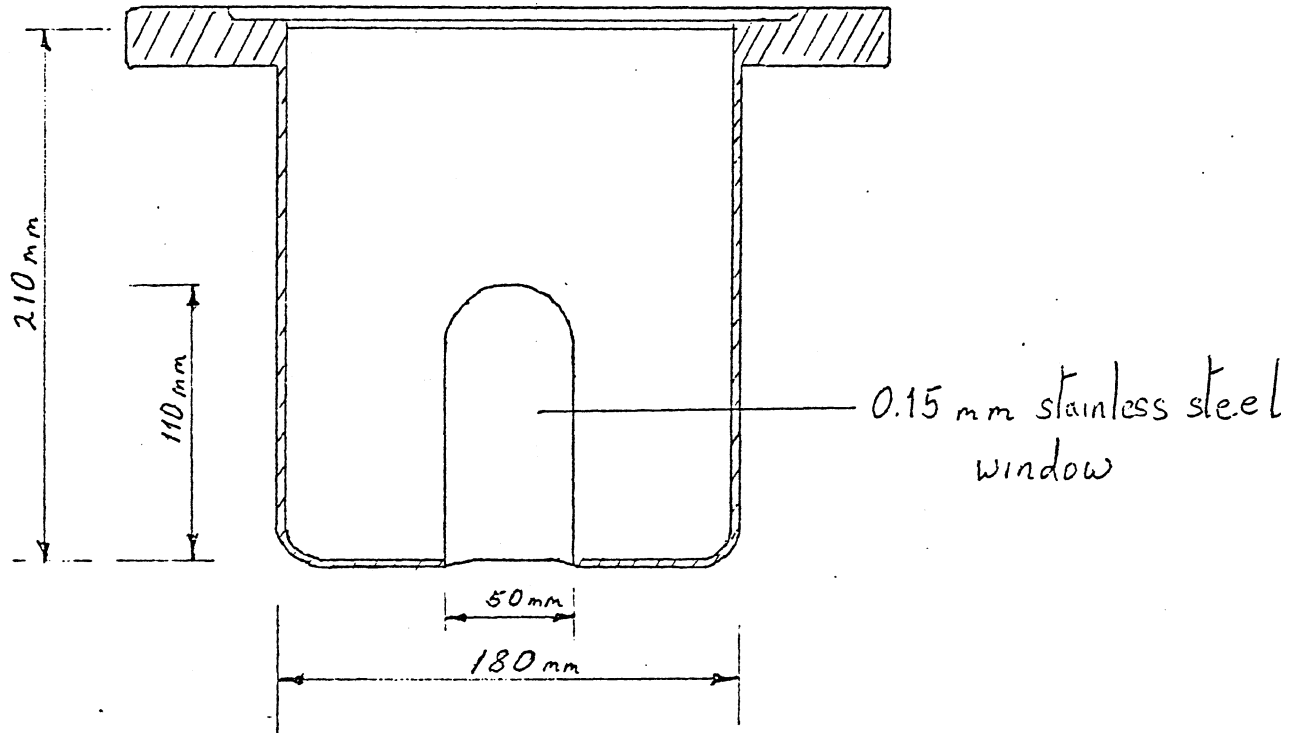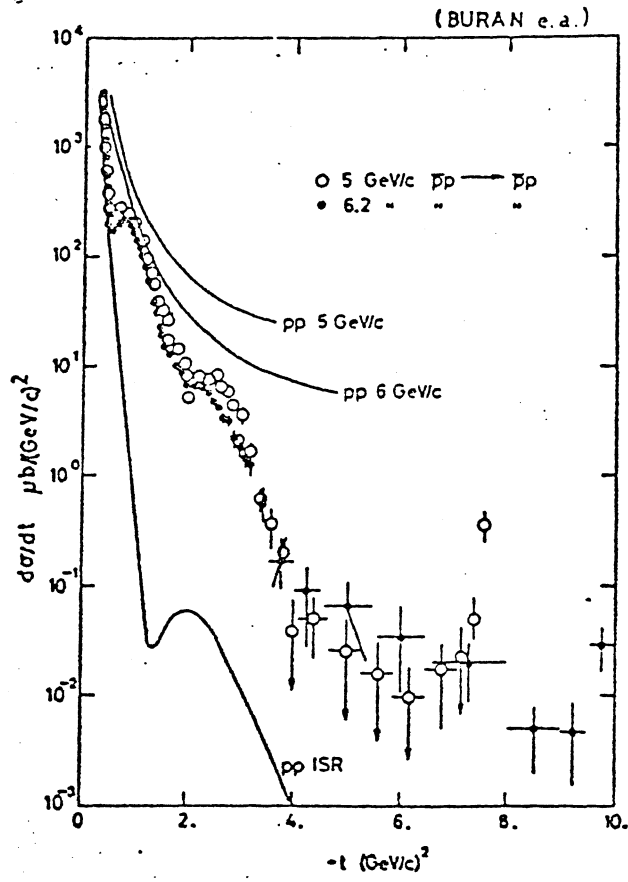0.15 mm stainless steel window

210 mm

110 mm

50 mm

180 mm
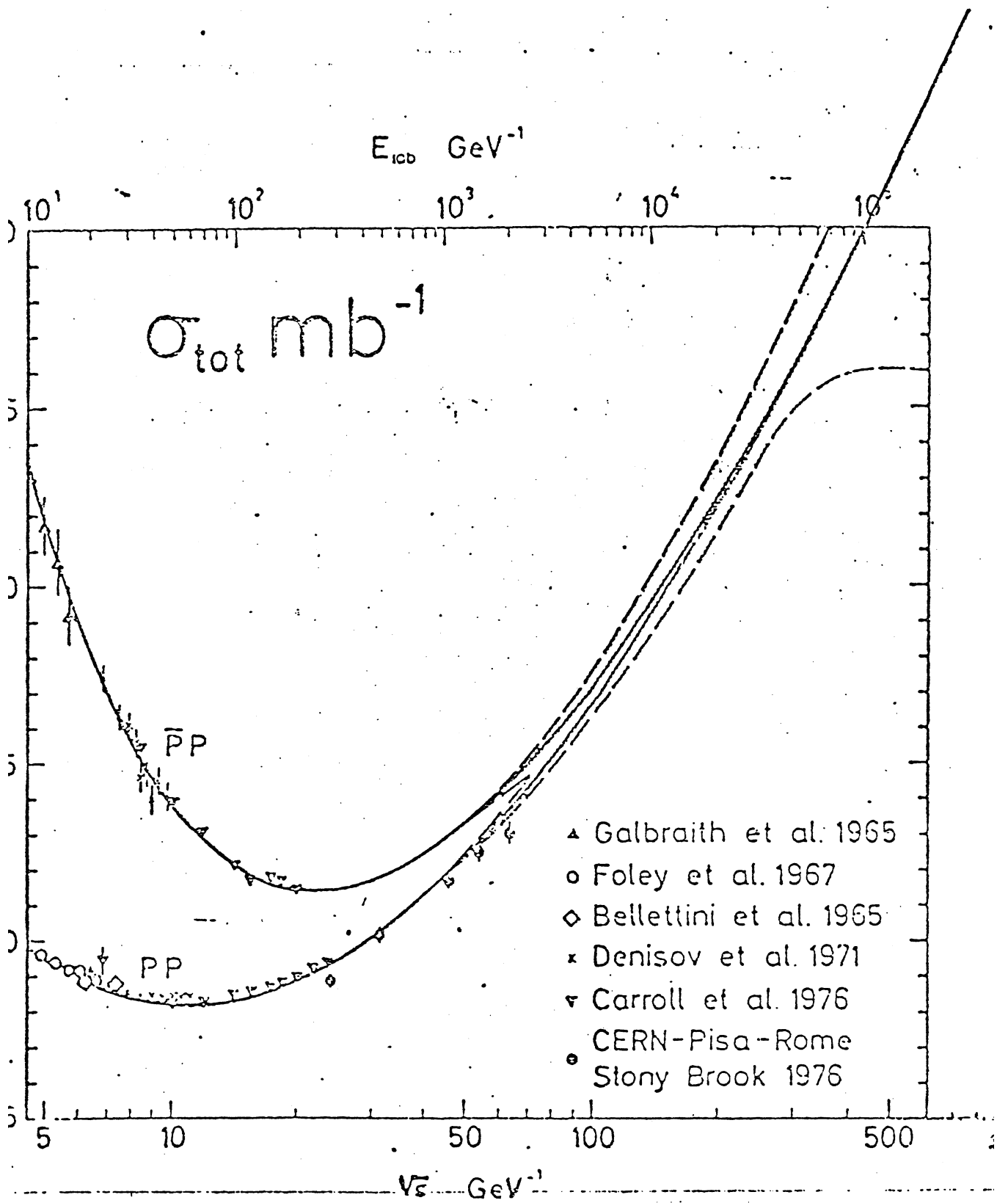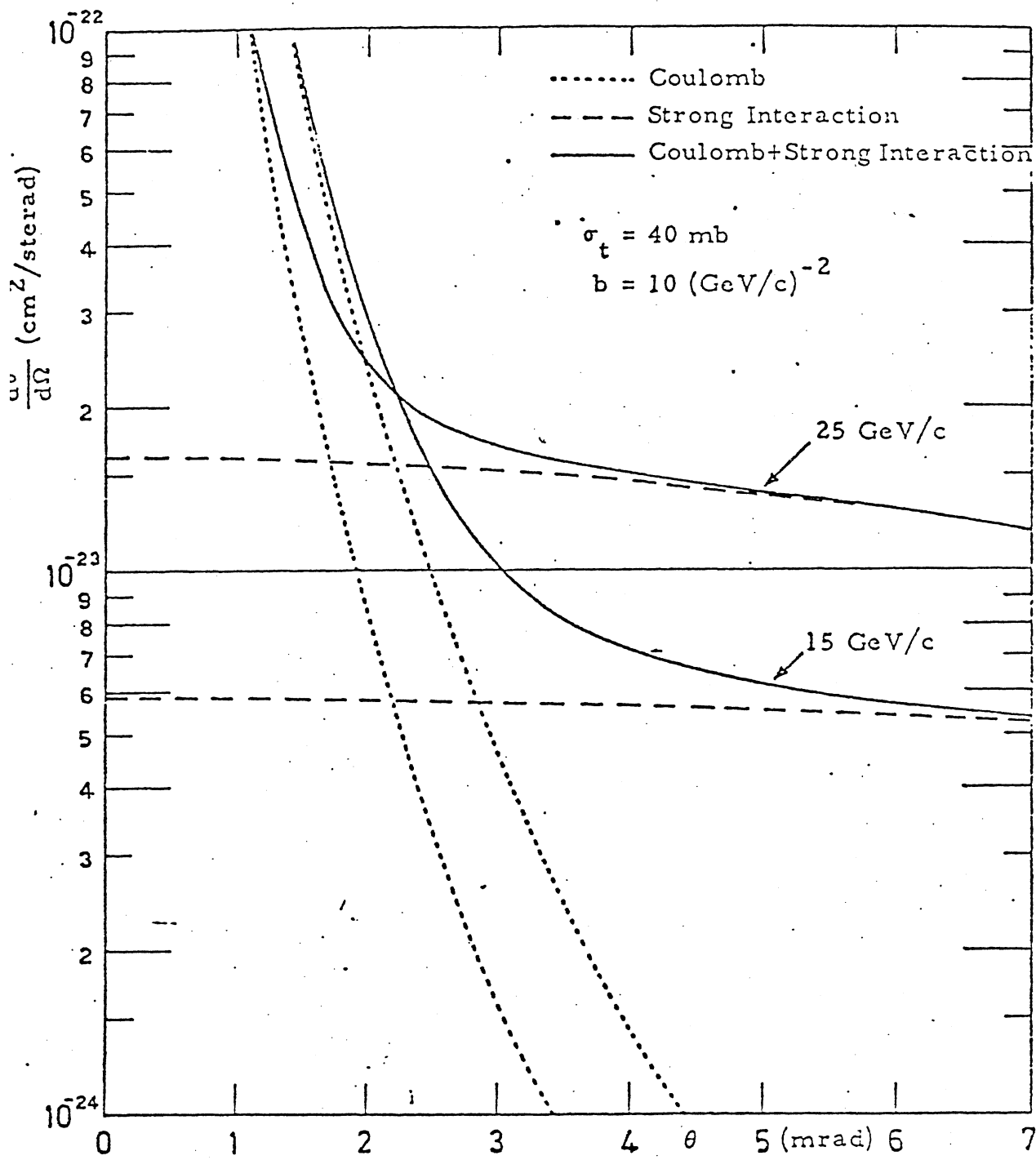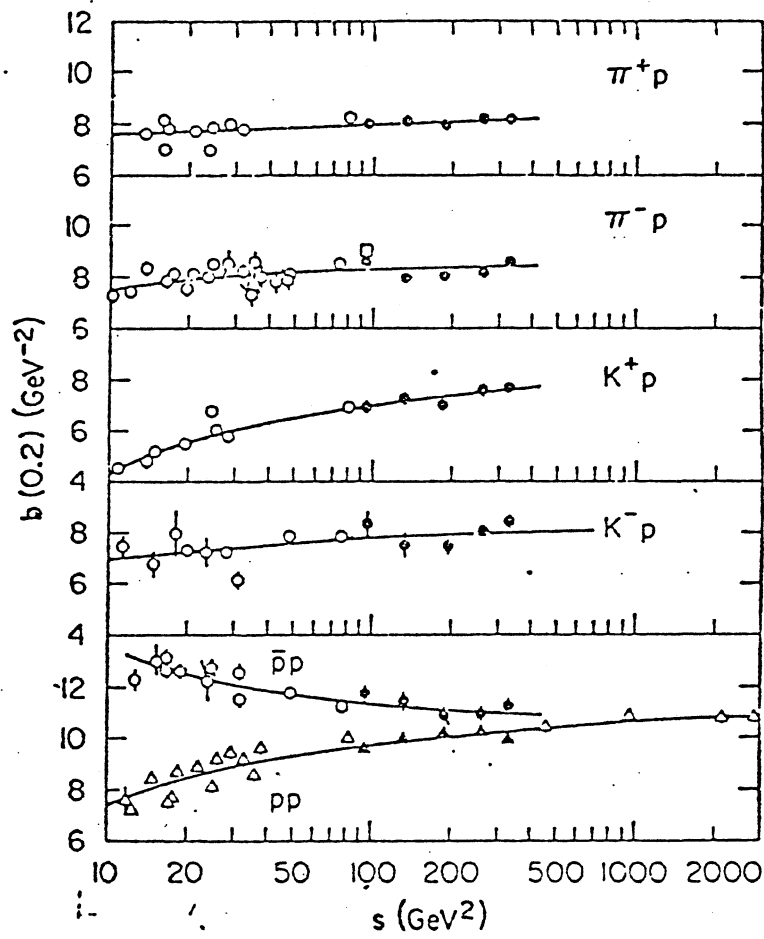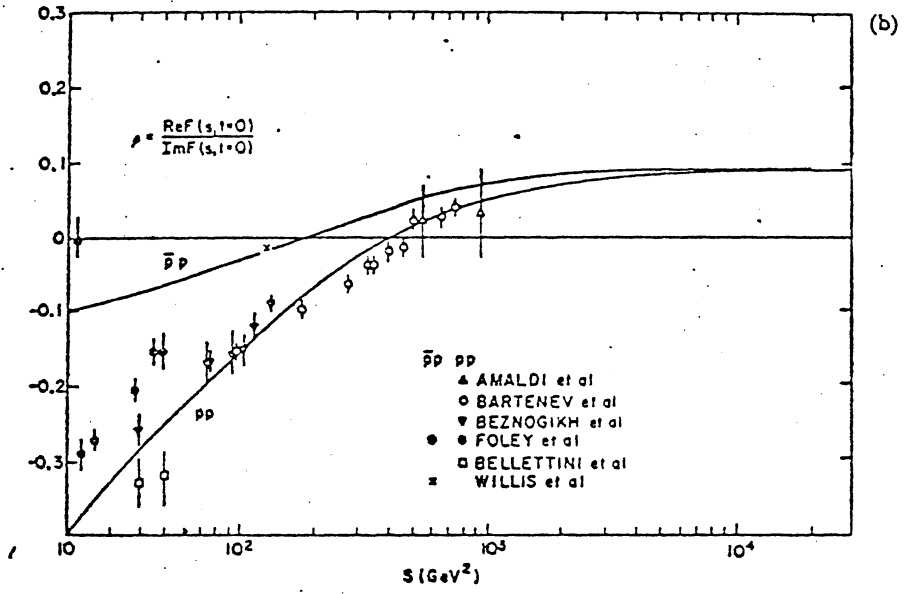
Fig. 6

Fig. 7

XI. PHYSICS WITH p̄p COLLISIONS IN EXPERIMENT R 608

CERN-Los Angeles-Saclay Collaboration

(presented by P. Schlein)

The goal of the recently approved ISR experiment, R 608, is to continue and expand on the type of physics program initiated in experiment R 603. In essence, this is the measurement of multi-particle systems of identified particles produced in a forward cone of angle $\pm$ 150 mradian and the correlations with 90° phenomena. The extension of this experiment to include p̄p studies is discussed in the following. The apparatus is shown in Figure 1. Figure 2 shows a $p\pi^{-}$ invariant mass spectrum from R 603 when the Λ° decays outside the vacuum pipe. This situation is approximately that of our new experiment because of its new thin-wall (0.3 mm) large volume vacuum pipe.

In physics terms, we will study the systematics of multi-body systems and try to understand them in terms of their presumed quark-parton or constituent structure. In our proposal, we stated 'all the physics we propose to do with our apparatus and especially the correlations between 0° and 90° finds a natural and exciting extension to p̄p interactions'.

In gross terms, forward systems produced in pp and pp interactions should be quite similar at ISR energies and therefore a coarse comparison will not be very interesting. The expected total cross-section difference between pp and p̄p interactions of $\simeq$ 1 mbarn obviously arises from more subtle effects having to do with central region phenomena which reflect the natures of the different interacting constituents in the two cases. Many central region phenomena are directly observable in the forward direction. Production of systems, whose dependence on longitudinal-x goes as a large power in $(1-x)^{n}$, such as pp $\rightarrow \bar{\Lambda}$ + X, are thought of as reflecting more complex 'sea' activity. Such processes may very well be different in pp and p̄p interactions. Even such a mundane process as inclusive pion production should, at some level, be different in pp and p̄p, owing to the antiquark in the pion.

Central region phenomena which lead to observable effects at 90°, such as production of systems of particles (jets) with high transverse momentum (quark-quark scattering) or di-lepton production (quark-antiquark annihilation) must, in some sense, deplete the forward direction and lead to striking 0° - 90° correlations. Another type of correlation that should exist arises from the pair production of, say, $\bar{s}s$ quarks. The observation of strangeness at 90° in,

for example, a K^- may be correlated with strangeness observation in the forward direction. All these correlations may be different in pp and $\bar{p}p$ interactions.

In short, everything that we study in pp interactions should also be studied in $\bar{p}p$ interactions. In this connection, it may be interesting to review some of the physics items that have emerged from R 603 and whose more extensive investigation is foreseen in R 608. Some of these results have emerged after the P98 proposal was written and hence suggest new directions for R 608.

1. Correlations at large-x ('quark recombination') :

As discussed in the P98 proposal, single mesons at large-x apparently reflect the quark-parton distributions of the incident proton. Our results from R 603 (PRL 41, 680 (1978)) on $\pi\pi$ and $\pi\pi\pi$ systems support this view. $\pi^-\pi^-$ systems fall off with increasing-x as $(1-x)^5$ compared with $(1-x)^3$ for $\pi^+\pi^-$ and $\pi^+\pi^+$, presumably reflecting the fact that there is only one d quark in the proton.

More recently, we have been impressed with the fact that :

$$\sigma(pp \to \Sigma^+(1385) + X) \gg \sigma(pp \to \Sigma^-(1385) + X) \tag{1}$$

see figure 3. Although charge conservation alone leads to the sense of the inequality (Σ^+ is most easily produced by $p \to \Sigma^+K^0$, whereas Σ^- is most easily produced in $p \to \Sigma^-K^+\pi^+$), the need for an additional pion in the latter case seems far too insignificant a cause for the order-of-magnitude difference in the cross-sections. On the other hand, a simple explanation exists in the fact that the quark structure of Σ^+ and Σ^- are, respectively, uus and dds. Thus the same reason for the suppression of $\pi^-\pi^-$ with respect to $\pi^+\pi^-$ and $\pi^+\pi^+$ also results in the inequality (1).

2. Λ^0 Polarization (Physics Letters - in press) :

The final analysis of our complete sample of pp $\to \Lambda^0$ + X at 26/26 and 31/31 GeV in R 603 (the x-distribution is shown in Figure 3a) has lead to the observation of a rather large polarization of the Λ^0 ($\bar{p} = -(0.357 \pm 0.055)$) in the ranges of longitudinal and transverse momenta, 15-24 and 0.6-1.4 GeV/c, respectively. Figure 4 shows a ratio of data which is equal to the quantity $(1 + \alpha P \cos\theta)/(1 - \alpha P \cos\theta)$ and demonstrates a substantial negative polarization (with respect to the production plane with $\hat{n} \propto \hat{p}_{beam} \times \hat{\Lambda}$). Figure 5 shows the final polarization values plotted vs. transverse momentum. Since the mechanism leading to this polarization is as yet unknown, it will be important to repeat more precise measurements of this type in both pp and $\bar{p}p$ interactions.

3. $\Lambda\bar{\Lambda}$ Pair Production :

A clear signal has been obtained for $\Lambda\bar{\Lambda}$ pair production in R 603. For the 4-track topology shown as the insert in Figure 6, when $p\pi^-$ is in the Λ-mass region, Figure 6 shows the $\bar{p}\pi^+$ invariant mass. Figure 6(a) assumes all +- pairs are $\bar{p}\pi^+$, Figure 6(b) shows only those events in which the $\bar{p}$ is identified by the Cerenkov counter and Figure 6(c) makes the additional requirement that both Λ^0 and $\bar{\Lambda}^0$ vertices occur outside the beam-beam crossing region. Clearly, the virtue of the sample in Figure 6(c) is that despite the loss in statistics, the background under the $\bar{\Lambda}^0$ mass peak is reduced to negligible proportions. Figure 6(d) shows a scatter plot of $p\pi^-$ vs. $\bar{p}\pi^+$ invariant mass for these events, in which the spot corresponding to simultaneous production is seen.

For these simultaneous $\Lambda^0\bar{\Lambda}^0$ events, the laboratory momentum p of the Λ is plotted vs. p of the $\bar{\Lambda}$ in Figure 7. While a group of events does cluster near the diagonal line, as expected for pair-produced events, there appears to be an asymmetric group of events for which $p_\Lambda > p_{\bar{\Lambda}}$. Given the fact that the dominant source of Λ in pp interactions is associated production with a K-meson, to be contrasted with central region pair production of $\bar{\Lambda}$, it appears that the accidental coincidence, in the same event, of a $\bar{\Lambda}$ with a Λ from a $K\Lambda$ pair may be a source of observed $\Lambda\bar{\Lambda}$ about half of the time.

A concentrated effort to obtain a large number of these $\Lambda\bar{\Lambda}$ pairs for both pp and $\bar{p}p$ interactions will be one worthwhile goal for R 608. The extent to which this central region phenomenon and their polarization correlations may be different in these two interactions will provide important information on the detailed quark and gluon interactions in the two cases. Moreover, as with all baryon-antibaryon states, $\Lambda\bar{\Lambda}$ will be an excellent channel in which to search for the elusive baryonium states.

4. Pomeron Factorization Breakdown :

As stated in our proposal, one of the interesting results from R 603 was the observation of a breakdown of Pomeron Factorization for momentum transfer $t > 0.5$ GeV^2. The breakdown appears to be related to the dip that occurs in elastic pp scattering at $t \simeq 1.4$ GeV^4. There is no reason to expect that this behaviour will be the same in pp and $\bar{p}p$ interactions and, indeed, it will be extremely interesting to discover in what way they are different.

The above are merely some examples of observations in the forward direction that probably will differ in pp and $\bar{p}p$ interactions. Even more striking differences may occur in the $0^\circ - 90^\circ$ correlations which we plan to study. They should shet important light on the quark and gluon dynamics in these processes.

Figure Captions

Fig. 1   :   Schematic layout of R 608 spectrometer

Fig. 2   :   Invariant mass spectrum for $p\pi^-$ around the Λ^o from experiment R 603.

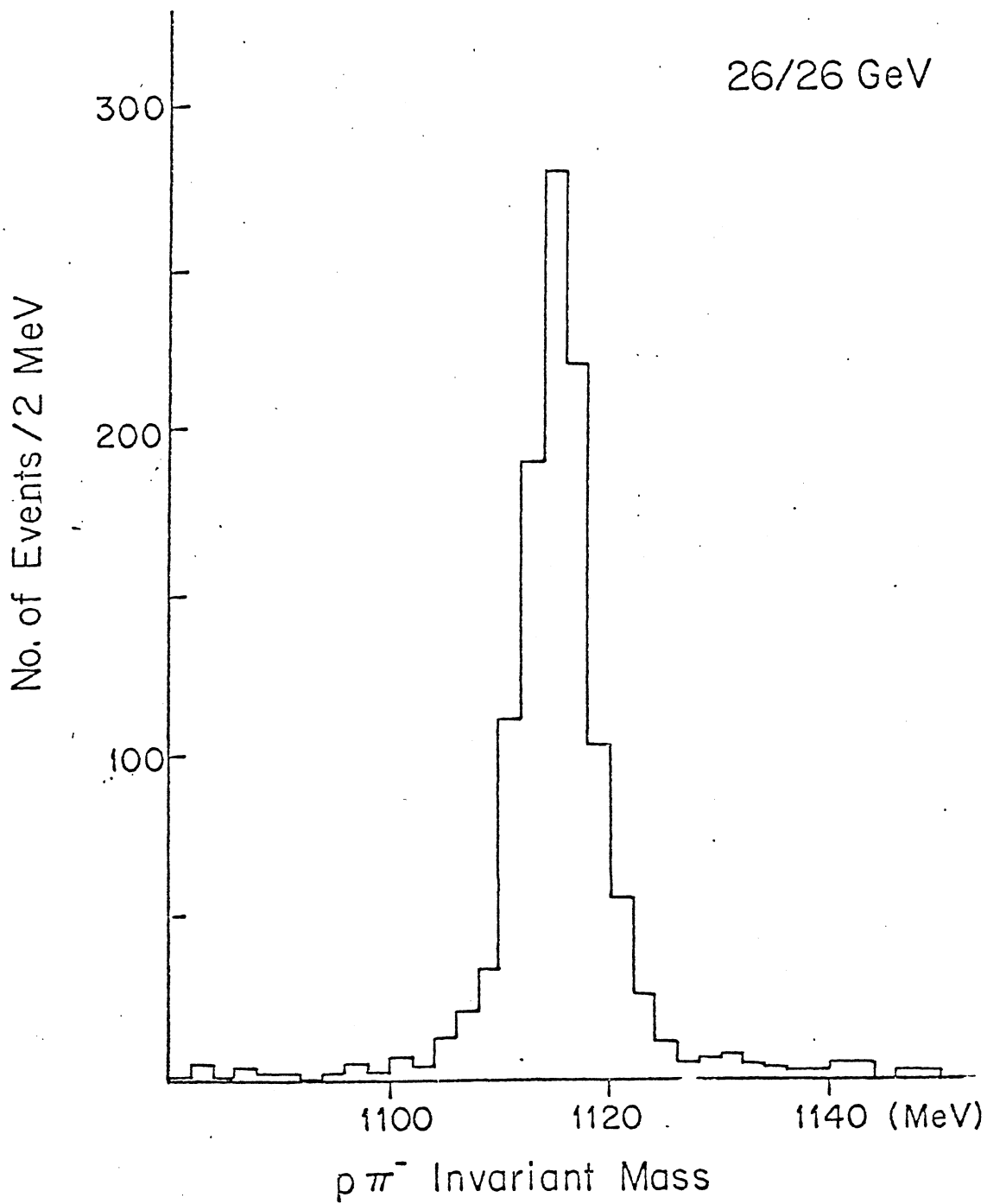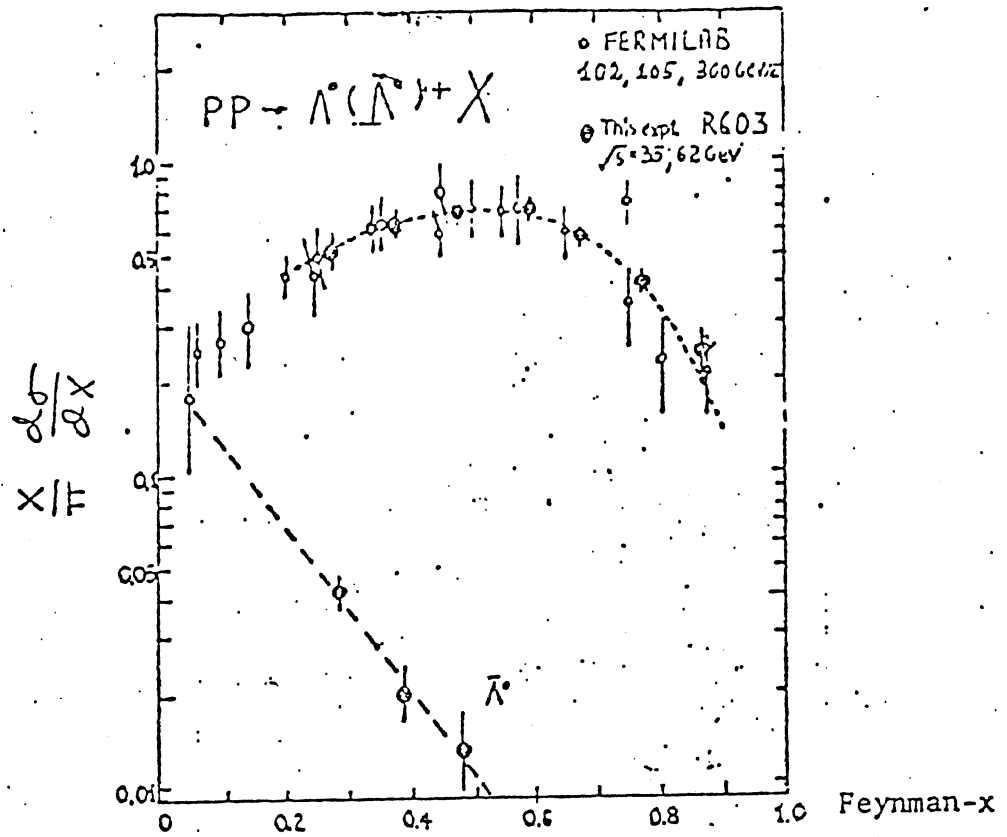Fig. 3   :   (a)   Inclusive cross-sections for Lambda and Anti-Lambda production in R 603 compared with lower energy bubble chamber results from FNAL, distribution in Feynmann-x.

                           (b) $\Lambda^o\pi^+$ and $\Lambda^o\pi^-$ invariant mass spectra from R 603 x > 0.6.

                           (c) $\Lambda^o\pi^-$ invariant mass spectrum from R 603 x > 0.4.

Fig. 4   :   Polarisation of Λ^o in R 603 $(1 + \alpha\rho \cos \theta)/(1 - \alpha\rho \cos \theta)$ as a function of $\cos \theta$.

Fig. 5   :   Polarisation of Λ^o in R 603 as a function of p_t (GeV/c).

Fig. 6   : $\Lambda\bar{\Lambda}$ pair production in R 603, 4 track topology

                           (a) $\bar{p}\pi^+$ invariant mass spectra

                           (b) $\bar{p}$ identified by $\hat{c}$

                           (c) $\bar{p}$ identified by $\hat{c}$ and vertices greater than 20 cm from the interaction region

                           (d) $p\pi^-$ versus $p\pi^+$ invariant mass plot in the mass region of simultaneous production of Λ^o and $\bar{\Lambda}^o$.

Fig. 7   :   Laboratory momentum distribution for $\Lambda\bar{\Lambda}$ events in R 603.

Figure 1

Figure 2

(a)

PP → $\Lambda^{\circ}(\bar{\Lambda}^{\circ}) + X$

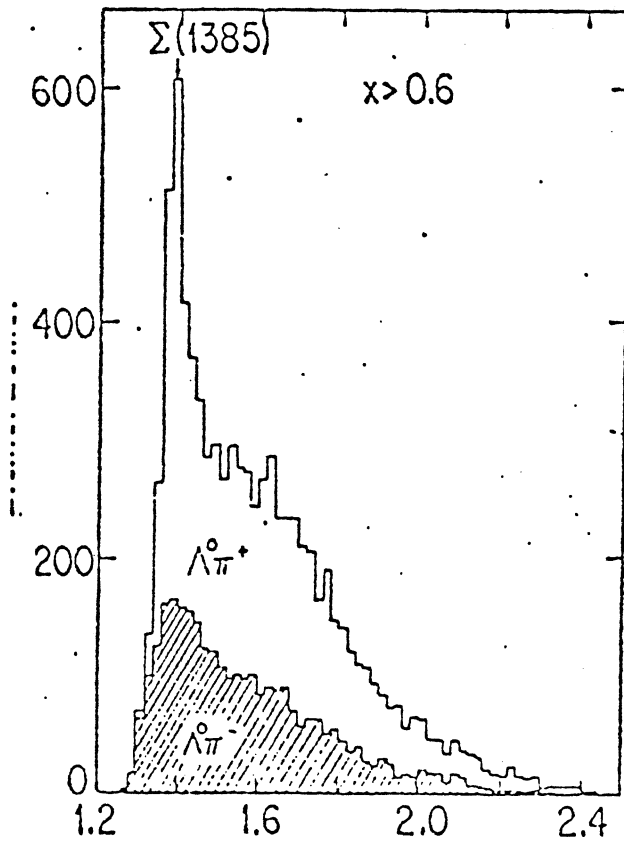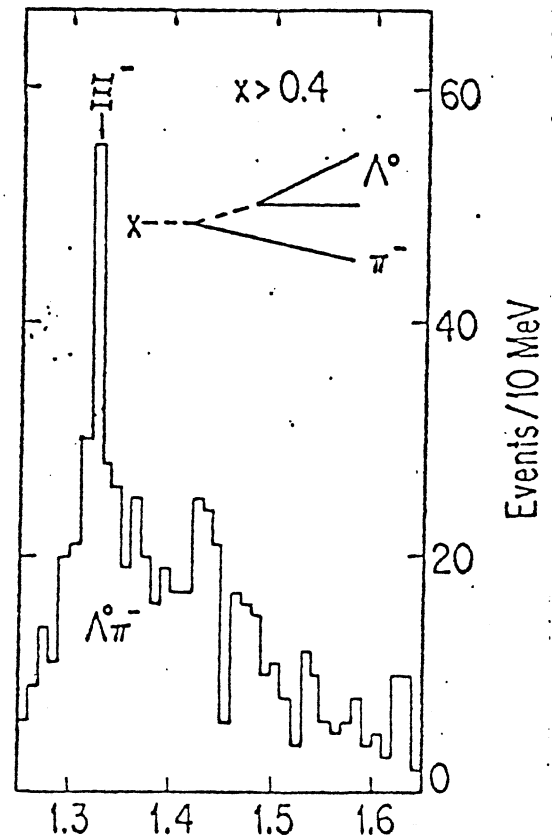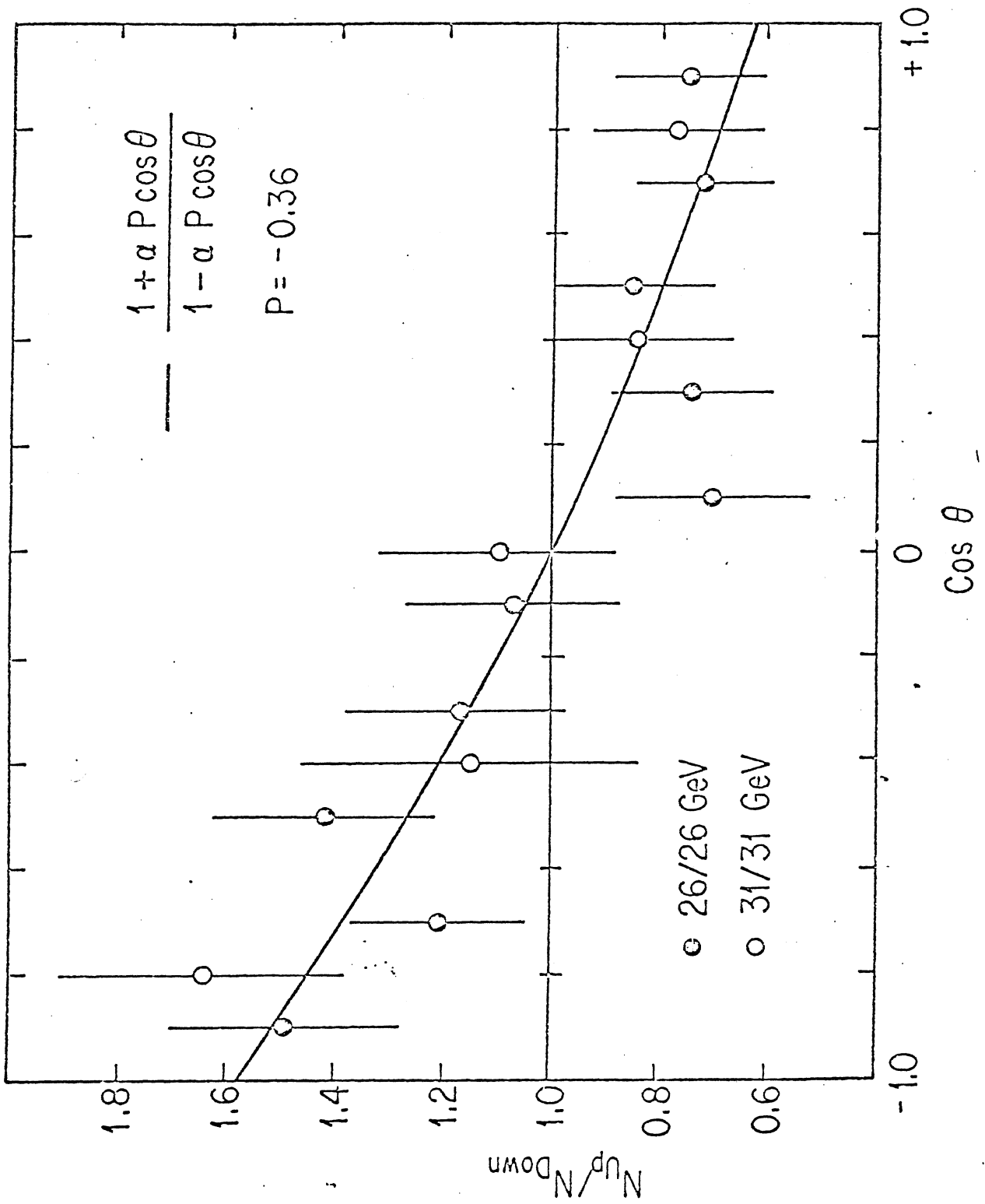FERMILAB 102, 105, 300 GeV

This expt R603 $\sqrt{s} = 35, 62$ GeV
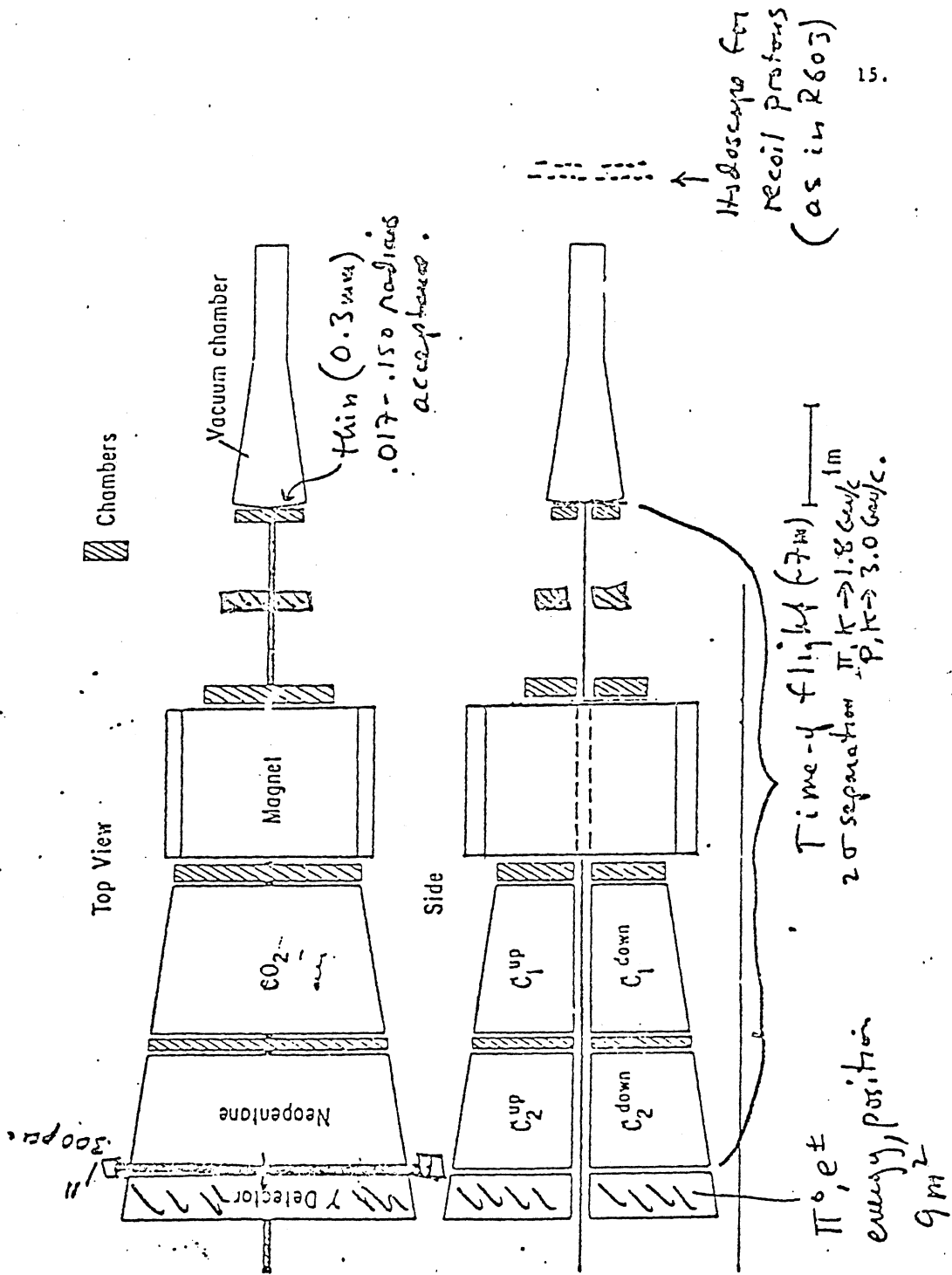
Inclusive cross sections for Lambda and anti-lambda production in R60? compared with lower energy bubble chamber results from FNAL
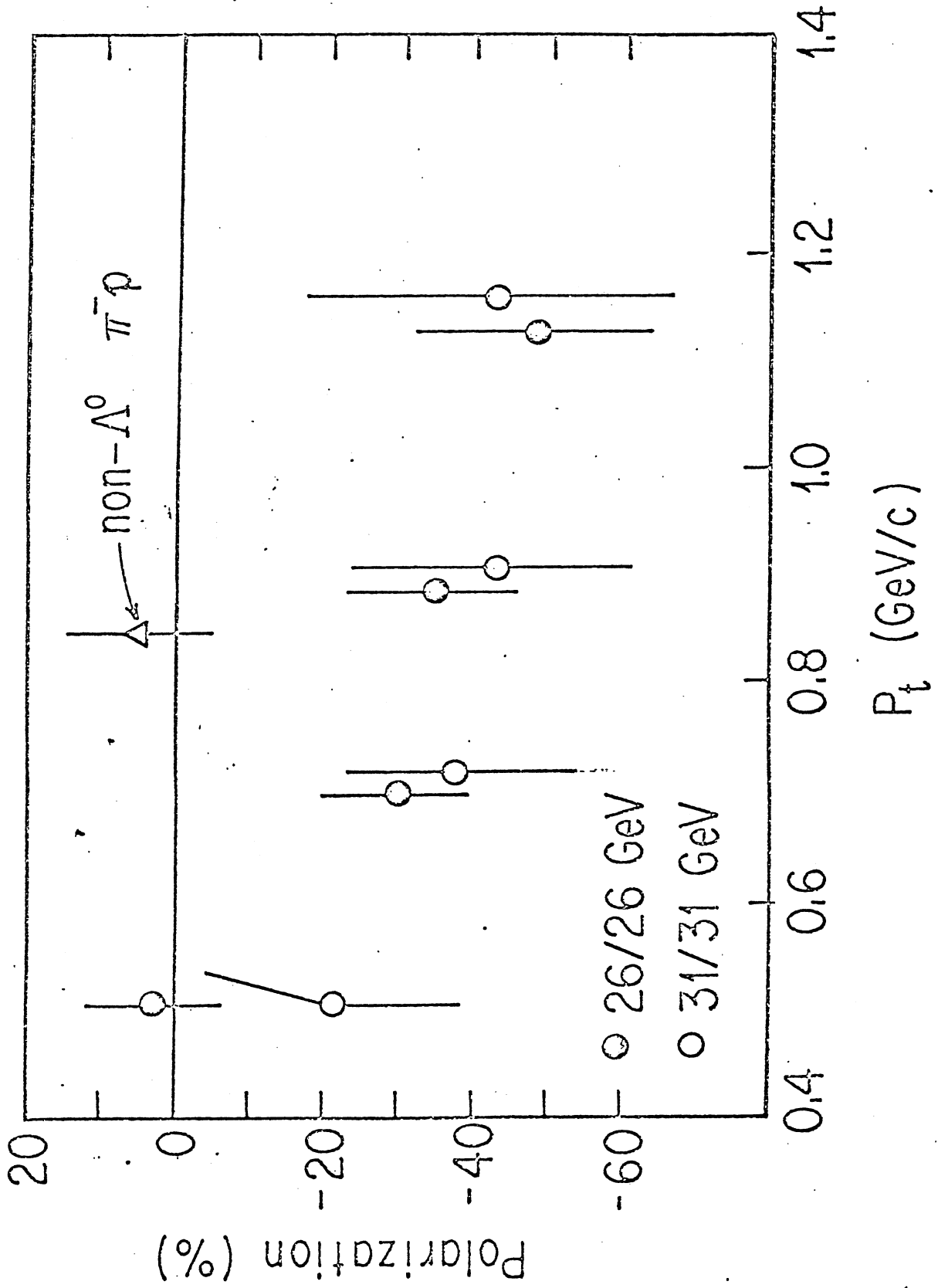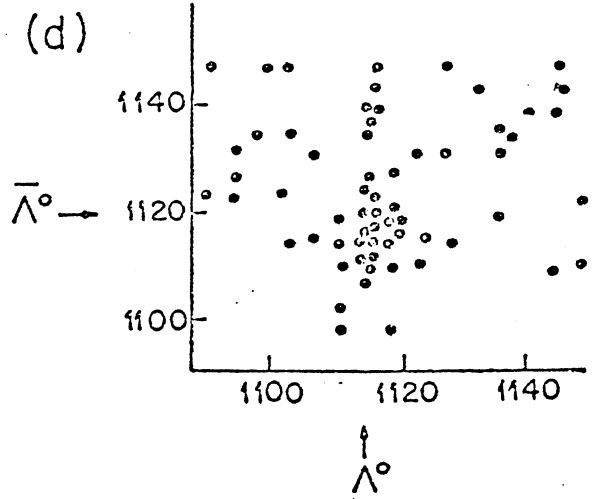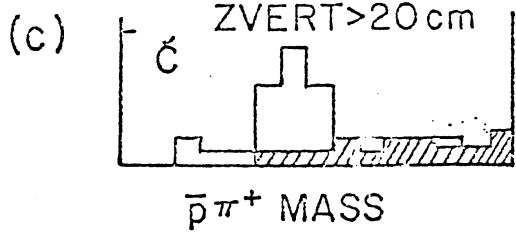
(b)

(c)

$\Sigma(1385)$ x > 0.6

$\Lambda^{\circ}\pi^{+}$

$\bar{\Lambda}^{\circ}\pi^{-}$

Ξ^{-} x > 0.4

$\Lambda^{\circ}\pi^{-}$

Invariant Mass (GeV)

Events / 10 MeV

Fig. 4

Fig. 5
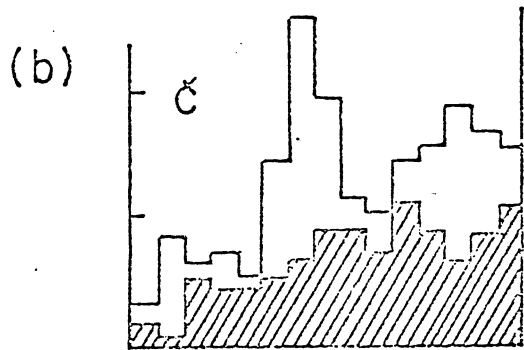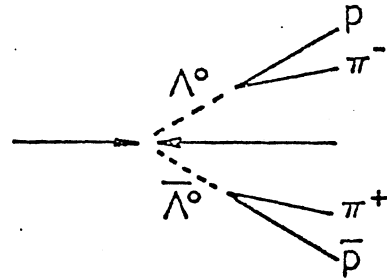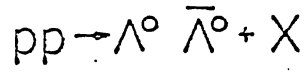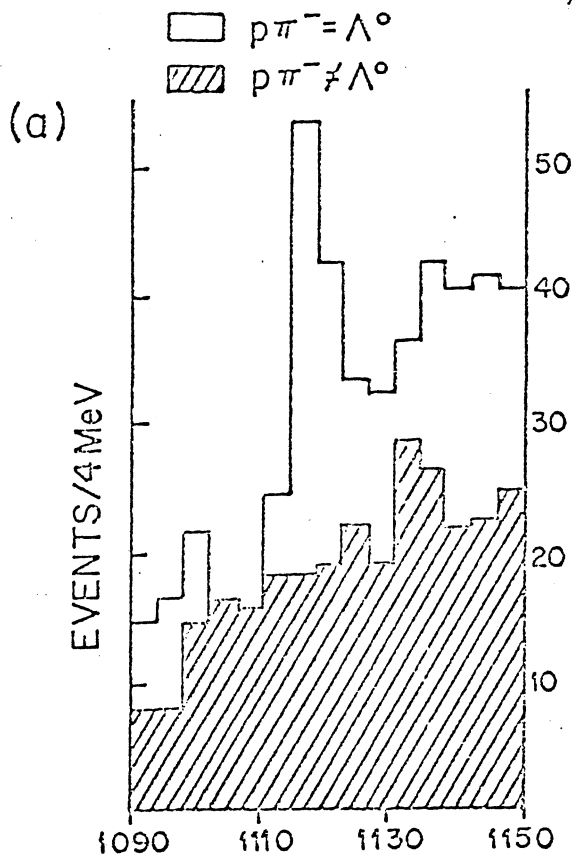
Fig. 6

$$pp \rightarrow \Lambda^{\circ} + \overline{\Lambda}^{\circ} + X$$
$$2.23 < M_{\Lambda\overline{\Lambda}} < 2.5 \text{ GeV}$$
$$0.5 < X(\Lambda\overline{\Lambda})$$
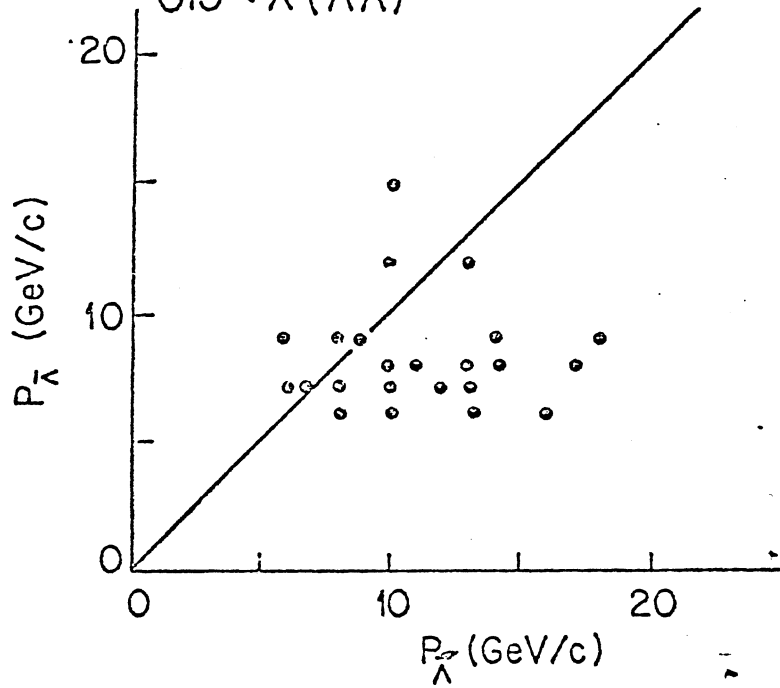
Preliminary
Cross section $\sigma \sim 10 \mu b$ in 1 hemisphere

Fig. 7

XII. POSSIBLE STUDIES OF $\bar{p}p$ INTERACTIONS AT THE ISR
WITH THE SUPERCONDUCTING SOLENOID OF CCOR

CERN-Columbia-Oxford-Rockefeller Collaboration

(presented by H.J. Besch - CERN-EP)

Introduction

The following is a brief review of the physics possibilities with antiprotons
in the ISR and using the superconducting solenoid detector at present being
used for experiment R 108 in intersection 1.

It is assumed that :

(a) the detector remains essentially in its present status

(b) the steel low-β insertion which increases the luminosity by about a
factor of two stays with the solenoid.

1. The Detector - technical data

The layout of the detector is shown in Figure 1. The solenoid has :

diameter ϕ = 1.4 m

length L = 1.7 m

field B = 1.4 T operating field (max. 1.5 T)

coil thickness d = 1 radiation length X_o

The inner detector consists of 4 drift chambers (DCM_{1-4}) of 2 planes each with
longitudinal readout by delay lines. The 'A,B' counters have TDC + ADC and there
are 336 lead glass blocks each with dimensions of $15 \times 15 \times 40$ cm^3 which provide
the trigger (40 cm ≈ 17 radiation lengths). Recently 2 strip chambers with
crossed 8 mm strips have been added between hodoscope B and the lead glass.
The performance can be summarized by :

Magnet : Momentum resolution $\frac{\Delta p}{p}$ = 0.04 p (in GeV/c)

Lead glass : Energy resolution $\frac{\Delta E}{E}$ = 0.004 + .043/√E (in GeV)

and the lead glass acceptance by $\Delta y \Delta \phi$ = 1.33 strad in the direction of c. of m. mot

$\Delta y \Delta \phi$ = 0.80 strad opposite to the direction of c.
motion

In order to calculate expected event rates for $\bar{p}p$ we compare the present luminosity

$$L_{pp}\text{peak} = 4.10^{31} \text{ cm}^{-2} \text{ sec}^{-1}$$

with that expected with $\bar{p}p$

$$L_{\bar{p}p}\text{peak} = 3.10^{29} \text{ cm}^{-2} \text{ sec}^{-1}$$

which is about 130 times lower.

In terms of integrated luminosity the experiment R 108 has used for T analysis :

$$\int L \, dt = 7.2 \times 10^{37} \text{ cm}^{-2}$$

This can be compared with the expected $\bar{p}p$ integrated luminosity, assuming two ten-day stacks per month[*] and 9 months of operation, one can hope for :

$$\int L \, dt = 2 \times 10^{36} \text{ cm}^{-2}$$

$$1 - 1.5 \text{ years}$$

which is still a factor of 40 down.

2. Lepton Pairs (e^+e^-)

There are expected to be significant differences in lepton pair production because of the presence of valence antiquarks in $\bar{p}p$.

(a) Drell Yan :

The ratio $\dfrac{\bar{p}p}{pp}$ depends on $\qquad \tau = \dfrac{m^2}{s}$

with $\qquad \sqrt{\tau} > 0.3$ it approaches 2 orders of magnitude

but for $\qquad \sqrt{\tau} \simeq 0.1$ it is $2 - 3$ depending on structure functions.

---

[*] see the notes of P. Bryant on Expected ISR Performance with Antiprotons in these proceedings, section VI.

However, large $\sqrt{\tau}$ is the domain of the fixed target machines

Assuming
$$\int \dot{L}\, dt = 2.10^{36}\ cm^{-2}$$

$$\sqrt{s} = 63\ GeV$$

$$s\ \frac{d^2\sigma}{d\sqrt{\tau}dy}\bigg|_{y=0} = 44.4\ e^{-25.6\sqrt{\tau}} \cdot 10^{-30}$$

Figure 2 shows the expected event rate in the solenoid detector for this integrated luminosity. Unfortunately it is not very promising.

(b) Resonance production

J/ψ production :

Approximately 700 events can be expected. It may be possible to study X-states.

T-production :

$\simeq$ 1 count in T-range can be expected if the cross-section stays as pp but a recent result from the Omega spectrometer gives

$$\frac{\bar{p}N \to J/\psi}{pN \to J/\psi} = 6 \quad \text{at similar x.}$$

Hadronic production of resonances is not well understood and experiments like this will help in the understanding of the production mechanisms, but it is clear that it will be necessary to increase the solid angle of the detector to allow a study of T. A factor of $\simeq$ 5 could be achieved, so one could expect about 30 T-events.

(c) Production of 'new' particles (Charm family)

In order to study the production of charmed particles it may be possible to make use of lower trigger thresholds because of the reduced luminosity, while the increase in production rate resulting from the presence of valence antiquarks in $\bar{p}p$
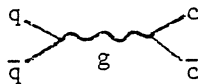
may improve the signal to noise ratio.

A handicap will be the lack of K-discrimination. The presence of strangeness would have to be detected via η and $\bar{\Lambda}$ ($|\eta_8 > = |2 \bar{s}s - \bar{u}u - \bar{d}d>$) Fig. 3 shows a $\bar{\Lambda}$-mass spectrum as measured with the solenoid detector. $\bar{\Lambda}$ can be identified by a large signal in the lead glass, caused by the annihilation of the decay $\bar{p}$.

3. Inclusive Π^o-production

The expected Π^o production rate obtainable with an integrated luminosity $\int L dt \cdot 2 \cdot 10^{36}$ cm^{-2} is approximated in Figure 4. Recent results from Fermilab on Π^o production[1] in $\bar{p}p$ and pp at $\sqrt{s}$ = 14 and 20 GeV show that

$\left(\dfrac{\sigma_{\bar{p}p}}{\sigma_{pp}}\right)_{90^o}$ lies between 0.5 and 2 for p_T = 1 - 3 GeV/c. It should be possible

to measure the distribution out to beyond 10 GeV/c. Also shown is an approximate upper limit for the proportion of single photons which may be detected in such a measurement (statistics only considered).

Finally, it should be noted that with a 2Π-acceptance in azimuth for charged tracks, correlation studies are possible.

4. Conclusion

The solenoid detector can do useful experiments in this 'new' field, sometimes handicapped by low rates, but this, on the other hand, may give an option to processes which were not accessible before.

References

1) G. Donaldson et al., PRL 40, 917 (1978).

Figure captions

Fig. 1   :   Layout of the detectors of experiment R 108

Fig. 2   :   The expected lepton pair event rate in the present detector
                     for an integrated luminosity of 2×10^{36} cm^{-2} , $\sqrt{s}$ = 63 GeV.

Fig. 3   :   Mass spectrum from experiment R 108 showing a $\bar{\Lambda}^{o}$ signal
                     identified by a large signal in the lead glass array from
                     annihilation of the decay $\bar{p}$

Fig. 4   :   Expected Π^{o} production for an integrated luminosity of
                     2×10^{36} cm^{-2} using results at $\sqrt{s}$ = 14, 20 GeV of
                     G. Donaldson et al. An approximate upper limit for the
                     proportion of direct single photons which could be detected
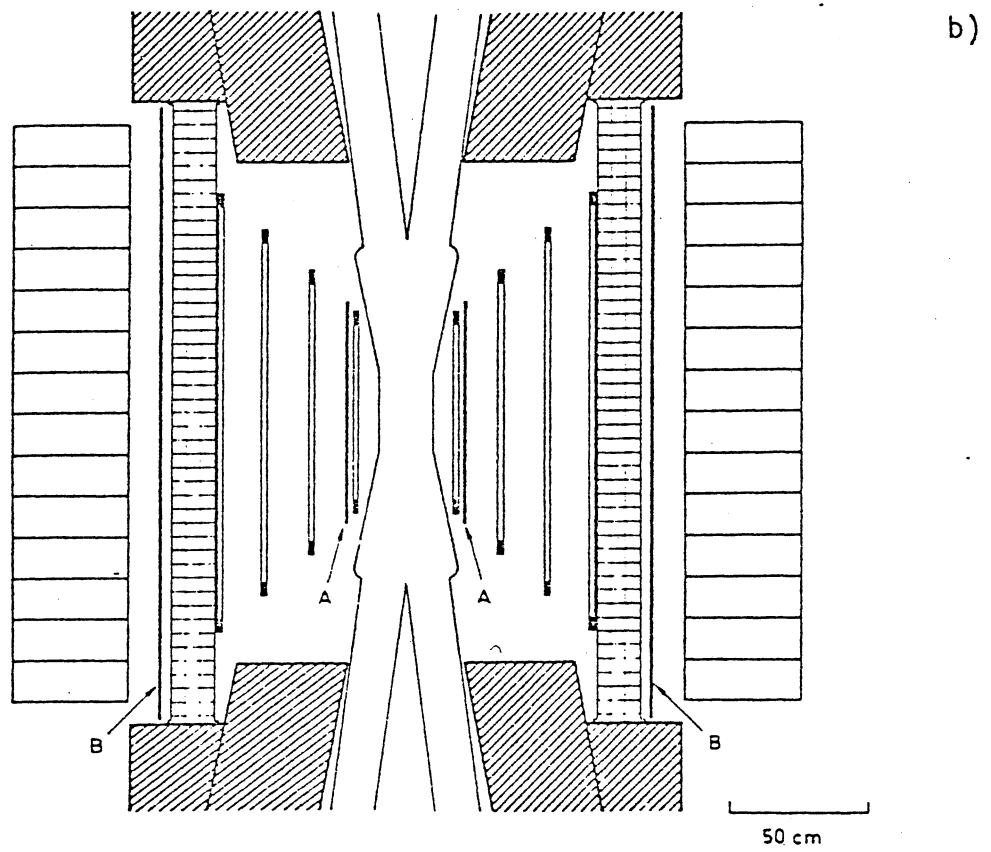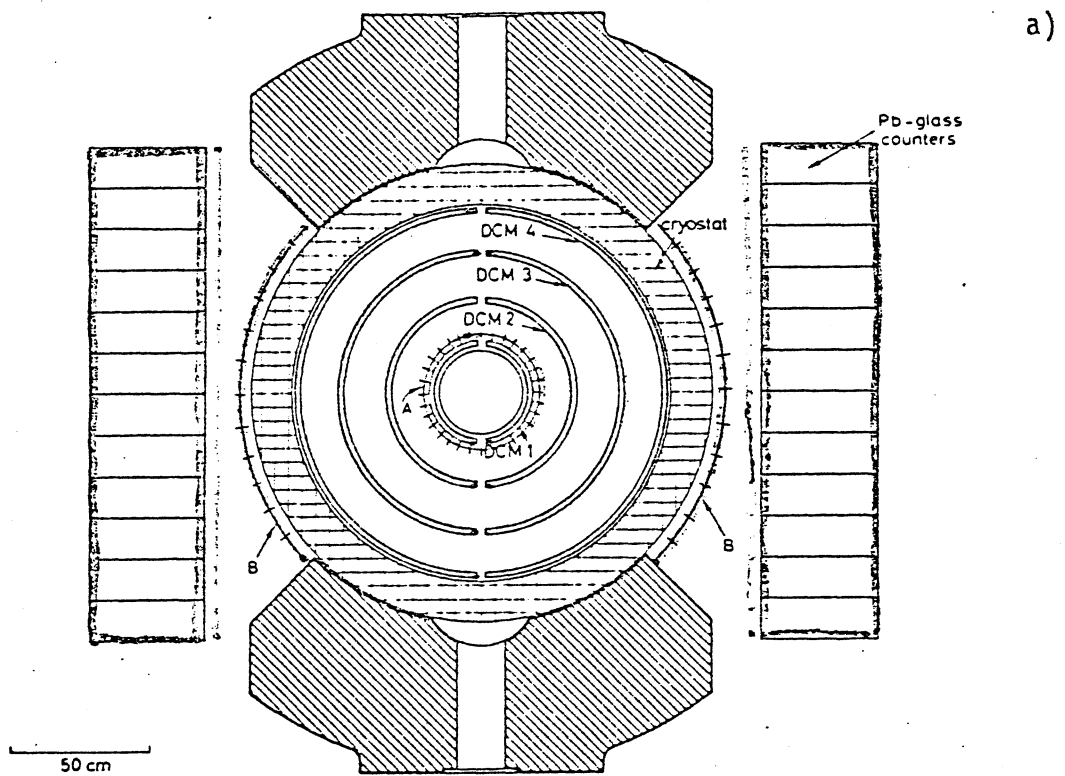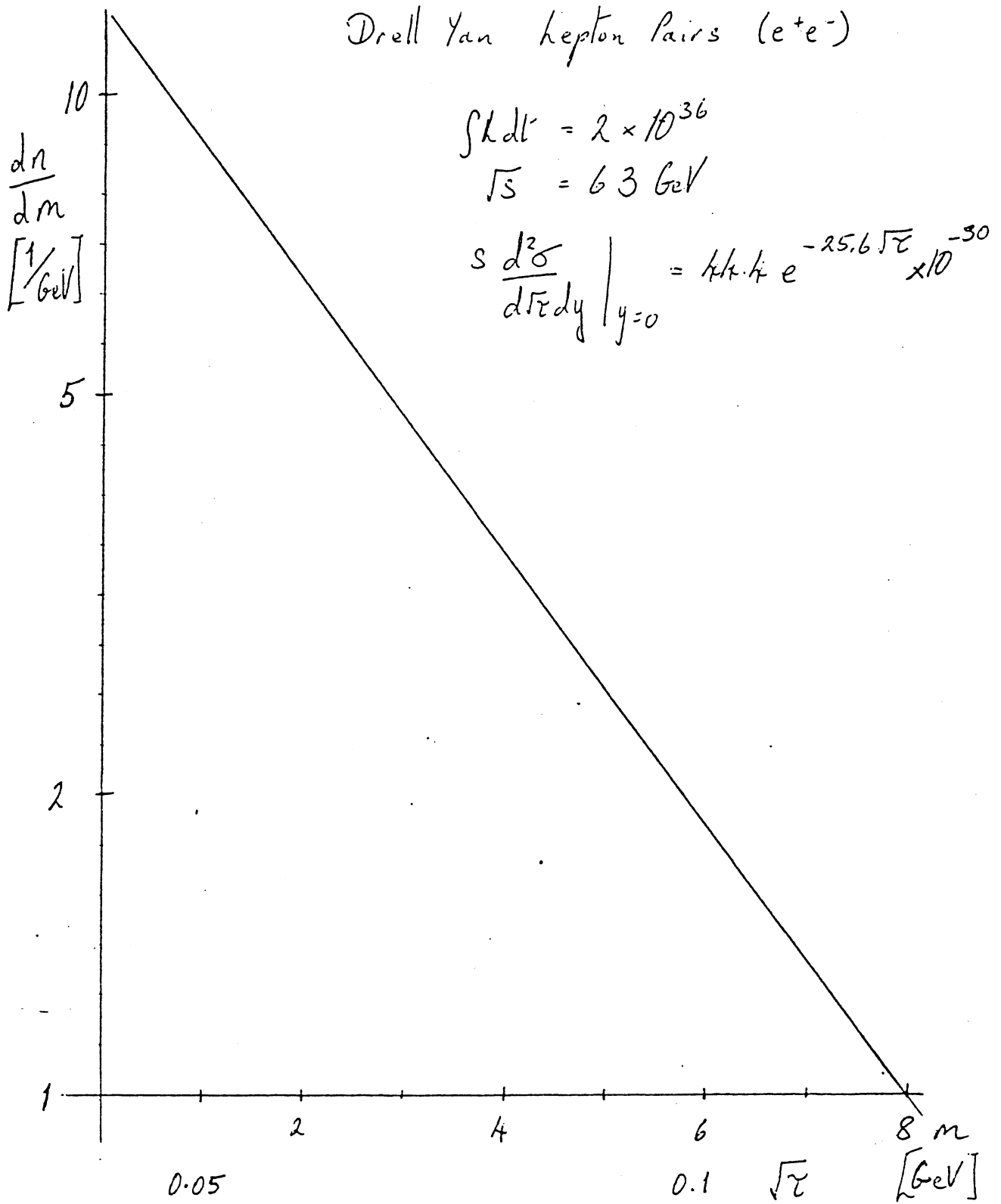   is also shown.

a)

b)

Fig. 1

Drell Yan Lepton Pairs (e^+e^-)

$$\int \mathcal{L} dt = 2 \times 10^{36}$$

$$\sqrt{s} = 63 \; GeV$$

$$s \frac{d^2\sigma}{d\sqrt{\tau}\,dy}\bigg|_{y=0} = 44.4 \; e^{-25.6\sqrt{\tau}} \times 10^{-30}$$

Fig. 2

Fig. 3

π° production in $\bar{p}p$.

$\frac{dn}{dp_T} \left[\frac{1}{0.5 \, \text{GeV/c}} \right]$

$\int \mathcal{L} \, dt = 2 \times 10^{36} \, \text{cm}^{-2}$

Single photon 1σ statistical limit from non conversion

Fig. 4